ไฮโดรจิเนชันของคาร์บอนไดออกไซด์บนตัวเร่งปฏิกิริยาฐานเหล็กสำหรับ
การสังเคราะห์เชื้อเพลิงเหลว

นางสาวรัชช์ประภา สัตถาวงษ์

วิทยานิพนธ์นี้เป็นส่วนหนึ่งของการศึกษาตามหลักสูตรปริญญาวิทยาศาสตรดุษฎีบัณฑิต
สาขาวิชาเคมีเทคนิค ภาควิชาเคมีเทคนิค
คณะวิทยาศาสตร์ จุฬาลงกรณ์มหาวิทยาลัย
ปีการศึกษา 2557

HYDROGENATION OF CARBON DIOXIDE ON IRON-BASED CATALYSTS FOR LIQUID FUEL SYNTHESIS

Miss Ratchprapa Satthawong

A Dissertation Submitted in Partial Fulfillment of the Requirements
for the Degree of Doctor of Philosophy Program in Chemical Technology
Department of Chemical Technology
Faculty of Science
Chulalongkorn University
Academic Year 2014

Thesis Title	HYDROGENATION OF CARBON DIOXIDE ON IRON-BASED CATALYSTS FOR LIQUID FUEL SYNTHESIS
By	Miss Ratchprapa Satthawong
Field of Study	Chemical Technology
Thesis Advisor	Professor Pattarapan Prasassarakich, Ph.D.
Thesis Co-Advisor	Professor Chunshan Song, Ph.D.

Accepted by the Faculty of Science, Chulalongkorn University in Partial Fulfillment of the Requirements for the Doctoral Degree

.....Dean of the Faculty of Science
(Professor Supot Hannongbua, Dr.rer.nat.)

THESIS COMMITTEE

.....Chairman
(Associate Professor Kejvalee Pruksathorn, Ph.D.)

.....Thesis Advisor
(Professor Pattarapan Prasassarakich, Ph.D.)

.....Thesis Co-Advisor
(Professor Chunshan Song, Ph.D.)

.....Examiner
(Associate Professor Pornpote Piumsomboon, Ph.D.)

.....Examiner
(Assistant Professor Chawalit Ngamcharussrivichai, Ph.D.)

.....External Examiner
(Ungkana Wongsiriwan, Ph.D.)

รัชช์ประภา สัตถาวงษ์ : ไฮโดรจิเนชันของคาร์บอนไดออกไซด์บนตัวเร่งปฏิกิริยาฐานเหล็กสำหรับการสังเคราะห์เชื้อเพลิงเหลว (HYDROGENATION OF CARBON DIOXIDE ON IRON-BASED CATALYSTS FOR LIQUID FUEL SYNTHESIS) อ.ที่ปรึกษาวิทยานิพนธ์หลัก: ศ. ดร.ภัทรพรรณ ประศาสน์สารกิจ, อ.ที่ปรึกษาวิทยานิพนธ์ร่วม: Prof. Chunshan SongPh.D., 122 หน้า.

ไฮโดรจิเนชันเชิงเร่งปฏิกิริยาของ CO_2 เพื่อสังเคราะห์สารเคมีและเชื้อเพลิงได้รับความสนใจเป็นอย่างมากเนื่องจากสามารถลดการปลดปล่อย CO_2 และการพึ่งพาเชื้อเพลิงฟอสซิล งานวิจัยนี้เป็นการพัฒนาตัวเร่งปฏิกิริยาที่มีประสิทธิภาพสำหรับการสังเคราะห์ไฮโดรคาร์บอนตั้งแต่ C_2 ขึ้นไป (C_2^+) จากไฮโดรจิเนชัน CO_2 โดยการดัดแปรสมบัติการดูดซับ CO_2 และ H_2 บนพื้นผิวตัวเร่งปฏิกิริยา งานวิจัยนี้ได้เตรียมตัวเร่งปฏิกิริยาโลหะเดี่ยวและโลหะคู่ Fe-M (M = Co, Ni, Cu, Pd) บนตัวรองรับอะลูมินาและทดสอบไฮโดรจิเนชัน CO_2 ที่ 573 เคลวิน และ 1.1 เมกะพาสคัล เมื่อเปรียบเทียบตัวเร่งปฏิกิริยาโลหะเดี่ยวมีเพียงตัวเร่งปฏิกิริยา Fe เท่านั้นที่สามารถสังเคราะห์ไฮโดรคาร์บอนสายยาวได้ ในขณะที่ตัวเร่งปฏิกิริยา Co และ Ni มีความจำเพาะเลือกเกิด CH_4 การผสม Fe กับ M (M/(M + Fe) = 0.10 โดยอะตอม) ส่งผลให้เกิดการส่งเสริมการเกิดไฮโดรคาร์บอนสายยาว จากการวิเคราะห์ H_2-TPR และ H_2-TPD พบว่าความสามารถในการถูกรีดิวซ์และสมบัติการดูดซับ H_2 ของตัวเร่งปฏิกิริยา Fe-Co/Al_2O_3 ขึ้นอยู่กับอัตราส่วน Co/(Co + Fe) อย่างมาก งานวิจัยนี้พบความสัมพันธ์เชิงเส้นระหว่างปริมาณ H_2 ที่ถูกดูดซับด้วยแรงปานกลางและ space-time yield ของไฮโดรคาร์บอนสายยาว ซึ่งชี้ให้เห็นถึงความสำคัญของ H_2 ชนิดนี้ต่อการเกิดไฮโดรคาร์บอนสายยาว การเติมโพแทสเซียม (K) ให้แก่ตัวเร่งปฏิกิริยา Fe-Co/Al_2O_3 สามารถเพิ่มการเกิดไฮโดรคาร์บอนสายยาวได้อย่างชัดเจนโดยเฉพาะอย่างยิ่งโอเลฟินส์โซ่ตรง ในขณะที่ลดการเกิด CH_4 สำหรับตัวเร่งปฏิกิริยา Fe-Co ที่มี K เป็นตัวส่งเสริมนั้น ไฮโดรจิเนชัน CO_2 เกิดผ่านปฏิกิริยาสองขั้นตอนคือ ปฏิกิริยา reverse water-gas shift ตามด้วยการสังเคราะห์ฟิสเชอร์-ทรอปส์ ซึ่งโอเลฟินส์และพาราฟินส์เกิดขึ้นในเวลาเดียวกัน แต่โอเลฟินส์ที่เกิดขึ้นบางส่วนอาจถูกไฮโดรจิเนตอีกครั้งไปเป็นพาราฟินส์ขึ้นอยู่กับปริมาณไฮโดรเจนที่ถูกดูดซับบนพื้นผิวตัวเร่งปฏิกิริยา การวิเคราะห์ H_2-TPD ชี้ให้เห็นว่าการเติม K เป็นการลดการดูดซับ H_2 บนตำแหน่งของโลหะ ส่งผลให้ปริมาณโอเลฟินส์เพิ่มขึ้น

ภาควิชา เคมีเทคนิค	ลายมือชื่อนิสิต .....
สาขาวิชา เคมีเทคนิค	ลายมือชื่อ อ.ที่ปรึกษาหลัก .....
ปีการศึกษา 2557	ลายมือชื่อ อ.ที่ปรึกษาร่วม .....

5373820023 : MAJOR CHEMICAL TECHNOLOGY
KEYWORDS: CO2 HYDROGENATION / IRON-BASED CATALYST / BIMETALLIC CATALYST / POTASSIUM PROMOTION / HIGHER HYDROCARBONS / SYNTHETIC NATURAL GAS / ADSORPTION PROPERTIES / LIGHT OLEFINS

RATCHPRAPA SATTHAWONG: HYDROGENATION OF CARBON DIOXIDE ON IRON-BASED CATALYSTS FOR LIQUID FUEL SYNTHESIS. ADVISOR: PROF. PATTARAPAN PRASASSARAKICH, Ph.D., CO-ADVISOR: PROF. CHUNSHAN SONG, Ph.D., 122 pp.

Catalytic CO_2 hydrogenation to chemicals and fuels has attracted great attention since it can reduce both CO_2 emission and dependence on fossil fuels. This research, the efficient catalyst for CO_2 hydrogenation to higher (C_2^+) hydrocarbons was developed by tailoring the adsorption properties for CO_2 and H_2 on the catalyst surfaces. The alumina supported monometallic and bimetallic Fe-M (M = Co, Ni, Cu, Pd) catalysts were prepared and tested for CO_2 hydrogenation at 573 K and 1.1 MPa. Among the monometallic catalysts, only Fe catalyst could synthesize C_2^+ hydrocarbons, while Co and Ni catalysts showed high CH_4 selectivity. The combination of Fe and M (M/(M + Fe) = 0.10 atom atom^{-1}) led to significant bimetallic promotion of C_2^+ hydrocarbons formation. H_2-TPR and H_2-TPD analyses suggested that the reducibility and H_2 adsorption properties of the Fe-Co/Al_2O_3 catalyst sensitively changed with the Co/(Co + Fe) atomic ratio. A linear relationship between the amount of moderately adsorbed H_2 and the space-time yield (STY) of C_2^+ hydrocarbons was observed, indicating an importance of this adsorbed H_2 specie on the formation of C_2^+ hydrocarbons. This research also discovered that potassium (K) addition to Fe-Co/Al_2O_3 catalyst significantly enhanced C_2^+ hydrocarbons formation, particularly linear olefins, while it suppressed CH_4 formation. H_2-TPD experiments revealed that K addition suppressed the hydrogen adsorption on metal sites, leading to an increase in the olefin content.

Department:	Chemical Technology	Student's Signature .....
Field of Study:	Chemical Technology	Advisor's Signature .....
Academic Year:	2014	Co-Advisor's Signature .....

ACKNOWLEDGEMENTS

The author would like to express heartfelt gratitude and sincere appreciation to her advisor, Prof. Dr.Pattarapan Prasassarakich and co-advisor, Prof. Dr.Chunshan Song for the encouraging guidance, supervision, helpful discussion and support throughout this research. The author also would like to acknowledge Assoc. Prof. Dr.Kejvalee Pruksathorn, Assoc. Prof. Dr.Pornpote Piumsomboon, Asst. Prof. Dr.Chawalit Ngamcharussrivichai, and Dr. Ungkana Wongsiriwan for serving as the dissertation chairman and members of thesis committee, respectively.

The author gratefully acknowledge the funding support from the Thailand Research Fund (through the Royal Golden Jubilee Project), Graduate School, Chulalongkorn University and the Pennsylvania State University.

Many thanks also go to EMS Energy Institute, Department of Energy and Mineral Engineering, Pennsylvania State University and Department of Chemical Technology, Faculty of Science, Chulalongkorn University for providing research facilities throughout this research work. The author deeply grateful to Dr. Naoto Koizumi who gave many valuable advices and taught her many important things about the research work. Special thanks are also extended to members of the Clean Fuels and Catalysis Program in the Energy Institute of the Pennsylvania State University and her friends in Department of Chemical Technology for friendship, support and encouragement.

Finally, the author would also express her deep gratitude to her family for their love, support and encouragement throughout the tenure of her Ph.D. program.

CONTENTS

Page

Page

Page

Page

LIST OF TABLES

LIST OF FIGURES

FIGURE PAGE

FIGURE PAGE

FIGURE PAGE

FIGURE PAGE

LIST OF ABBREVIATIONS

α	:	Chain growth probability
ASF	:	Anderson–Schulz–Flory
BET	:	Brunauer-Emmett-Teller
BJH	:	Barrett-Joyner-Halenda
CCS	:	Carbon Capture and Storage
DME	:	Dimethyl ether
DRIFTS	:	Diffuse Reflectance Infrared Fourier Transform Spectroscopy
FTIR	:	Fourier Transform Infrared Spectroscopy
FTS	:	Fischer-Tropsch Synthesis
GTCC	:	Gas Turbine Combined Cycle
$\Delta G_{298\ K}$	:	Gibb Free Energy
$\Delta H_{298\ K}$	:	Heat of Reaction
IGCC	:	Integrated Gasification Combined Cycle
MS	:	Mass Spectrometry
MWCNTs	:	Multi-Walled Carbon Nanotubes
NIST	:	National Institute of Standards and Technology
ppm	:	Parts-Per-Million
RWGS	:	Reverse Water–Gas Shift
SNG	:	Synthetic Natural Gas
SSITKA	:	Steady-state Isotopic Transient Kinetic Analysis
STY	:	Space-Time Yield

TOF	:	Turnover-Frequency
TOS	:	Time-On-Stream
TPD	:	Temperature-Programmed Desorption
TPR	:	Temperature-Programmed Reduction
WGS	:	Water-Gas Shift
XPS	:	X-Ray Photoelectron Spectroscopy
XRD	:	X-Ray Diffraction

CHAPTER I

INTRODUCTION

1.1 Motivation

Nowadays, many global issues originate from the pollutant emissions of fossil fuel combustion (coal, petroleum, and natural gas) in various stationary and mobile energy systems such as manufacturing industries and transportations. The pollutants are not limited to only NO_x, SO_x, and particulate matter (PM). Carbon dioxide (CO_2) emission has also become a major global problem due to its culpability to the greenhouse effect and global warming [1-4]. The atmospheric CO_2 concentration has increased steadily during the last 200 years from approximately 270 ppm to 385 ppm [5,6]. It should be mentioned that the atmospheric CO_2 also has important and positive roles in the ecological system, since it is a carbon source for photosynthesis and food production, and also an original carbon source of the fossil fuels used today. However, too high a CO_2 concentration could prevent the re-emission of an infrared, leading to an increase in the atmospheric temperature and a global climate change [7].

Currently, an ongoing research aiming to find ways for reducing CO_2 emission in the atmosphere such as capturing the CO_2 released from combustion of fossil fuels and sequestration of the CO_2. Since 2006, more than 30 billion tonnes of CO_2 is discharged into the atmosphere every year [8], but less than 100 million tonnes is utilized (2010) [9]. The consumption of the fossil hydrocarbon resources worldwide also continuously increase. Over 80 percent of the current energy demands are met by the combustion of coal, oil and natural gas, with the unavoidable production and emission of CO_2 [10,11]. The representation of a current global energy scenario based on fossil fuels and the distribution of energy source consumption is shown in Figure

1.1 [12]. A rapid consumption of the fossil hydrocarbon resources worldwide has become a major challenge. Although coal resources are more abundant which could last for several hundred years based on a current consumption rate, but they are still limited [13,14]. Weisz has pointed out that the energy demand and the population growth are exhausting the world's supplies of oil, gas and coal [15,16]. Although other nonconventional fossil fuels such as tar sands, oil shale, and natural gas hydrates are also being considered, all of these hydrocarbon resources are still non-renewable, so they can be exhausted [16]. Therefore, utilization of CO_2 to produce energy-rich compounds has attracted great attention since this could mitigate both the current CO_2 emission levels and the dependence on the depleting non-renewable fuels [4,10,16-18].

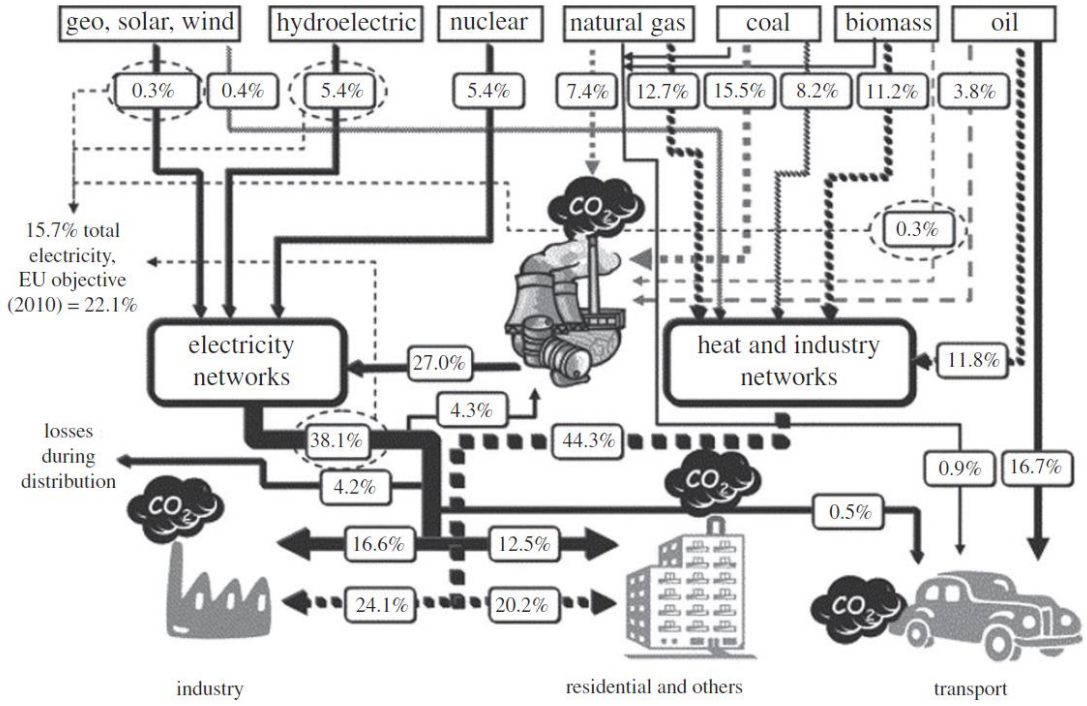

Figure 1.1 Current global energy scenario based on fossil fuels [12].

So far, CO_2 hydrogenation to hydrocarbons has been studied mainly on traditional catalysts for Fischer-Tropsch synthesis (FTS) such as Fe, Ni, Co and Ru catalysts. Attentions have been paid on improving the catalytic performances of Fe-based catalysts since the higher hydrocarbons could be synthesized from CO_2 hydrogenation [19-22]. Though the K promoted Fe/Al_2O_3 catalysts are known to show activity for higher hydrocarbons synthesis from CO_2 but their activity and selectivity to higher hydrocarbons are still very low [19,20]. How to achieve the substantial activity improvement in synthesis of higher hydrocarbons remains a major challenge.

1.2 Carbon Dioxide Control and Utilization

Controlling CO_2 is a major challenge and long-term task. There are five possible technical options for reducing the CO_2 concentration in the atmosphere including energy choices, energy efficiency, CO_2 capture, CO_2 sequestration, and CO_2 utilization [16]. Energy choices can be performed by selecting the primary energy input for new installations of energy systems or switching from a carbon-rich energy carrier (coal) toward less carbon intensive energy sources (oil or natural gas) for decreasing the produced CO_2. The large reduction of CO_2 would be achieved by changing an energy input from fossil fuels to the non-fossil fuels such as renewable energy ie. hydropower, solar energy, wind energy, and biomass [16,18].

The second option is to improve the energy efficiency of energy utilization systems, which has a strong influence on CO_2 reduction [5,16,18]. An average efficiency of the existing energy systems in the fossil fuel-based electricity generators in the United States is about 35%, while that for the automobiles is less than 20% [16,23]. The energy efficiencies could be notably increased by developing and implementing the new energy utilization systems such as an integrated gasification combined cycle (IGCC) for coal-based power plants, a gas turbine combined cycle (GTCC) for natural gas-based power plants, or fuel cell-based hybrid motors for

transportation. For the chemical industry, more efficient process or more selective catalyst can make a process such as oxidation reaction more selective, resulting in a minimization of CO_2 formation at the source, which improve the process efficiency and conserve hydrocarbon resources [4,24].

To reduce the amount of CO_2 emitted from large-scale fossil fuel based facilities such as power stations and cement works, carbon capture and storage (CCS) are primarily focused [12]. There are three generic options for CCS being proposed: pre-combustion capture, post-combustion capture, and oxy fuel combustion, which are based on different physical and chemical processes involving absorption, adsorption and cryogenic capture of CO_2. [25,26].

Recently, utilization of CO_2 has gained great attention worldwide since it can turn CO_2 to hydrocarbon fuels which are still compatible with the current facility infrastructure. Due to the high stability of CO_2, a large amount of energy, effective reaction conditions, and active catalysts, are necessary for CO_2 conversion [16]. However, the thermodynamic considerations reveal that high energy is required if only CO_2 is used as a single reactant, but it becomes thermodynamically easier if CO_2 is used as a co-reactant with another molecule that has higher Gibbs free energy, such as CH_4 and H_2. CO_2 Hydrogenation is one of the interesting routes for synthesizing hydrocarbon fuels using CO_2 as a carbon source [16-18]. Moreover, it is also possible to convert CO_2 using the energy from renewable, carbon-free sources (e.g. electricity derived from solar, wind, wave or nuclear, associated with hydrogen or methane), which make this process sustainable [17,27,28].

1.3 Reverse Water-Gas Shift Reaction

The reverse water–gas shift (RWGS) reaction is also a reaction in the catalytic CO_2 hydrogenation process. It is the first step in the hydrogenation of CO_2 into fuels. The RWGS reaction is a mildly endothermic reaction with heat of reaction ($\Delta H_{298\ K}$) of

41.2 kJ mol^{-1} and Gibb free energy ($\Delta G_{298\ K}$) of 28.6 kJ mol^{-1} [17]. The RWGS reaction is shown in Eq. (1.1).

$$CO_2 + H_2 \leftrightarrow CO + H_2O \quad (1.1)$$

The equilibrium of this reaction can be shifted to the right by increasing the concentration of CO_2 or H_2 to force the complete consumption of the other reactant or removing water vapor from the reactor [17]. The water vapor could be removed using a desiccant bed, or a membrane permeoselective to water. In the FTS, water formed as a by-product during the reaction can deactivate the FT catalysts and also inhibit the reaction rate. Therefore, various types of membranes such as silico-alumina or zeolitic membranes are applied for the selective H_2O removal during the FTS [29,30]. The same concept might possibly be applied for the RWGS reaction to shift the reaction equilibrium [17].

Since the RWGS reaction is a reversible reaction, the active catalysts in the water gas shift (WGS) reaction (such as copper- and cerium-based catalysts) are frequently active in the reverse reaction as well [17,31,32]. The copper-based (Cu-based) bimetallic catalyst such as Cu–Ni catalysts supported on gamma alumina have also been tested for CO_2 hydrogenation [33]. The ratio of Cu/Ni strongly affected the conversion and product selectivity, since Cu favors CO formation, while Ni is active for CO_2 methanation. The Cu-based catalysts used for methanol synthesis such as CuO/ZnO and Cu–Zn/Al_2O_3 with various Cu/Zn ratio have also been applied for the RWGS reaction and the results showed that the alumina supported Cu rich (Cu/Zn $>$ 3) catalyst was the most active one for this reaction. A linear relationship between the activity of the catalyst and the surface area of metallic Cu was proposed [34]. Potassium (K) was also used as a promoter for Cu catalyst. The K-promoted Cu/SiO_2 catalyst showed higher CO_2 conversion (12.8%) than the unpromoted catalyst (5.3%) at 600 ^{o}C, since K enhanced CO_2 adsorption and provided the additional active sites for the decomposition of formate species, which is the intermediate of RWGS reaction [18,35].

The ceria-supported Ni catalyst (2 wt% Ni) also showed high activity, selectivity and stability for the RWGS reaction, with CO yield ~35% at 600 °C, while the bulk Ni favors the CO_2 methanation [36]. The active components for the reaction over Ni/CeO_2 catalyst are the oxygen vacancies formed in the lattice of CeO_2 and highly dispersed Ni. However the CeO_2-supported catalysts are easily suffer from a deposition of carbon, leading to strong deactivation of the catalyst [18,37].

Two main reaction mechanisms of the RWGS reaction have been proposed, namely redox and formate mechanisms, but it is still controversial [38,39]. The redox mechanism for the RWGS reaction over Cu-based catalyst can be written as shown in Eq. (1.2) and (1.3).

$$CO_2 + 2Cu^0 \rightarrow Cu_2O + CO \quad (1.2)$$

$$H_2 + Cu_2O \rightarrow 2Cu^0 + H_2O \quad (1.3)$$

In the redox mechanism, CO_2 dissociatively adsorbs on the metallic Cu sites to form CO. The oxidized Cu (Cu_2O) is subsequently reduced by H_2 back to the metallic state (Cu^0). Hydrogen is proposed to be a reducing reagent without direct participation in the formation of intermediates in the RWGS reaction [40,41]. In the case of formate mechanism, the main reaction intermediate is a bidentate formate formed from the reaction between CO_2 and H_2, suggesting that CO is formed from decomposition of the formate intermediates [17,18,35,42].

Another RWGS mechanism over a Pt/CeO_2 catalyst was also proposed [43]. The results from a detailed spectrokinetic analysis, monitored by diffuse reflectance Fourier transform infrared spectroscopy (DRIFTS) and mass spectrometry (MS) using steady-state isotopic transient kinetic analysis (SSITKA) suggest that Co formation over Pt/CeO_2 catalyst proceeds via three kinds of mechanism as showed in Figure 1.2. CO was mainly formed via surface carbonate intermediates, including reaction between the surface carbonates and oxygen vacancies or the diffusion of the vacancies in the CeO_2. However, the formates and Pt-bound carbonyls species were also observed, but at lower extent compared with the carbonate intermediates [18,43].

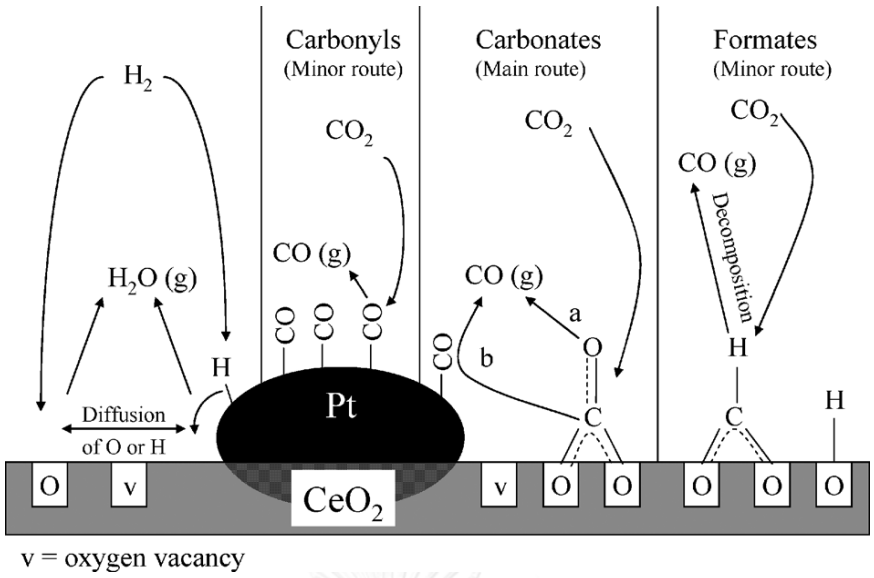

Figure 1.2 The proposed model for the reaction mechanism of the RWGS reaction over Pt/CeO_2 [43].

1.4 CO_2 Hydrogenation to Alcohol

1.4.1 Synthesis of Methanol

Methanol is a common solvent, a starting material in chemical industry and also an alternative fuel. Methanol could be synthesized via CO_2 hydrogenation using a single or two step approaches. The RWGS reaction and the methanol synthesis are integrated in a single reactor for the single step approach, while they are separated into two reactor for the two step approach [17]. Methanol synthesis via CO_2 hydrogenation is an exothermic reaction with $\Delta H_{298\ K}$ of -49.5 kJ mol^{-1} and can be written as shown in Eq. (1.4) [18].

$$CO_2 + 3H_2 \rightarrow CH_3OH + H_2O \qquad (1.4)$$

From the thermodynamic point of view, the synthesis of methanol could be driven by decreasing the reaction temperature or increasing the reaction pressure. However, since CO_2 has low reactivity, the reaction temperature need to be higher than 513 K in order to activate CO_2 for the methanol formation [44]. In addition, the side reaction such as RWGS reaction, higher alcohols or hydrocarbon

formations also consume H_2, resulting in a reduction of the methanol formation. The water formed during methanol synthesis and side reactions should also be considered, since water can deactivate the catalysts or inhibit the methanol formation [17,44]. To avoid the formation of undesired by-products, the highly selective catalysts are crucial for methanol synthesis via CO_2 hydrogenation.

Until now, most catalysts used for CO_2 hydrogenation to methanol are the modified catalysts used for methanol synthesis from CO hydrogenation. They are based on Cu/ZnO catalysts containing various additives such as Zr, Ga, Si, Al, B, Cr, Ce, V, Ti [45,46]. The addition of these additives to the Cu/ZnO-based catalysts could improve the dispersion and stability of Cu particles significantly, leading to an increase in the total surface area of the metal phase, thus CO_2 conversion and methanol yield were enhanced [46-49]. Furthermore, the crystal types of ZrO_2 also affected performance of the catalysts, ie., the activity of Cu supported on m-ZrO_2 was higher than that of the Cu/t-ZrO_2, due to the higher concentration of adsorbed active intermediates such as HCOO and CH_3O [18,50,51]. A simplified reaction paths for CO_2 hydrogenation to methanol over the Cu/ZrO_2 catalyst surface was proposed as shown in Figure 1.3 [18,52]. Hydrogen dissociatively adsorbed on the Cu surface, while CO_2 adsorbed on the surface of ZrO_2 formed bicarbonate species. The bicarbonate species are then hydrogenated by the adsorbed hydrogen on metallic Cu (spillover) to form formate intermediate species, which subsequently hydrogenated to methanol [53,54].

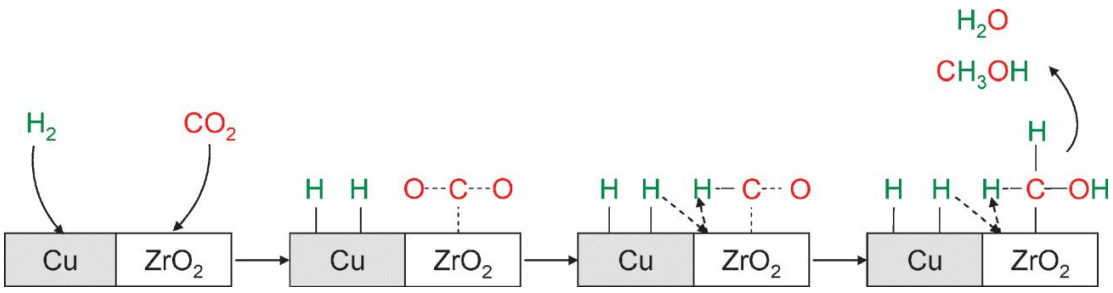

Figure 1.3 Proposed reaction pathway of the methanol formation from CO_2 hydrogenation over Cu/ZrO_2 catalyst [18,52].

Ga or Cr could increase the specific activity per unit Cu surface area of the catalysts, and Ga, Al or B can also decrease the adsorption rate of water that inhibits the methanol formation [46,55,56]. Further studies demonstrated that the Cu/ZnO-based multicomponent catalysts such as $Cu/ZnO/ZrO_2/Al_2O_3$, $Cu/ZnO/ZrO_2/Al_2O_3/SiO_2$ and $Cu/ZnO/ZrO_2/Al_2O_3/Ga_2O_3$ showed better performances for CO_2 hydrogenation to methanol. The addition of a small amount of SiO_2 significantly improved the long-term stability of the multi-component catalysts during the reaction [57].

In addition to the Cu/ZnO-based catalysts, the noble metal-based catalysts also exhibit high activity for methanol synthesis via CO_2 hydrogenation. The supported Pd catalysts are the most commonly used catalysts due to their high activity and selectivity for CO_2 hydrogenation to methanol. Several researchers reported that support materials also play a crucial role on the performance of Pd catalyst [44,58,59]. The La_2O_3 supported Pd catalyst could synthesize methanol with more than 89% selectivity at 623 K and 12 MPa, while methane (CH_4) was the major product when the acidic supports (e.g. SiO_2, Al_2O_3) were used [44]. The multi-walled carbon nanotubes (MWCNTs) were also used as a support for Pd-ZnO catalysts. The 16% Pd0.1Zn1/CNTs(h-type) catalyst showed high efficiency for CO_2 hydrogenation to methanol at 523 K and 3.0 MPa with the observed turnover-frequency (TOF) of 1.15 x 10^{-2} s^{-1} [58]. Recently, Koizumi et al. [59] investigated the effect of the pore size and pore structure of the SiO_2 support (amorphous SiO_2, MCM-48, MCM-41, SBA-15 and MSU-F) on the catalytic activity of alkali promoted Pd catalysts for methanol synthesis from CO_2 hydrogenation. The alkali promoted Pd supported on MCM-41 and SBA-15 exhibited high activity for methanol synthesis at 523 K and 4.1 MPa, due to that the small Pd^0 nanoparticles can be formed in the small mesopores of MCM-41 and SBA-15 which confine the nanoparticle growth [59].

1.4.2 Synthesis of Higher Alcohol

Higher alcohols are preferable to methanol as products from CO_2 hydrogenation in terms of easier transport/storage and excellent compatibility to gasoline [17,18]. Higher alcohol synthesis from CO_2 could be proceed via two-step reaction; RWGS reaction (for producing syngas) and subsequent hydrogenation of CO to higher alcohols [17]. Therefore, a catalyst that is active for both reactions under the same condition (ie. Fe-based and Rh-based catalysts) would be favorable for the overall reaction [18,60-63]. Catalysts for higher alcohol synthesis should provide active sites for promoting several reactions including partial reduction of CO_2 to CO, C-C bond formation, and OH group insertion, such as the combination of Cu-based catalysts, which has the RWGS ability, and Fe-based catalysts with the FTS ability [18,62,63]. The addition of alkaline promoter such as K to the Fe-based FT catalysts could promote the C-C bond formation, leading to an increase in C_2^+-alcohols formation [63]. The ethanol selectivity from CO_2 hydrogenation at 300 °C and 7 MPa was increased from 6% to 20% by adding K_2CO_3 to a Cu/Fe/ZnO catalyst. However, the major products were C_2^+ hydrocarbons and the deactivation rate was relatively high [17,64,65].

Rh-based catalyst is also known as an efficient catalyst for ethanol synthesis from CO hydrogenation [60]. By modifying this catalyst, ethanol can be synthesized from CO_2 hydrogenation. The Li promoted Rh/SiO_2 catalyst could yield ethanol with 15.5% selectivity and 7.0% CO_2 conversion. In situ FTIR analysis suggested that CO_2 was hydrogenated to ethanol via CO intermediate and the addition of Li could increase CO formation [60]. An ethanol selectivity of 16% with 26.7% CO_2 conversion were obtained using SiO_2 supported Rh-Fe catalyst (5 wt%) [61]. According to the XPS and in situ FTIR analyses, the authors have concluded that the electronic states of Rh was changed by Fe^{3+}, and the presence of Fe^0 promotes methanation and prevented the formation of methanol, ethanol, and CO [61]. Rh-Fe-Li(1:1:1)/SiO_2 catalyst (5 wt%) gave high ethanol selectivity (14%) at 34% CO_2 conversion at 260 °C [18,64].

The carbon nanotubes (CNTs) were also used as a support for the Rh-based catalysts for CO hydrogenation [66,67]. Rh and Mn nanoparticles with Li and Fe as the additives (Rh:Mn:Li:Fe was 1:1:0.075:0.05 by weight; denoted as RMLF), were deposited on the inner (RMLF-in-CNTs) or outer (RMLF-out-CNT) surface of the CNTs (4-8 nm inner diameter and 250-500 nm length; 1.2 wt% Rh loading). The results showed a significantly different behavior between RMLF-in-CNT and RMLF-out-CNT catalysts in the formation of C_2 oxygenates from CO hydrogenation (Figure 1.4). The C_2 oxygenates yield with more than 76% ethanol was obtained from RMLF-in-CNTs, which is about one order of magnitude higher than that of the analogous RMLF-out-CNT sample, and also larger than that of similar catalysts prepared supported on silica [17,66].

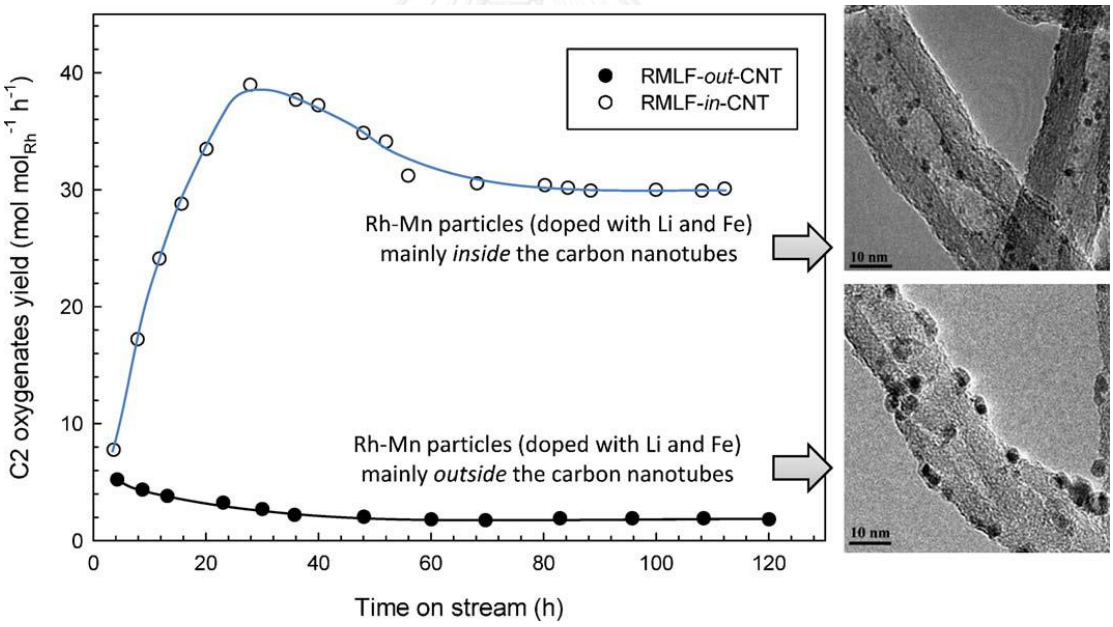

Figure 1.4 Time-on-stream profiles of C_2 oxygenate yield from CO hydrogenation at 320 °C over RMLF-in-CNT and RMLF-out-CNT catalysts, accompanied with the transmission electron microscopy images of the respective fresh samples [17,66].

The effects of different carbon support materials; carbon black (CB), CMK-3 and activated carbon (AC); on the catalytic activity of C_2 oxygenate synthesis from syngas were also studied by the same authors [67]. Among the four catalysts with different carbon supports, RMLF/CNTs exhibited the highest activity. Even though Rh is very well dispersed on the AC with high surface area, this catalyst showed the lowest overall activity and C_2 oxygenate yield. These results suggest that the combination of the nanochannels and graphitic structure may be crucial in promoting this reaction in addition to the metal dispersion, particle size and presence of dopants [17,67]. These results could provide a direction for the direct synthesis of ethanol from CO_2 hydrogenation in addition to the CO hydrogenation.

1.5 CO_2 Hydrogenation to Dimethyl Ether

Dimethyl ether (DME) is a clean-burning substitute for diesel oil due to its high-efficiency for compression ignition with reduced NO_x, SO_x, and particulate matter [68,69]. Though, it is a volatile organic compound, but it is non-toxic, non-carcinogenic non-mutagenic, and non-teratogenic [68]. There are two routes for synthesizing DME from hydrogenation of CO_2, namely a two-step process and a single-step process [70,71]. For the two-step process (traditional route), CO_2 is firstly hydrogenated to methanol (Eq. (1.4)) on a metallic catalyst (Cu-based catalyst is commonly used) followed by the dehydration of methanol (Eq. (1.5); $\Delta H_{298\ K}$ of 23.4 kJ mol^{-1} [68]) on an acid catalyst [72].

$$2CH_3OH \leftrightarrow CH_3OCH_3 + H_2O \qquad (1.5)$$

The bifunctional catalyst is used in the single-step process to perform the two steps simultaneously. The favorable thermodynamics of the dehydration reaction can drive the methanol synthesis reaction, leading to an increase in the reactor productivity [17,70,71]. Therefore, selection of acidic support is greatly important.

The water formed during the reaction also needs to be considered, since it could decrease the activity of the acid supports [73]. Furthermore, the water formed from CO_2 hydrogenation (RWGS or methanol synthesis) is more than that from the CO hydrogenation. HZSM-5 zeolite has been chosen as a part of the bifunctional catalyst, since it is not sensitive to the water concentration [74-76]. However, the drawback of using HZSM-5 zeolite is that it also catalyzes DME conversion into hydrocarbons. Some of these hydrocarbons are considered as precursor for coke formation that could deactivate the zeolite by blocking its pores [77]. The addition of an appropriate amount of Na to the HZSM-5 zeolite could prevent the hydrocarbons formation from DME by decreasing number and strength of the Brønsted acid sites of the zeolite [78]. There is no irreversible deactivation observed for Cu–Zn–Al/NaHZSM-5 catalysts at the temperature below 300 ^{o}C [18,73]. A suitable amount of La in the CuO-ZnO-Al_2O_3-La_2O_3/HZSM-5 catalyst could enhance the dispersion of Cu on the surface by reducing the crystallite size of CuO, which resulted in an increase of CO_2 conversion [79]. However, according to the thermodynamic analysis, the DME synthesis from CO_2 hydrogenation is a less worthy alternative compared to that using syngas, due to the greater thermodynamic stability of CO_2 as compared to H_2O [17].

1.6 CO_2 Hydrogenation to Formic Acid

Formic acid synthesis is an alternative to convert CO_2 to liquid products that can be used as both fuels and chemicals. Formic acid is widely used in many fields such as the leather and rubber industries [80]. Since the early 1990s, attentions have been paid on the hydrogenation of CO_2 to formic acid and formates [81]. Recently, formic acid has also been considered as hydrogen storage material by combining CO_2 hydrogenation with selective decomposition of formic acid, resulting in a continuously study on an improvement of the catalyst activity and stability [18,81,82]. Synthesis of formic acid via CO_2 hydrogenation is shown in Eq. (1.6).

$$CO_2 + H_2 \leftrightarrow HCOOH \qquad (1.6)$$

To shift the reaction equilibrium, it is necessary to add an inorganic or organic base to the reaction system [80]. By adding an inorganic base, formate is formed which subsequently needs strong acid for converting formate to formic acid, while in the case of an organic base, recovery of formic acid is complicated and consume high energy because of the volatility of the base [18,80].

CO_2 hydrogenation to formic acid and formates typically use organometallic complexes such as the transition-metal catalysts based on rhodium, ruthenium, and iridium at low temperatures, rather than the heterogeneous systems [81,83]. By using $RhCl(PPh_3)_3$ catalyst (Wilkinson catalyst) for CO_2 hydrogenation, formic acid was formed in the presence of rhodium complexes with a phosphine ligand [84,85]. The catalyst activity is strongly dependent on the solvent nature, where high rates can be achieved using polar solvents such as DMSO and MeOH. The beginning and the end of CO_2 hydrogenation is corresponded to the presence of $RhCl(PPh_3)_2(NEt_3)$, which is a precursor of the catalytically active complex. An excess of PPh_3 could inhibit the reduction of the complex to metallic Rh, leading to a significant increases in the yield of formic acid [18].

Addition of a small amount of water can improve the catalytic CO_2 hydrogenation to formic acid effectively [86,87]. It was suggested that hydrogen-bonding interaction between a hydrogen atom of H_2O and an oxygen atom of CO_2 enhanced the electrophilicity of carbon and facilitated its insertion into the metal-hydride bond [87,88]. Water can also be used as the solvent for synthesizing formic acid, especially for the formation of formate, since it is an inexpensive, abundant, and innocuous solvent, and also provide many advantages such as high absorption for some gases, amphoteric behavior in Brønsted sites, and easily to be separated from a polar compounds [89]. However, catalysis in water system requires the catalysts with water-soluble ligands such as Ir and Ru complexes [18].

Although homogeneous catalysts have been proved to be efficient catalysts for the synthesis of formic acid from CO_2 hydrogenation, but they still have some drawbacks in terms of product separation and recycle of the catalyst. These

problems are possibly solved by immobilizing a complex onto a support material to improve the reusability and stability of the catalyst. Ruthenium complexes immobilized on amine-functionalized-silica prepared by an in situ synthetic approach exhibited high activity and 100% selectivity for the formic synthesis from CO_2 hydrogenation, and this catalyst was also easily to be separated and recycled [18,90].

1.7 CO_2 Hydrogenation to Hydrocarbons

1.7.1 Methanation of Carbon Dioxide

The methanation of CO_2 has a wide range of applications including the production of syngas and the formation of compressed natural gas. Catalytic hydrogenation of CO_2 to methane or Sabatier reaction (Eq. (1.7); $\Delta H_{298\ K}$ of -252.9 kJ mol^{-1}) is an important catalytic process [18].

$$CO_2 + 4H_2 \rightarrow CH_4 + 2H_2O \qquad (1.7)$$

Although, CO_2 methanation is a thermodynamically favorable reaction ($\Delta G_{298\ K}$=-130.8 kJ mol^{-1}); the reduction of the stable CO_2 molecule to CH_4 is an eight-electron process with significant kinetic limitations, which requires a catalyst that can offer acceptable activity and selectivity [18,91]. The metal-based heterogeneous catalysts have been studied extensively for the CO_2 hydrogenation to methane, especially Ni and VIIIB metals (such as Ru and Rh) supported on various oxides. The nature of support plays an important role in the interaction between nickel and support, which determines the catalytic activity and selectivity of CO_2 methanation [92]. Ni catalysts supported on amorphous silica are active for CO_2 methanation, and more active than Ni on silica gel support [93,94]. Since the dispersion of the active phase depends on the support, many researches have focused on preparation of highly dispersed metal supported catalysts. Ni/MCM-41 catalysts with different amount of Ni was studied for CO_2 methanation, and the activity and selectivity of Ni/MCM-41 with 3 wt% Ni loading were higher than those of Ni/SiO_2 catalysts and comparable to that of Ru/SiO_2 catalysts [18,95,96].

However, Ni-based catalysts would deactivate at low temperature due to the interaction of the metal particles with CO and the mobile nickel subcarbonyls formation [97]. In contrast, VIIIB metals such as Ru, Pd, and Pt are stable at operating conditions and could provide higher activity for CO_2 methanation than Ni [98]. The reaction rate of Ru/Al_2O_3 (15 wt% Ru loading) at steady-state was about 10 times higher than that of the Ni-based catalysts. The turnover frequency (TOF) of Ru-based catalysts were dependent on the Ru dispersion and the type of supports (metal-support interaction). The TOF of Ru/Al_2O_3 was 16.5×10^3 s^{-1}, which is higher than those of $Ru/MgAl_2O_4$ (8.8×10^3 s^{-1}), Ru/MgO (7.9×10^3 s^{-1}) and Ru/C (2.5×10^3 s^{-1}) [99]. The low activity of Ru/C catalyst could be explained by decrease in active sites due to the partial covering of metal surface by carbon [99]. Highly dispersed Ru nanoparticles were also synthesized on TiO_2 prepared by a barrels-sputtering method, which could provide higher yield (100% yield) at 433 K compared to that of the catalyst prepared by conventional wet impregnation method [100]. Moreover, the addition of yttrium (Y) to Ru-based catalysts could increase the active surface area, Ru dispersion and also catalytic activity [18,101].

Although the CO_2 methanation is a simple reaction, but its reaction mechanism is somewhat difficult to establish and still controversial. Two mechanisms for CO_2 methanation have been proposed with different intermediates. For the first mechanism, CO_2 is first converted to CO via RWGS reaction, and the formed CO is then hydrogenated to CH_4 following the same mechanism as CO methanation [102-104]. Another mechanism is the direct hydrogenation of CO_2 to CH_4 via the formation of the formate through a carbonate species, without forming CO as an intermediate [103,105,106].

1.7.2 Synthesis of C_2^+ Hydrocarbons

CO_2 hydrogenation to hydrocarbons is basically a modification of the FTS, where CO_2 is used as a carbon source instead of CO, and in which the catalyst composition is tailored to maximize the production of hydrocarbons [18]. Hydrocarbons can be synthesized from hydrogenation of CO_2 either by direct or indirect routes (via CO and/or CH_3OH intermediate formation) [17]. For the indirect route, a multistage approach using separated reactors or a single-stage approach using hybrid catalysts which are able to perform simultaneously the multi-step transformation, can be applied [17,18]. Many researchers reported that the hydrogenation typically takes place via the formation of CO intermediate, while the direct hydrogenation of CO_2 to hydrocarbons (Eq. (1.8)) rarely occurs. The possible pathway was proposed; CO_2 is first converted to CO via RWGS reaction (Eq. (1.1)), and the formed CO is subsequently hydrogenated to form the monomers (CH_x species) (Eq. (1.9)), which finally form the different hydrocarbons via a FT mechanism [107].

$$CO_2 + 3H_2 \rightarrow -(CH_2)- + 2H_2O \quad (1.8)$$

$$CO + 2H_2 \rightarrow -(CH_2)- + H_2O \quad (1.9)$$

Until now, the catalysts used for CO_2 hydrogenation to hydrocarbons are based-on those for FTS such as Fe, Co, Ni and Ru catalysts [108]. However, when supported Co, Ni and Ru catalysts are used for CO_2 hydrogenation, CH_4 becomes a major product with only small amounts of higher hydrocarbons are observed [109-111]. During CO_2 hydrogenation, C/H ratio on the catalyst surface is low due to the slow CO_2 adsorption rate, which favors the hydrogenation of surface-adsorbed intermediates to form CH_4 [112]. Riedel et al. [113] and Gnanamani et al. [114] studied the activities and selectivities for the hydrogenation of CO, CO_2 and their mixtures over Co and Fe catalysts. In the case of Co-based catalyst, by increasing partial pressure of CO_2 (CO partial pressure decreased), the product composition was shifted from an FT synthesis type to almost only CH_4, while the product composition was only slightly changed when Fe catalyst was used. Different behaviors of Fe and

Co catalysts are explained in terms of different types of the kinetic regime of FTS, where strong CO adsorption is crucial for Co catalysts, while carbide formation is important for Fe catalysts [113,115].

As a consequence of the prior studies including those mentioned above, attentions have been paid on improving the catalytic performances of Fe-based catalysts to increase the yield of higher hydrocarbon products, by adding some promoters such as Li, K and Mn or selecting the proper support materials [19-22,116-118]. The addition of K to Fe-based catalysts increased CO_2 conversion and higher hydrocarbon selectivity, while decreased CH_4 selectivity. Olefin content in the products were also increased with K content, since K could suppress further hydrogenation of the produced olefins [20]. Many researchers reported that the addition of K to Fe catalysts increased CO_2 adsorption, while it suppressed H_2 adsorption [19,35,119-122]. K also facilitated the formation of iron carbide, which is believed as the active sites for the formation of higher hydrocarbon in FTS and CO_2 hydrogenation [119,120,123]. Mn could perform as both structural promoter and electronic modifier for Fe-based catalysts. It enhanced the reduction and carburization of iron oxides and increased the dispersion of Fe_2O_3 [118,124]. The addition of Mn also increased surface basicity of the catalysts, resulting in a decrease in CH_4 formation and increase in an olefin/paraffin ratio in FTS and CO_2 hydrogenation [20,118,124]. Cu could also promote CO_2 hydrogenation as well, by facilitating the catalyst reduction and providing the active sites for H_2 dissociation [118,125].

The product distributions from CO_2 hydrogenation are also dependent on type of support materials, where it affects the dispersion of the active metals and prevents the sintering of the metals during the reaction [126]. Al_2O_3 is known as a good support, since it could prevent sintering due to the strong metal-support interaction, followed by SiO_2 and TiO_2 [113,119,126]. Different type of zeolites with characteristic pore structures and acidity strongly affected the catalytic performances of the catalysts and the distribution of hydrocarbon products [127,128].

Though K promoted Fe/Al_2O_3 catalysts ($K \geq 0.5$ mol-K mol^{-1} of Fe) are viewed as most promising catalysts for higher hydrocarbons synthesis from CO_2 hydrogenation so far, these catalysts still have low performances for converting CO_2 [16-19]. How to achieve substantial activity improvement in synthesis of higher hydrocarbons remains a major challenge.

1.8 Objectives and Scope of Dissertation

The principle objective of this research is to develop efficient catalysts for CO_2 hydrogenation to higher (C_2^+) hydrocarbons. One approach is to tailor the adsorption properties of CO_2 and H_2 on the catalyst surfaces using various catalyst formulations, for facilitating the carbon-carbon bond formation. The effects of catalyst formulations on the physical and chemical properties of the catalysts were also investigated.

Chapter I of this thesis provides a review of the global challenges and strategies for control, conversion and utilization of CO_2 with focusing on the catalytic hydrogenation of CO_2.

The experimental procedures for the catalyst preparation as well as the CO_2 hydrogenation and the various techniques used for the catalyst characterization are given in Chapter II.

The catalytic activities and selectivities of the monometallic (Fe, Co, Ni, Cu, Pd) catalysts for CO_2 hydrogenation are reported in Chapter III. The effect of combining Fe with the second metal (M; Co, Ni, Pd, Cu) at the same M/(M + Fe) atomic ratio, on the catalytic properties are also studied, accompanied with an investigating the effect of Ni/(Ni + Fe) atomic ratio on the bimetallic promotion of higher hydrocarbons.

In Chapter IV, the Fe-Co bimetallic catalysts were studied in more details to understand the bimetallic promotion in CO_2 hydrogenation to higher hydrocarbons. The Fe-Co bimetallic catalysts were prepared at various Co/(Co + Fe) atomic ratio from 0 -1 and tested for CO_2 hydrogenation. The effect of K promoter is also investigated.

To investigate the physical and chemical properties of Fe-Co bimetallic catalysts, these bimetallic catalysts were characterized by X-ray diffraction (XRD), temperature-programmed reduction (TPR), diffuse reflectance Infrared Fourier transform spectroscopy (DRIFTS) and temperature-programmed desorption (TPD), and their results are reported in Chapter V. To clarify the influence of Fe and Co combination on the adsorption properties of H_2 and CO_2, and their impact on the CO_2 hydrogenation activities, the in-situ and quasi in-situ techniques were used to characterize the catalysts after H_2 reduction and CO_2 hydrogenation at high-pressure conditions, respectively.

In Chapter VI, the pathway for light olefin (C_2-C_4) formation from CO_2 hydrogenation over K-promoted Fe-Co bimetallic catalyst was investigated. The influence of K-promoter on adsorption properties of H_2 and CO_2 and their impact on the CO_2 hydrogenation activities of the Fe-Co bimetallic catalysts with different K/Fe atomic ratios were also studied by N_2 adsorption-desorption, TPR, TPD and DRIFTS.

Finally, the conclusions from this research and recommendations for future work are provided in Chapter VII. The results of this research will contribute the understanding and useful guidance to the development of Fe-based bimetallic catalysts for CO_2 hydrogenation to higher hydrocarbons.

CHAPTER II

EXPERIMENTAL AND CHARACTERIZATION

2.1 Materials

Gamma-alumina (γ-Al_2O_3; PURALOX TH 100/150, BET surface area = 150 m^2 g^{-1}, average pore diameter = 22 nm) was purchased from Sasol North America Inc. and was calcined at 823 K for 2 h before being used. $Fe(NO_3)_3{\cdot}9H_2O$ (99.99%), $Co(NO_3)_2{\cdot}6H_2O$ (≥ 98%), $Ni(NO_3)_2.6H_2O$ (99.999%), K_2CO_3 (99.995%) were purchased from Sigma-Aldrich Chemical Company. $Cu(NO_3)_2{\cdot}2.5H_2O$ (98-102%) and $(NH_3)_4Pd(NO_3)_2$ (99.9%) were purchased from Alfa-Aesar Chemical Company. All of the precursors were used without further purification. Mixed gas of 24 vol% CO_2/ 72 vol% H_2/ 4 vol% Ar (purity > 99.999%), H_2 gas (99.999%) and He (99.999%) were supplied by Praxair Inc.

2.2 Catalyst Preparation

2.2.1 Unpromoted Catalyst

Gamma-alumina was used as support material. The total metal loading was kept constant at 15 wt% (support weight basis) except Pd catalyst (5 wt% metal loading). Supported monometallic catalysts (Fe, Co, Ni, Cu and Pd) were prepared by incipient wetness impregnation method using aqueous solutions containing $Fe(NO_3)_3{\cdot}9H_2O$, $Co(NO_3)_2{\cdot}6H_2O$, $Ni(NO_3)_2.6H_2O$, $Cu(NO_3)_2{\cdot}2.5H_2O$ and $(NH_3)_4Pd(NO_3)_2$ as a precursor, respectively. The impregnated sample was dried at 333 K in a rotary evaporator for 2 h, and then dried in an electrical oven at 383 K for 3 h in ambient air followed by calcination at 623 K for 2 h under flowing dry air (ca. 100 mL (NTP) min^{-1}) (Figure 2.1).

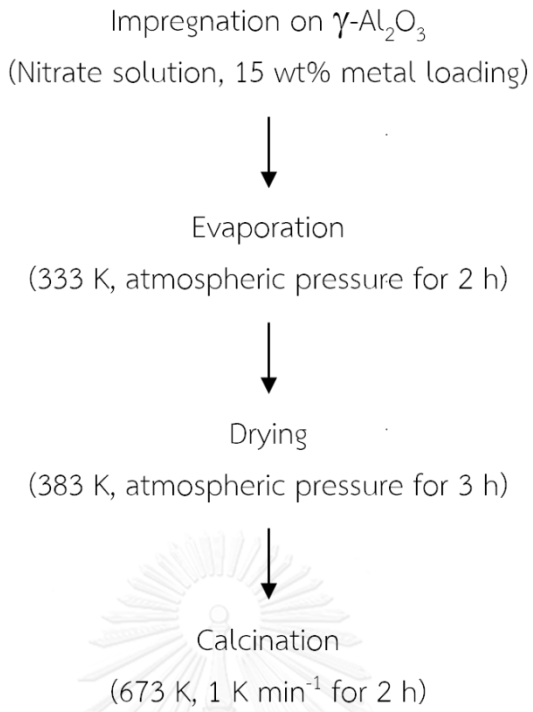

Figure 2.1 Procedure for preparation of supported Fe-based catalysts.

The supported bimetallic catalysts Fe-Co/Al_2O_3, Fe-Ni/Al_2O_3, Fe-Cu/Al_2O_3 and Fe-Pd/Al_2O_3 were prepared by co-incipient wetness impregnation method using the aqueous solution containing both bimetallic precursor $Fe(NO_3)_3{\cdot}9H_2O$ and $Co(NO_3)_2{\cdot}6H_2O$, $Fe(NO_3)_3{\cdot}9H_2O$ and $Ni(NO_3)_2.6H_2O$, $Fe(NO_3)_3{\cdot}9H_2O$ and $Cu(NO_3)_2{\cdot}2.5H_2O$, $Fe(NO_3)_3{\cdot}9H_2O$ and $(NH_3)_4Pd(NO_3)_2$, respectively and prepared in accordance with the procedures used for supported monometallic catalysts. The total metal (Fe + Co, Fe + Ni, Fe + Cu and Fe + Pd) loading was also kept constant at 15 wt% (support weight basis). The Co/(Co + Fe) atomic ratio and Ni/(Ni + Fe) were varied in the range of 0.0-1.0, while Cu/(Cu + Fe) and Pd/(Pd + Fe) were fixed at 0.10 atomic ratio.

2.2.2 K-promoted Catalyst

K promoted catalysts were prepared by a two-step impregnation method; an aqueous solution of K_2CO_3 was impregnated onto the alumina support in the first step and the sample was dried in a rotary evaporator at 333 K for 2 h

followed by drying in an electric oven at 383 K overnight. This sample was then impregnated with the mixed metal nitrate solution (Fe-Co, Fe-Ni, Fe-Cu and Fe-Pd) followed by drying and calcination under the same conditions mentioned in section 2.2.1 (Figure 2.2). The catalysts prepared in this work are denoted as Fe-M(X)/K(Y)/Al_2O_3; M = Ni, Cu, Pd, Co, where X and Y represent the M/(M + Fe) and K/Fe atomic ratios, respectively. Loadings of metal and K of prepared catalysts are listed in Table 2.1.

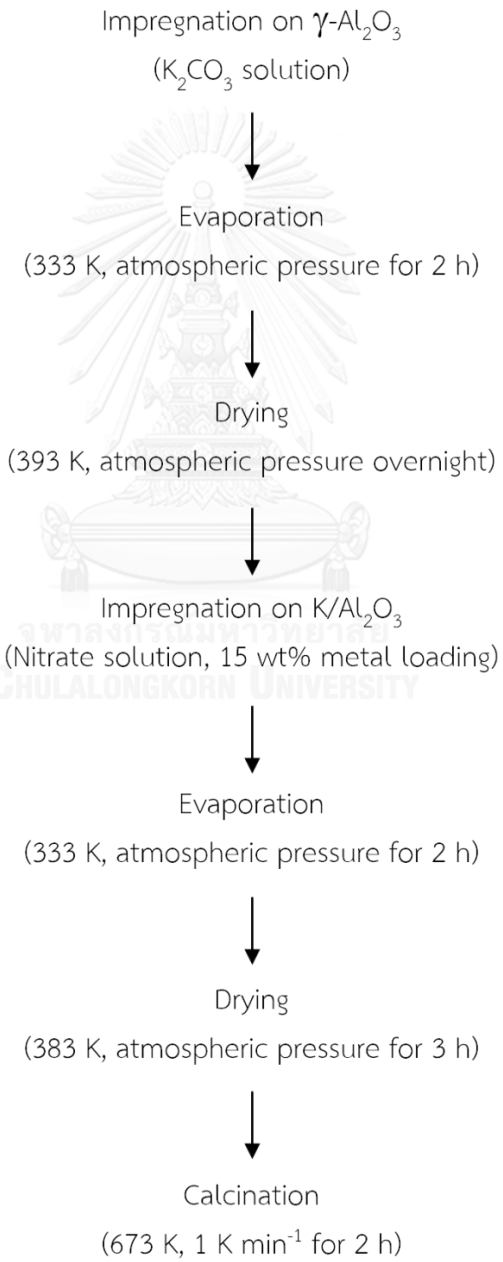

Figure 2.2 Procedure for preparation of K-promoted Fe-based catalysts.

Table 2.1 Fe, Co, Ni, Cu, Pd and K loadings of unpromoted and K-promoted Fe-M/Al_2O_3 catalysts (M = Ni, Cu, Pd, Co).

Catalyst	Loading / wt% (support weight basis)					
	Fe	Co	Ni	Cu	Pd	K
Fe	15.0	-	-	-	-	-
Co	-	15.0	-	-	-	-
Ni	-	-	15.0	-	-	-
Cu	-	-	-	15.0	-	-
Pd	-	-	-	-	5.0	-
Fe-Co(0.10)	13.4	1.6	-	-	-	-
Fe-Co(0.17)	12.4	2.6	-	-	-	-
Fe-Co(0.25)	11.1	3.9	-	-	-	-
Fe-Co(0.50)	7.3	7.7	-	-	-	-
Fe-Ni(0.03)	14.5	-	0.5	-	-	-
Fe-Ni(0.10)	13.4	-	1.6	-	-	-
Fe-Cu(0.10)	13.3	-	-	1.7	-	-
Fe-Pd(0.10)	12.4	-	-	-	2.6	-
Fe/K(0.3)	15.0	-	-	-	-	3.2
Co/K(0.3)	-	15.0	-	-	-	3.0
Fe-Co(0.10)/K(0.3)	13.4	1.6	-	-	-	2.8
Fe-Co(0.17)/K(0.3)	12.4	2.6	-	-	-	2.6
Fe-Co(0.17)/K(0.5)	12.4	2.6	-	-	-	4.3
Fe-Co(0.17)/K(1.0)	12.4	2.6	-	-	-	8.7
Fe-Co(0.25)/K(0.3)	11.1	3.9	-	-	-	2.3
Fe-Co(0.50)/K(0.3)	7.3	7.7	-	-	-	1.5
Fe-Ni(0.03)/K(0.3)	14.5	-	0.5	-	-	3.0
Fe-Ni(0.10)/K(0.3)	13.4	-	1.6	-	-	2.8
Fe-Cu(0.10)/K(0.3)	13.3	-	-	1.7	-	2.8
Fe-Pd(0.10)/K(0.3)	12.4	-	-	-	2.6	2.6

2.3 Catalyst Evaluation

The performance of catalysts on CO_2 hydrogenation to hydrocarbons was carried out in a high-pressure fixed-bed flow reactor system (Figure 2.3). Typically, about 0.2 g of catalyst was mixed with amorphous SiO_2 (75-250 μm particle size) in order to dilute the heat generated from the exothermal reaction and maintain an aspect ratio. The diluted catalyst was charged into a stainless steel reactor (internal diameter = 6 mm) between two glass wool layers. The upper part of the catalyst bed was packed with SiO_2 glass ball (2 mm diameter) as a pre-heating zone. The catalyst was reduced under a 50 mL (STP) min^{-1} H_2 flow (purity > 99.999%) at 673 K for 2 h, and then cooled down to 573 K before CO_2 hydrogenation reaction. The feed gas, 24 vol% CO_2/ 72 vol% H_2/ 4 vol% Ar (purity > 99.999%), was then fed into the system. The reaction conditions are 573 K and 1.1 MPa with GHSV of 3600 mL (STP) g^{-1} h^{-1}, unless otherwise stated.

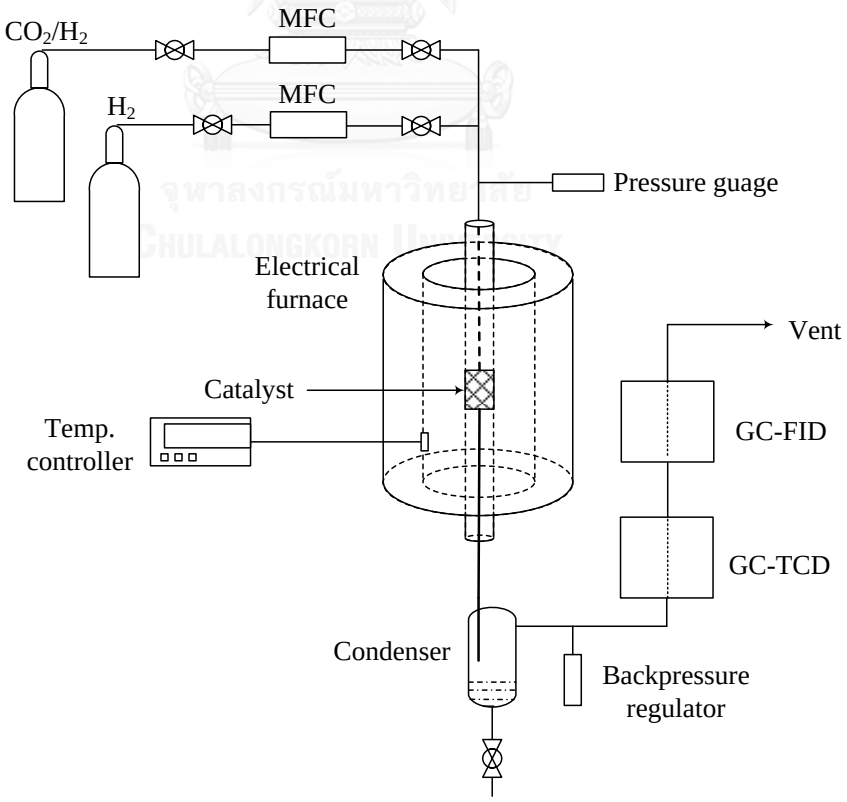

Figure 2.3 High-pressure fixed-bed flow system for CO_2 hydrogenation.

2.4 CO_2 Hydrogenation Product Analysis

2.4.1 Gas Product

The gas products including Ar, CO, CH_4 and CO_2 were analyzed online using an Agilent 3000 micro Gas Chromatography (GC) with molecular sieve type column for Ar, CO, CH_4 and Plot-Q column for CO_2. The gas-phase hydrocarbon products were analyzed online using SRI 8610C GC equipped with Flame Ionization Detector (GC-FID) (Porapak Q column). The condition and temperature program used for micro GC and GC-FID are described in detail in Appendix A.

2.4.2 Liquid Hydrocarbon Products

The liquid hydrocarbons were collected in an ice trapped condenser connected to the reactor and analyzed after the reaction with Gas Chromatography-Mass Spectrometry (GC/MS) (Shimadzu, QP-5000) with a capillary column Rxi®-5HT (Crossbond® 5% diphenyl/ 95% dimethyl polysiloxane, 30 m x 0.25 mm i.d. x 0.25 μm film thickness) and a split mode injector (ratio 20:1) was used with ultra-high purity helium as a carrier gas. The condition and temperature program for GC/MS are described in Appendix B.

2.5 Catalyst Passivation

After CO_2 hydrogenation at 573 K and 1.1 MPa for 15-16 h, the catalyst was cooled down to 298 K under flowing 24 vol% CO_2/ 72 vol% H_2/ 4 vol% Ar and subsequently passivated using 0.95 vol % O_2/He (purity > 99.999%) at a flow rate of 30 mL min^{-1}. An area of O_2 peak (effluent of O_2) observed by Micro GC equipped with TCD was used as a mark for the catalyst passivation. The passivation finished after the O_2 peak area became constant and the catalyst then collected from the reactor for characterizations, hereafter simply denoted as *spent catalyst*.

2.6 Adsorption/Desorption of N_2

The physical properties of catalyst were measured using a fully automated TriStar II (Micromeritics) surface area and porosity analyzer. The catalyst surface area (SA), pore volume (PV) and average pore diameter (D_p) were determined from the nitrogen (N_2) adsorption/desorption isotherms measured at 77 K. Before analysis, all the samples (ca. 0.20–0.25 g) were degassed under a N_2 flow at 363 K for 1 h and 473 K for 12 h. The isotherms were elaborated according to the Brunauer-Emmett-Teller (BET) method for surface area calculation, while Barrett-Joyner-Halenda (BJH) model was used to obtain pore volume and average pore diameter of the catalysts.

2.7 Temperature-Programmed Reduction

2.7.1 Calcined Catalyst

Temperature-programmed reduction (TPR) experiments were carried out at ambient pressure in a Micromeritics AutoChem 2910 Automated Catalyst Characterization System using hydrogen (H_2-TPR) as reducing agent. About 100 mg of catalyst was introduced in a U-shaped quartz tube reactor (held by quartz wool). To remove adsorbed species on the catalyst surface, the catalyst was heated *in situ* to 393 K (10 K min^{-1}) under Ar (purity > 99.999%) flow (25 mL min^{-1}) for 1 h prior to reduction process. The catalyst was then cooled down to 323 K and the flowing gas was subsequently switched to 5.04 vol% H_2/Ar at 20 mL min^{-1} and sustained throughout the analysis. After a baseline was established, the temperature program started by a ramp of 10 K min^{-1} up to 1173 K and held at 1173 K for 30 min. The effluent gas was cooled down by a viscous solution of isopropanol mixed with liquid N_2 located between a reactor and detector to trap the water formed during the reduction process. The gas was then analyzed using a thermal conductivity detector (TCD).

2.7.2 Pre-reduced Catalyst

About 100 mg of catalyst was charged to the U-shaped quartz tube reactor and pre-reduced *in situ* at 673 K at the ramp rate of 5 K min^{-1} under a 50 mL min^{-1} H_2 flow (purity > 99.999%) for 2 h prior to the TPR experiment. After pre-reduction process, in order to remove H_2 gas that might be remained in the reactor, the catalyst was cooled down to 423 K under flowing 20 mL min^{-1} Ar (purity > 99.999%) for 30 min. The gas was then switched to 5.04 vol% H_2/Ar at 20 mL min^{-1} and followed the same procedures used for calcined catalyst in section 2.7.1.

2.8 Temperature-Programmed Desorption

Temperature-programmed desorption (TPD) experiments were conducted using the same instrument as TPR experiments.

2.8.1 H_2-TPD

In a typical experiment, about 150 mg of catalyst was placed in a U-shaped quartz tube reactor and pre-reduced *in situ* before the H_2-TPD experiment, at 673 K (5 K min^{-1}) for fresh catalyst or 573 K (5 K min^{-1}) for spent catalyst under a 50 mL min^{-1} H_2 flow (purity > 99.999%) for 2 h. The catalyst was then cooled down to 200 K under flowing H_2 using an isopropanol-liquid N_2 mixture in order to prevent desorption of weakly adsorbed hydrogen from the catalyst surface. To remove H_2 gas that might be remained in the reactor, the catalyst was purged by 30 mL min^{-1} 0.95 vol% Ar/He (purity > 99.999%) flow until H_2 pressure (observed from Mass Spectrometer) became constant. The TPD experiment was started by heating at a ramp of 10 K min^{-1} to 1173 K under 30 mL min^{-1} 0.95 vol% Ar/He (purity > 99.999%) flow, Ar was used as an internal standard. The temperature program was started at around 280 K. The effluent gas was analyzed using a Dycor Dymaxion Mass Spectrometer DM200M (AMETEK).

2.8.2 CO_2-TPD

About 150 mg of catalyst was placed in a U-shaped quartz tube reactor and pre-reduced *in situ* before the CO_2-TPD experiment at 673 K (5 K min^{-1}) for fresh catalyst or 573 K (5 K min^{-1}) for spent catalyst, under a 50 mL min^{-1} H_2 flow (purity > 99.999%) for 2 h. The catalyst was then purged with 0.95 vol% Ar/He (purity > 99.999%) at a flow rate of 30 mL min^{-1}, at 573 K for 30 min to remove H_2 gas that might be remained in the reactor. The catalyst was subsequently dosed with 15 vol% CO_2/He (at 573 K) at a flow rate of 30 mL min^{-1} for 1 h, followed by cooling down to room temperature. The catalyst was then purged with 30 mL min^{-1} 0.95 vol% Ar/He (purity > 99.999%) to remove any trace of CO_2 until CO_2 pressure (observed from Mass Spectrometer) became constant. The TPD experiment was performed by following the same procedures used for H_2-TPD in section 2.8.1.

2.9 In situ Diffuse Reflectance Infrared Fourier Transform Spectroscopy (DRIFTS)

The surface species formed during CO_2 hydrogenation on the spent catalysts were characterized by Fourier transform infrared (FTIR), using a Thermo Nicolet NEXUS 470 FTIR spectrometer equipped with a diffuse reflectance cell (Spectra Tech), an mercury cadmium telluride (MCT-A) detector cooled by liquid N_2 and a KBr beamsplitters. The infrared cell with a ZnSe window was employed at high temperatures. The cell was directly connected to a gas flow system, equipped with rotameter and a set of valves to choose gas type and control gas flow rate. The temperature of the catalyst was monitored by a K-type thermocouple placed 2 mm underneath the crucible surface.

Before the experiment, about 50 mg of the spent catalyst was gently mixed and grinded with 50 mg of NaCl powder until homogeneous since the color of all the spent catalysts was black. The mixed powder of spent catalyst and NaCl was then charged into the sample holder and was purged in N_2 (purity > 99.999%) at 298 K for

1 h to remove any moisture and gases, before recording the DRIFT spectrum. Successively, the catalyst was pre-reduced *in situ* at 573 K (10 K min^{-1}) under H_2 flow (purity > 99.999%) for 2 h, and then cooled down to 310 K under a H_2 flow. The DRIFT spectrum was then recorded after flushing the catalyst with N_2 for 30 min. These spectra were transformed to Kubelka-Munk functions using a NaCl background spectrum measured under a N_2 flow at ambient temperature.

The adsorption states of CO_2 on the reduced catalysts were also studied by DRIFTS coupled with CO_2 adsorption. The calcined catalyst was charged into the sample holder and then pre-reduced in situ at 573 K (heating at 10 K min^{-1}) under a H_2 flow for 1 h, followed by flushing with N_2 at this temperature for 30 min. Background was collected at this temperature after the system was equilibrated for 30 min. The in situ DRIFT spectra of the adsorbed CO_2 were recorded at 573 K under a 10 vol% CO_2/Ar flow through the cell after reaction times of 10 and 20 min, and then a final spectrum was collected after flushing with N_2. The total flow of all gases through the Infrared cell was kept constant at 50 mL min^{-1}.

2.10 X-ray Diffraction

XRD patterns of calcined and spent catalysts were obtained using a PANalytical Empryean X-Ray Diffractometer with Cu Kα (λ = 0.154059 nm) radiation, fixed slit incidence (0.25° divergence, 0.5° anti-scatter, specimen length 10 mm) and diffracted (0.25° anti-scatter, 0.02 mm nickel filter) optics. Samples were prepared by the back-loading method in which a powder sample was pressed into the cavity of a quartz low-background support. Data was obtained at 45 kV and 40 mA from 30-90 (2θ) using a PIXcel detector in scanning mode with a PSD length of 3.35° (2θ), and 255 active channels for a duration time of 20-40 min. Resulting patterns were adjusted for 2θ position using NIST 640c silicon and analyzed with Jade+9 software by MDI of Livermore, CA.

CHAPTER III

COMPARATIVE STUDY OF Fe-BASED BIMETALLIC CATALYSTS FOR CO_2 HYDROGENATION TO HIGHER HYDROCARBONS

3.1 Introduction

Until now, traditional Fischer-Tropsch synthesis (FTS) catalysts such as Fe, Co, Ni and Ru catalysts have been applied for CO_2 hydrogenation to hydrocarbons. However, CH_4 was the main product from CO_2 hydrogenation over supported Ni and Ru catalysts [109-111,129,130]. Riedel et al. [113] and Gnanamani et al. [114] made a comparative study of the hydrogenation of CO, CO_2 and their mixtures on Co and Fe catalysts, and reported that the product composition from hydrogenation using Co-based catalyst shifted from an FTS type to CH_4 with increasing partial pressure of CO_2, while it was almost not changed in the case of Fe catalyst. Therefore, attentions have been paid on improving the catalytic performance of Fe catalyst by adding promoters such as K and Mn or using various types of support materials [19,20,22]. Recently, Fe/Al_2O_3 catalysts with these promoters have been viewed as one of the promising catalysts for higher hydrocarbons synthesis from CO_2 hydrogenation [19,20,116]. However, these catalysts still have low activities for CO_2 hydrogenation to higher hydrocarbons.

In this chapter, a comparative study on the CO_2 hydrogenation to higher hydrocarbon over several Fe-based bimetallic catalysts was conducted. Al_2O_3 supported Fe-M (M = second metal) bimetallic catalysts were prepared and tested for CO_2 hydrogenation. Co, Ni, Cu and Pd as second metal with different abilities for activating H_2 were selected. The activities and selectivities of these monometallic catalysts were investigated. The effect of K addition to the bimetallic catalysts was also studied.

3.2 Equilibrium Conversion of CO_2 Hydrogenation

Before starting CO_2 hydrogenation experiments, the equilibrium CO_2 conversion and composition at various reaction temperature were calculated using Aspen HYSYS 3.2 (molar ratio of H_2/CO_2=3 and 1.0 MPa total pressure) as shown in Figure 3.1. Equations (3.1) - (3.6) were used for calculating the equilibrium CO_2 conversion as curves (a), (b) and (C). CH_4 as the most stable product and C_3H_8 as relatively stable species of the organic components were selected for being the representatives of the hydrocarbon products.

Curve (a): CO_2 hydrogenation to CO (RWGS)

$$CO_2 + H_2 \leftrightarrow CO + H_2O \quad (3.1)$$

Curve (b): CO_2 hydrogenation to CO and hydrocarbons

$$CO_2 + H_2 \leftrightarrow CO + H_2O \quad (3.2)$$

$$CO + 3H_2 \leftrightarrow CH_4 + H_2O \quad (3.3)$$

$$3CO + 7H_2 \leftrightarrow C_3H_8 + 3H_2O \quad (3.4)$$

Curve (c): CO_2 hydrogenation to hydrocarbons

$$CO_2 + 4H_2 \leftrightarrow CH_4 + 2H_2O \quad (3.5)$$

$$3CO_2 + 10H_2 \leftrightarrow C_3H_8 + 6H_2O \quad (3.6)$$

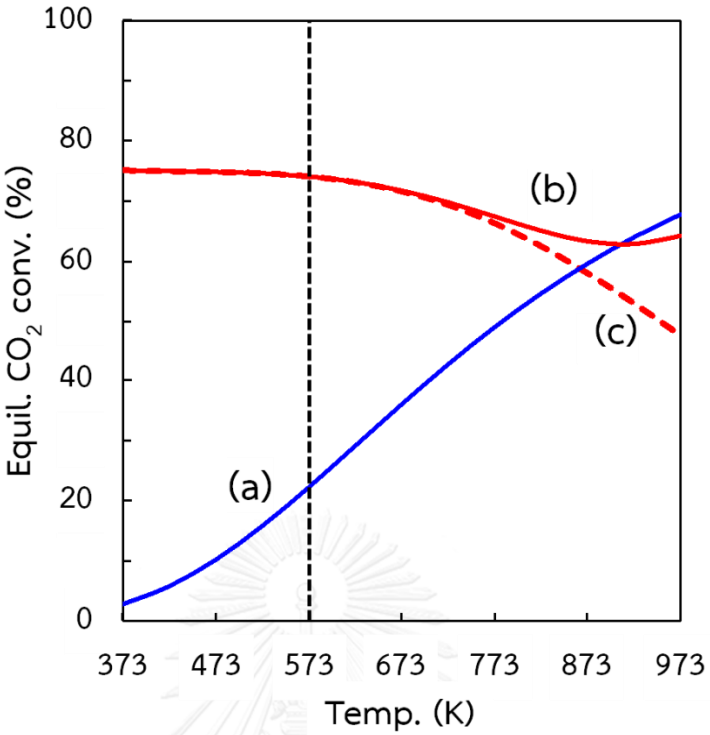

Figure 3.1 Equilibrium CO_2 conversions for a molar ratio of H_2/CO_2=3 as a function of reaction temperature (1.0 MPa total pressure).

3.3 Monometallic Catalysts

To investigate the unique catalytic properties of each monometallic catalyst (Fe, Co, Ni, Cu and Pd), the Al_2O_3 supported monometallic catalysts were prepared and tested for CO_2 hydrogenation at 573 K and 1.1 MPa. The fairly constant CO_2 conversions were obtained after 4-5 h on stream for all catalysts. Time-on-stream (TOS) stabilities of CO_2 conversions on Ni and Cu catalysts are shown in Figure 3.2 as examples. The conversions and product yields at about 15-16 h on stream were chosen for evaluating the catalytic activity and selectivity.

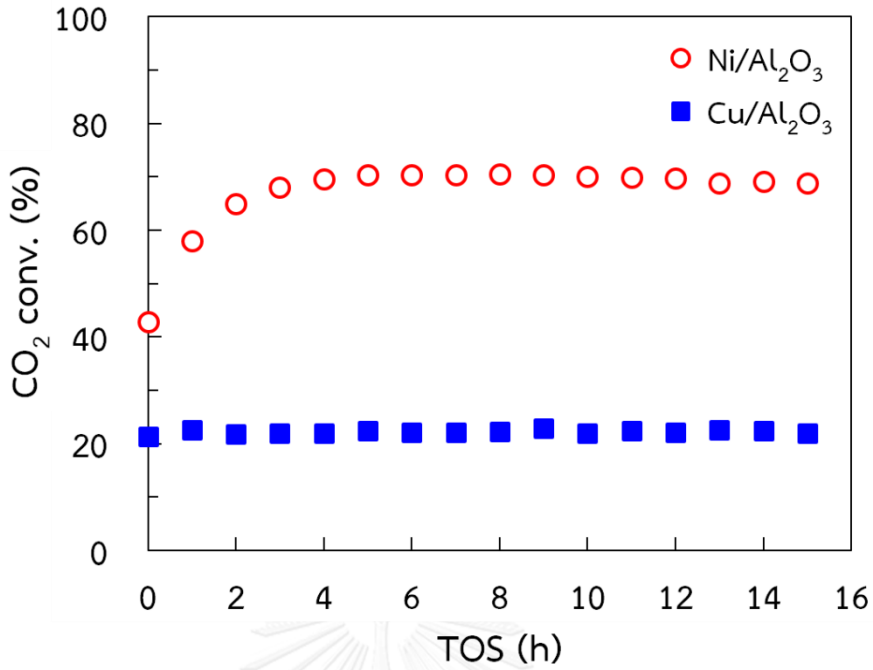

Figure 3.2 Time-on-stream stabilities of CO_2 conversions over Ni/Al_2O_3 and Cu/Al_2O_3 catalysts.

CO_2 hydrogenation activities and selectivities of monometallic catalysts are presented in Table 3.1. The results show that among the monometallic catalysts studied here, only Fe/Al_2O_3 catalyst could yield C_2^+ hydrocarbons (38% selectivity) from CO_2 hydrogenation, but with lower CO_2 conversion (12.1%) compared to other catalysts. Riedel et al. [113] suggested that C_2^+ hydrocarbons could be formed on Fe catalyst via the irreversible carbide (active phase) formation on the catalyst surface. This carbide species was a prerequisite for carbon-carbon bond formation. On the contrary, Co/Al_2O_3 and Ni/Al_2O_3 catalysts provided higher CO_2 conversion at 49% and 70%, respectively, but yielded almost only CH_4 as the hydrocarbon products. This suggests that Co and Ni catalysts have strong ability to dissociate H_2, resulting in a high coverage of hydrogen on the catalyst surface, which promoted CH_4 formation. It is also worth noting that CO_2 conversion on Ni/Al_2O_3 catalyst approached the equilibrium value for CO_2 methanation at this reaction condition (ca. 74%), which makes this catalyst suitable for synthesizing the SNG from CO_2 hydrogenation.

Table 3.1 CO_2 hydrogenation activities and selectivities of the monometallic catalysts.

Catalyst	CO_2 conv. (%)	HC selectivity (%, carbon based)		STY (μmol $g^{-1}s^{-1}$)		
		CH_4	C_2-$C_{5(7)}$	CH_4	C_2-$C_{5(7)}$	CO
Fe/Al_2O_3	12.1	62	38	0.54	0.13	0.65
Co/Al_2O_3	48.8	99	1	3.61	0.01	0.07
Ni/Al_2O_3	70.1	100	0	6.57	0	0.01
Cu/Al_2O_3	22.6	0	0	0	0	2.33
Pd/Al_2O_3 *	12.5	100	0	0.22	0	1.18

Total metal loading = 15 wt% (support weight basis) (* Pd = 5 wt%)

Pretreatment: H_2 red. at 673 K, 2 h

Operating cond: 573 K, 1.1 MPa, 3600 mL (STP) g^{-1} h^{-1}

In the case of Cu/Al_2O_3 catalyst, CO was the main product from CO_2 hydrogenation, and the conversion (22.6%) was nearly the same as the equilibrium one for the RWGS reaction at this reaction condition, indicating the high activity for RWGS reaction of Cu catalyst. Pd/Al_2O_3 catalyst also yielded CO selectively with small amount of CH_4 formation. The selective CO formation over Cu/Al_2O_3 and Pd/Al_2O_3 catalysts is possibly due to that CO adsorbs molecularly on the Cu and Pd surfaces [131,132]. However, the lower abilities of Cu and Pd for CO and CO_2 dissociation compared to Co and Ni catalysts would result in the less CH_4 formation, even though Pd has higher ability for H_2 dissociation. These results suggested that the nature of active phase on monometallic catalysts possibly depended on the nature of the individual transition metals.

3.4 Bimetallic Catalysts

3.4.1 Unpromoted Bimetallic Catalyst

As mentioned in section 3.3, Fe catalyst exhibited highest C_2^+ hydrocarbons formation from CO_2 hydrogenation but the conversion was very low (12.1%). To improve the CO_2 hydrogenaion activity of Fe catalyst, the Al_2O_3 supported Fe-based bimetallic catalysts (Fe-M; M = Co, Ni, Cu or Pd) with 15 wt% total metal loading (Fe + M) (support weight basis) were prepared and tested under the same reaction condition. The M/(M + Fe) was kept constant at 0.10 atomic ratio for all bimetallic catalysts.

The CO_2 hydrogenation activities and selectivities of Fe/Al_2O_3 and Fe-M(0.1)/Al_2O_3 catalysts are shown in Figure 3.3 and also summarized in Table 3.2. The results show that combining Fe and the second metal (Co, Ni, Cu or Pd) could enhance the CO_2 conversion of Fe catalyst significantly (from 12.1 to 20.4 - 37.6%). C_2^+ hydrocarbon yields also notably increased by combining Fe with Co, Cu or Pd at this ratio.

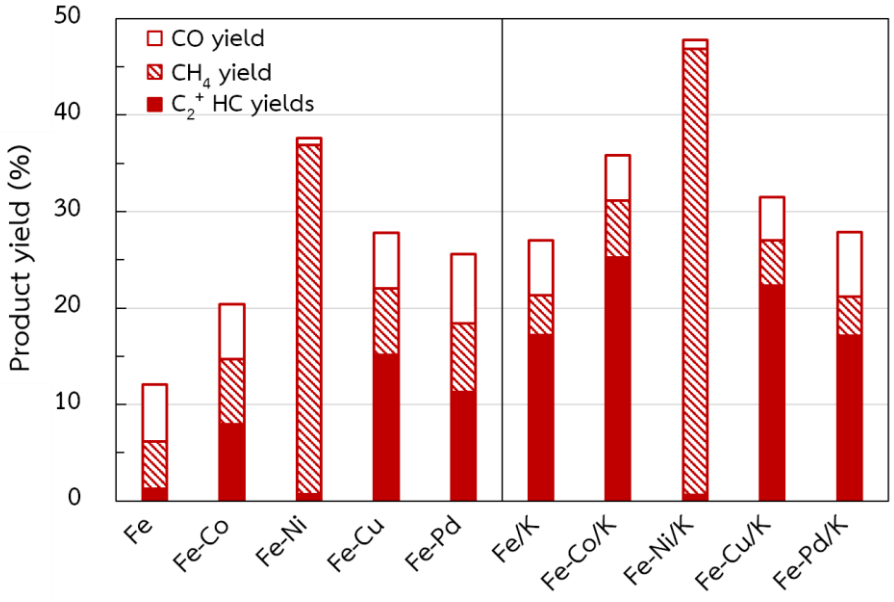

Figure 3.3 Product yields from CO_2 hydrogenation over unpromoted and K-promoted Fe/Al_2O_3 and Fe-M(0.1)/Al_2O_3 catalysts.

Table 3.2 CO_2 hydrogenation activities and selectivities of Al_2O_3 supported bimetallic catalysts.

Catalyst	CO_2 conv. (%)	HC selectivity (%, carbon based)		STY (μmol g-1 s-1)			Alpha [a)]
		CH_4	C_2-C_7	CH_4	C_2-C_7	CO	
Fe	12.1	62	38	0.54	0.13	0.65	0.27
Fe-Co(0.1)	20.4	52	48	0.67	0.22	0.65	0.37
Fe-Ni(0.1)	37.6	98	2	3.53	0.03	0.07	0.07
Fe-Cu(0.1)	27.8	41	59	0.78	0.37	0.66	0.43
Fe-Pd(0.1)	25.6	48	52	0.77	0.29	0.78	0.44
Fe/K	27.0	29	71	0.46	0.34	0.63	0.55
Fe-Co(0.1)/K	35.8	34	66	0.68	0.44	0.53	0.48
Fe-Ni(0.1)/K	47.8	87	13	3.94	0.26	0.10	0.18
Fe-Cu(0.1)/K	31.5	29	71	0.55	0.42	0.52	0.54
Fe-Pd(0.1)/K	27.9	30	70	0.46	0.34	0.79	0.53

Total metal loading = 15 wt% (support weight basis), K/Fe = 0.3

Pretreatment: H_2 red. at 673 K, 2 h

Operating cond: 573 K, 1.1 MPa, 3600 mL (STP) g^{-1} h^{-1}

[a)] Alpha (chain growth probability) were calculated from mass fractions of C_1-C_7 HCs hydrocarbons

According to section 3.3, the monometallic Co, Cu and Pd did not yield any C_2^+ hydrocarbons at this reaction condition, so these results indicated the synergistic promotion of C_2^+ hydrocarbons formation by combining Fe and the second metal. The effectiveness of the second metals at X = 0.1 atom $atom^{-1}$ (without K-promoter) in terms of C_2^+ hydrocarbons formation is Cu > Pd > Co >> Ni (Figure 3.3). The promoting effects of Cu and Pd could be explained by their selectivity for RWGS reaction, which provided CO for further hydrogenation to C_2^+ hydrocarbons by FTS over the Fe surface. The promotion effect of Co is more interesting, since Co/Al_2O_3 catalyst alone only catalyzed CO_2 methanation as shown in Table 3.1. This

promoting effect is possibly due to an enhancement of hydrogen coverage on the catalysts surfaces. Though the combination of Fe and Ni at the X of 0.1 atom atom^{-1} provided the strongest enhancement of CO_2 conversion, in contrast to other bimetallic catalysts, Fe-Ni catalyst selectively produced CH_4 from CO_2 hydrogenation.

3.4.2 K-Promoted Bimetallic Catalyst

The addition of K (K/Fe=0.3 atom atom^{-1}) to the Fe-Co, Fe-Ni, Fe-Cu and Fe-Pd catalysts with M/(M + Fe) = 0.1 atom atom^{-1} enhanced both the CO_2 conversion and C_2^+ hydrocarbon yields irrespective of the combination of metals (Table 3.2 and Figure 3.3). The chain growth probability of hydrocarbons was also improved since K addition significantly suppressed the CH_4 selectivity (Table 3.2). The K promoter effectively increased the CO_2 conversions and C_2^+ hydrocarbon formation on the Fe-Co (35.8%) and Fe-Ni (47.8%) bimetallic catalysts, while it had weaker effects on the activities and selectivities of the Fe-Cu and Fe-Pd catalysts. In the presence of K-promoter, the C_2^+ hydrocarbon yield is followed this order: Fe-Co > Fe-Cu > Fe-Pd >> Fe-Ni. These results indicated that K could enhanced the CO_2 hydrogenation activity to higher hydrocarbons for all catalysts, but the extent of K promotion still depended on the combination of metals.

Choi et. al. and Cubeiro et. al. [19,120] studied the effect of K addition to Fe-based catalysts by chemisorption experiments and reported that the addition of K decreased H_2 chemisorption capacity of Fe based catalyst, while it enhanced CO_2 adsorption. This indicated that K addition performed different manner compared to that by the combination of Fe and other transition metals, which enhanced hydrogen coverage. Thus, relatively lower activities of K-promoted Fe-Cu and Fe-Pd bimetallic catalysts might be due to that the bimetallic promotion effects are partly suppressed by K addition since Cu and Pd have lower hydrogenating abilities compared to Co and Ni.

Among the K-promoted catalysts, Fe-Co/Al_2O_3 and Fe-Cu/Al_2O_3 catalysts were the most effective ones in terms of higher hydrocarbon formation from CO_2 hydrogenation. These bimetallic catalysts could yield C_2^+ hydrocarbons more effectively than K-promoted Fe/Al_2O_3 catalyst which is known as one of most promising catalysts so far.

3.5 Fe-Ni Bimetallic Catalysts

As mentioned in section 3.3, Fe-Ni(0.1)/Al_2O_3 catalyst yielded higher CH_4 selectivity (98%) compared to other bimetallic catalysts (41-62%). This might be due to that the surface of Fe-Ni catalyst has much stronger ability for activating hydrogen compared to others, so it is difficult for carbon-carbon bond to be formed. Furthermore, the surface carbon species from dissociative chemisorption of CO_2 was favorably hydrogenated to CH_4. Therefore, it might be possible to synthesize higher hydrocarbons from CO_2 hydrogenation over Fe-Ni catalyst if the hydrogenating ability of this catalyst could be suppressed. To confirm this idea, the Fe-Ni bimetallic catalyst with low Ni loading (Ni/(Ni + Fe)=0.03 atom atom^{-1}) was prepared and tested for CO_2 hydrogenation.

Figures 3.4a and 3.4b illustrate CO_2 conversion and STY of C_2-C_7 hydrocarbons over the Fe-Ni bimetallic catalyst as a function of the Ni/(Ni + Fe) atomic ratio, respectively. As shown in these figures, CO_2 conversion increased with increasing Ni/(Ni + Fe) atomic ratio, and the STY of C_2-C_7 hydrocarbons of the Fe-Ni(0.03)/Al_2O_3 catalyst (0.30 μmol g^{-1} s^{-1}) was higher than that of the monometallic Fe catalyst (0.13 μmol g^{-1} s^{-1}). The addition of K (K/Fe=0.3 atom atom^{-1}) to this catalyst further increased the STY of C_2-C_7 hydrocarbons to 0.41 μmol g^{-1} s^{-1}, which was comparable to that of the Fe-Co(0.1)/K(0.3)/Al_2O_3 catalyst (0.44 μmol g^{-1} s^{-1}) (section 3.4.2). These results support the idea that controlling adsorption properties of hydrogen on the catalyst surface is important for enhancing higher hydrocarbons formation and suppressing CH_4 formation in CO_2 hydrogenation reaction.

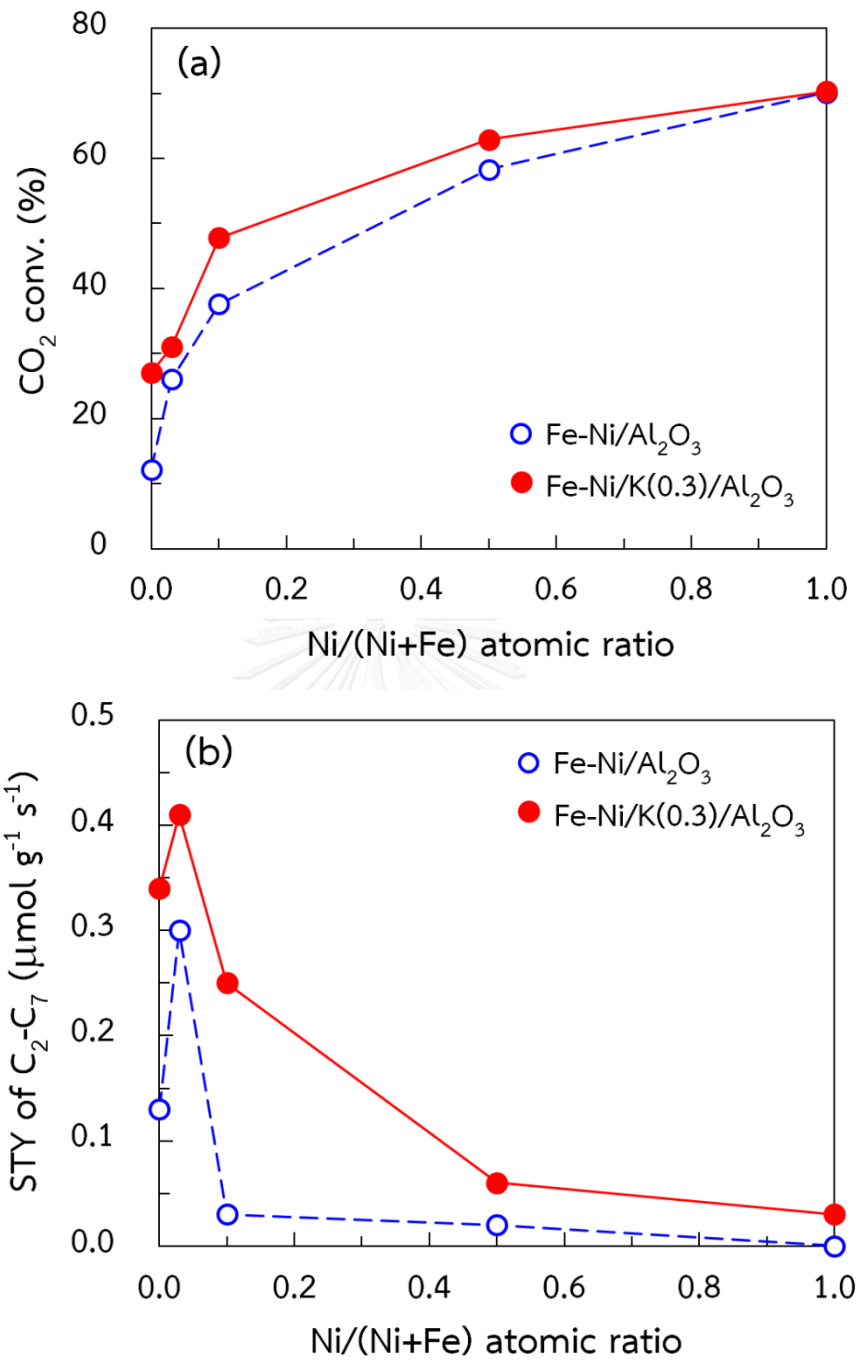

Figure 3.4 (a) CO_2 conversion and (b) STY of C_2-C_7 hydrocarbons as a function of Ni/(Ni+Fe) atomic ratio over Fe-Ni/Al_2O_3 and Fe-Ni/K(0.3)/Al_2O_3 catalysts.

3.6 Physical Properties of Fe-M Bimetallic Catalysts

To investigate a correlation of the catalytic activity to the physical properties of the catalysts, the N_2 adsorption-desorption analyses of the monometallic and bimetallic catalysts were performed. The physical properties of all catalysts are summarized in Table 3.3. According to the results in Tables 3.1, 3.2 and 3.3, there is no relation between physical properties of the catalysts and CO_2 conversions. Without the K promoter, BET surface area of monometallic Fe (137 m^2 g^{-1}) and Fe based bimetallic catalysts (129-145 m^2 g^{-1}) were larger than those of other catalysts (115-121 m^2 g^{-1}). The addition of K to the bimetallic catalysts slightly decreased BET surface area (124-130 m^2 g^{-1}) of the catalysts but strongly increased CO_2 conversion (Table 3.2). These results suggest that the selection of combining the transition metals significantly affects the nature of the active phase or active site(s) of the catalysts.

Table 3.3 The physical properties of Al_2O_3 supported monometallic and bimetallic catalysts prepared in this work.

Catalyst	SA [a] (m^2 g^{-1})	PV [b] (cm^3 g^{-1})	D_p [c] (nm)
Al_2O_3	139	1.03	24
Fe	137	0.71	18
Co	121	0.86	23
Ni	117	0.84	23
Cu	115	0.87	24
Pd	138	1.03	24
Fe-Co(0.10)	145	0.75	18
Fe-Ni(0.03)	141	0.70	18
Fe-Ni(0.10)	143	0.73	18
Fe-Ni(0.50)	129	0.77	20
Fe-Cu(0.10)	143	0.74	19
Fe-Pd(0.10)	141	0.77	19
Fe-Co(0.10)/K	130	0.63	17
Fe-Ni(0.03)/K	125	0.64	18
Fe-Ni(0.10)/K	128	0.60	16
Fe-Ni(0.50)/K	127	0.73	20
Fe-Cu(0.10)/K	127	0.66	18
Fe-Pd(0.10)/K	124	0.67	19

[a] BET surface area

[b] BJH desorption cumulative pore volume

[c] BJH desorption average pore diameter

CHAPTER IV

CO_2 HYDROGENATION TO HIGHER HYDROCARBONS OVER Fe-Co BIMETALLIC CATALYSTS

4.1 Introduction

As mentioned in section 3.1, the comparative studies of the hydrogenation of CO, CO_2 and their mixtures on Co and Fe catalysts demonstrated that the product composition with Co-based catalyst shifted from an FTS type to CH_4 with increasing CO_2 partial pressure, while it was barely changed in the case of using Fe catalyst [113,114]. These dramatically different catalytic properties of Co and Fe catalysts imply the importance of controlling CO_2 and H_2 coverage over active metal surface for carbon – carbon bond formation.

The idea behind this work is that surface chemisorption properties of H_2 and CO_2 could be tailored over bimetallic surface involving Fe and Co by changing their composition for enhancing higher hydrocarbons [133]. Several research groups have studied bimetallic effect on CO hydrogenation in Fischer-Tropsch synthesis (FTS) and suggested that bimetallic alloy formation was associated with their improved activities and selectivities [134-141]. Systematic study on the effect of the catalyst composition (Co/(Co + Fe) atomic ratio) on the CO_2 hydrogenation activity and selectivity has not been reported and the effect of K addition on the activity and selectivity of the Fe-Co bimetallic catalyst is still unknown.

In this work, a series of Fe-Co/Al_2O_3 catalysts with a wide range of Co/(Co + Fe) atomic ratios were prepared and tested for CO_2 hydrogenation. The effect of K content on the CO_2 hydrogenation activity and selectivity to higher hydrocarbons over Fe-Co bimetallic catalysts was also studied. K-promoted Fe-Mn catalyst as a reference catalyst was also prepared and tested, since this catalysts has been known

as one of the promising catalysts for CO_2 hydrogenation to higher hydrocarbons [19,20].

4.2 Time-On-Stream Stabilities of Fe-Co Catalysts

The time-on-stream (TOS) stabilities of CO_2 conversions and product yields on Fe-Co(0.17)/K(0.3)/Al_2O_3 and Fe-Co(0.17)/K(1.0)/Al_2O_3 catalysts are shown in Figures 4.1a and b respectively, as examples. The stable CO_2 conversion and selectivities were obtained after 3-4 h on stream for the Fe-Co bimetallic catalysts with low Co/(Co + Fe) atomic ratios (≤ 0.25), and no deactivations of the catalysts were observed for more than 50 h. However, the time-dependent behaviors of the catalysts with higher Co/(Co + Fe) atomic ratios (≥ 0.5) were slightly different (see Appendix E). CO_2 conversion over these catalysts slightly decreased with time on stream, but the decreasing rates were less than 0.4% per hour at 15-16 h on stream. In addition, these catalysts produced almost only CH_4 and their product selectivities did not change with TOS.

4.3 Effect of Co/(Co + Fe) Atomic Ratios

4.3.1 CO_2 Conversions

From Chapter III, Fe-Co bimetallic catalysts showed high activity for CO_2 hydrogenation to C_2^+ hydrocarbons compared to other bimetallic catalysts. In this chapter, the Al_2O_3 supported Fe-Co bimetallic catalysts with various Co/(Co + Fe) atomic ratios were prepared and tested for CO_2 hydrogenation at 573 K and 1.1 MPa to investigate their activities and selectivities in more details.

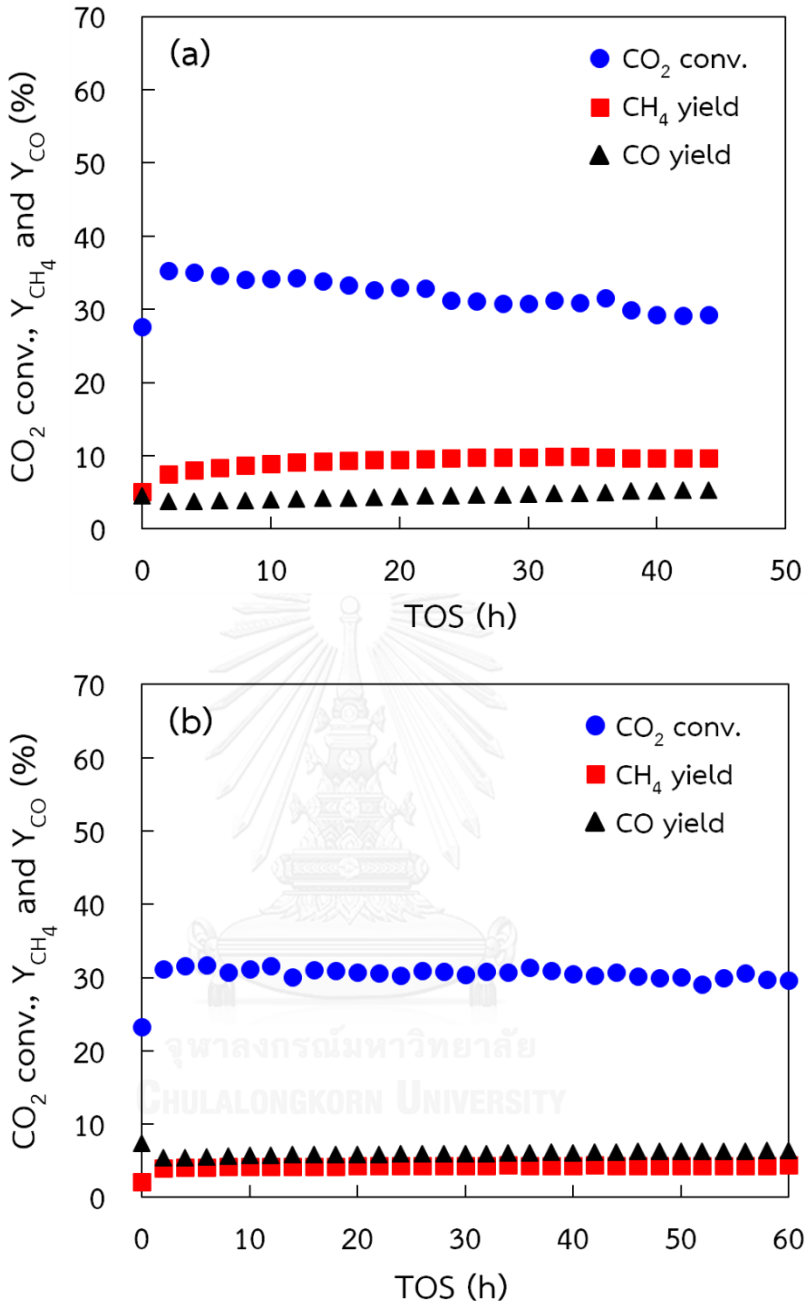

Figure 4.1 Time-on-stream stabilities of CO_2 conversions and product yields over (a) Fe-Co(0.17)/K(0.3)/Al_2O_3 and (b) Fe-Co(0.17)/K(1.0)/Al_2O_3 catalysts.

The change in CO_2 conversion over Fe-Co/Al_2O_3 bimetallic catalysts as a function of the Co/(Co + Fe) atomic ratio is shown in Figure 4.2. CO_2 conversion over Fe/Al_2O_3 catalyst (15 wt% Fe loading) was 12% at this reaction condition. Riedel et al. [113] reported the relatively similar activity of Fe/Al_2O_3 catalyst with 20 wt% Fe loading, where CO_2 conversion was about 23% at the same reaction temperature and pressure but nearly half of GHSV (~1900 mL g^{-1} h^{-1}). The combination of Fe and a small amount of Co (Co/(Co + Fe) = 0.17 atom $atom^{-1}$) increased the conversion almost twice compared to that of monometallic Fe/Al_2O_3 catalyst. The conversion increased almost linearly with further increase in the Co/(Co + Fe) atomic ratio, and reached almost 50% at Co/(Co + Fe) atomic ratio of unity, namely Co/Al_2O_3 catalyst.

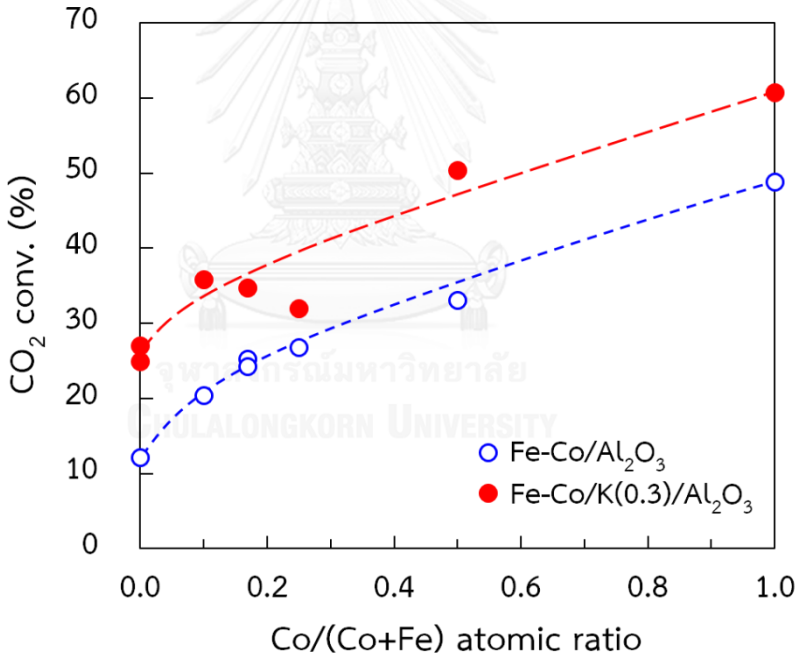

Figure 4.2 CO_2 conversion over Fe-Co(X)/K(0.3)/Al_2O_3 and Fe-Co(X)/Al_2O_3 catalysts as a function of Co/(Co+Fe) atomic ratio.

4.3.2 Hydrocarbon Product Yields

The influence of Co content on space-time yields (STYs) of C_2-C_7 hydrocarbons and CH_4 over Fe-Co/Al_2O_3 catalysts are illustrated in Figures 4.3a and 4.3b, respectively. As shown in these figures, the STY of C_2-C_7 hydrocarbons showed a maximum value at the Co/(Co + Fe) ~ 0.17 atom atom^{-1}, while that of CH_4 increased almost linearly with increasing the Co/(Co + Fe) atomic ratio up to 0.50. The maximum STY of C_2-C_7 hydrocarbons is clearly much higher than the simple summation of those over the monometallic Fe/Al_2O_3 and Co/Al_2O_3 catalysts (Figure 4.3a), which indicated that combining Fe and a small amount of Co led to significant bimetallic promotion of CO_2 hydrogenation to C_2^+ hydrocarbons. Furthermore, the STYs of C_2-C_7 hydrocarbons and CH_4 increased at similar rates (2-3 folds) at the Co/(Co + Fe) $\leq$ 0.17 atom-Co atom^{-1}. These results revealed that the Fe-Co bimetallic formulation with a low Co content enhanced the CO_2 conversion without losing an ability for carbon - carbon bond formation for synthesizing the higher hydrocarbons. However, further increasing Co/(Co + Fe) atomic ratios ($\geq$ 0.5 atom-Co atom^{-1}) resulted in a significant decrease of the STY of C_2-C_7 hydrocarbons. Only small amounts of C_2^+ hydrocarbons were observed in the product stream from hydrogenation using high Co loading catalysts, and CH_4 formation accounted for 90-99% of the total hydrocarbons product. These results are similar to the previous work by Park et al. [142], in which they reported that Fe-Co/Al_2O_3 catalyst with 5 wt% Fe and 5 wt% Co loading showed higher CO_2 conversion, but lower selectivity for C_2-C_5 hydrocarbons compared to 10 wt% Fe/Al_2O_3 catalyst. Therefore, these results clearly demonstrated an importance of Fe-Co combination with high Fe concentration for C_2^+ hydrocarbons synthesis from CO_2 hydrogenation, which has never been reported previously. The high activity and selectivity to higher hydrocarbons of the bimetallic catalyst suggested that the combination of Fe and Co made the surface adsorption properties for CO_2 and H_2 suitable for facilitating the carbon chain growth thus leading to an increase in the higher hydrocarbon yield.

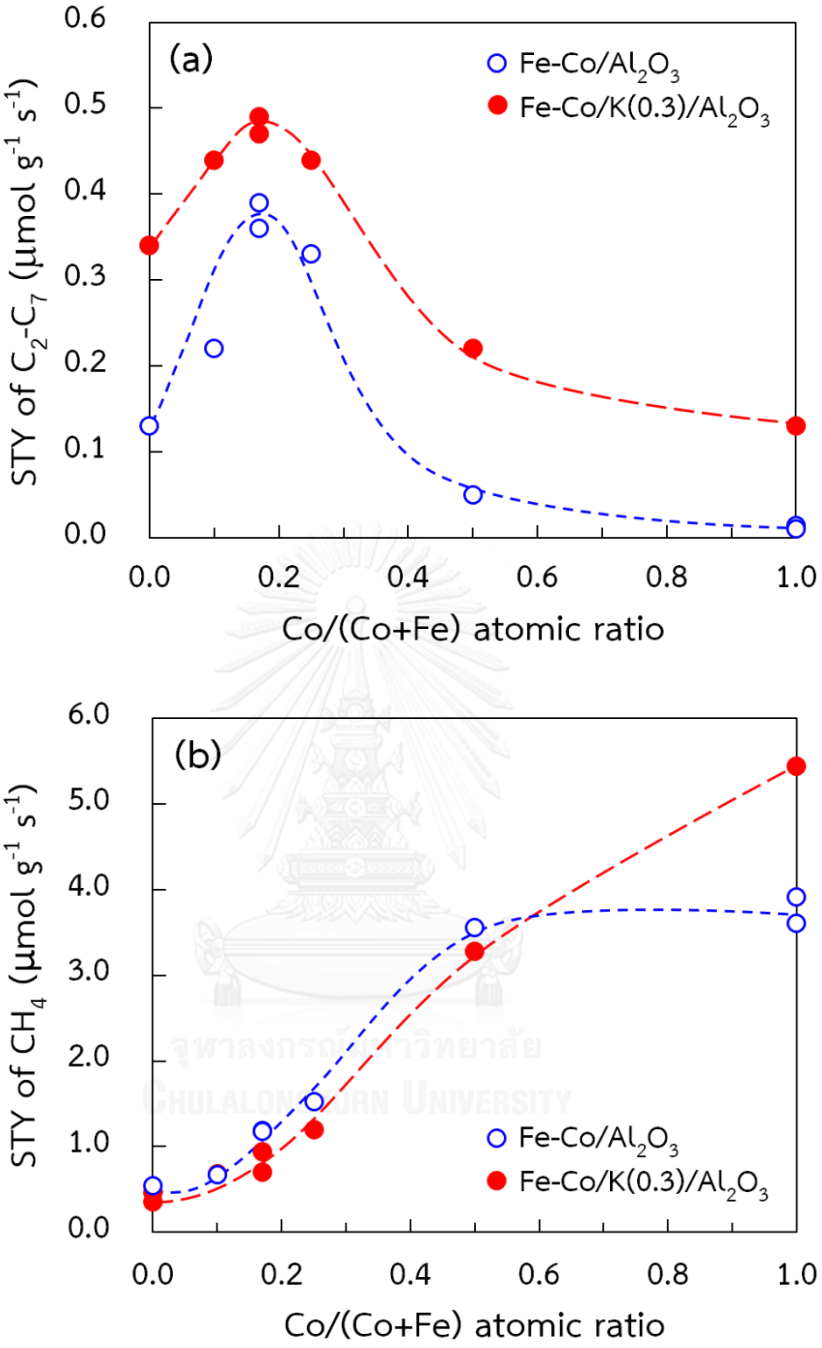

Figure 4.3 Effect of Co/(Co + Fe) atomic ratio on STY of (a) C_2-C_7 hydrocarbons and (b) CH_4 over Fe-Co bimetallic catalysts.

It should also be noted that Fe-Co bimetallic catalysts were used for CO hydrogenation and the optimum Co/(Co + Fe) atomic ratio was 0.5-0.75 [134,137], which was different from the optimum ratio for CO_2 hydrogenation reported in this work. This was possibly due to the different site requirements for CO and CO_2 hydrogenation. Hence, the optimum catalyst composition for CO_2 hydrogenation cannot be simply predicted from the previous studies on CO hydrogenation.

The conversions and selectivities of all monometallic and bimetallic catalysts are summarized in Table 4.1. Fe-Co(0.17)/Al_2O_3 catalyst exhibited more than 4 times higher C_2^+ selectivity than the monometallic Fe catalyst with significantly lower CO selectivity, and rarely change in CH_4 selectivity. For the unpromoted Fe-Co/Al_2O_3 bimetallic catalysts, CH_4 selectivity was quite high (30-40%) even at the low Co/(Co + Fe) atomic ratios compared to that in typical Fischer-Tropsch synthesis (FTS). However, these bimetallic catalysts, in particular monometallic Co catalyst, are still useful for fuel production from CO_2 hydrogenation since CH_4 can be used as synthetic natural gas. No olefins were observed in the gas phase hydrocarbons with these unpromoted monometallic and bimetallic catalysts.

4.4 Effect of K Addition

The effect of K addition on the activities and selectivities of Fe-Co bimetallic catalysts were also studied. CO_2 conversions over K-promoted (K/Fe = 0.3 atom $atom^{-1}$) and unpromoted Fe-Co bimetallic catalysts are compared as illustrated in Figure 4.2. K-promoted catalyst exhibited higher CO_2 conversion than the unpromoted catalysts regardless of the Co/(Co + Fe) atomic ratios. The addition of K also improved the STY of C_2-C_7 hydrocarbons over bimetallic catalysts without changing the overall trend (Figure 4.3a), while it suppressed CH_4 formation when the Co/(Co + Fe) atomic ratio was less than 0.5 (Figure 4.3b).

Table 4.1 CO_2 conversion and product selectivities of unpromoted and K-promoted Fe-Co/Al_2O_3 in comparison to monometallic catalysts [115].

Catalyst	CO_2 conversion (%)	Selectivity (%, carbon based)			O/P [a]	Alpha [b]
		CO	CH_4	C_2^+ [d]		
Fe	12.1	49	41	10	0.0	0.27
Fe-Co(0.10)	20.3	28	33	39	0.0	0.37
Fe-Co(0.17)	25.2	13	44	43	0.0	0.36
Fe-Co(0.17) [c]	25.7	12	44	44	0.0	0.40
Fe-Co(0.25)	26.8	10	54	36	0.0	0.31
Fe-Co(0.50)	33.1	1	87	12	0.0	0.04
Co	48.8	2	97	1	0.0	0.00
Fe/K(0.3)	27.0	21	15	64	1.1	0.55
Fe-Co(0.10)/K(0.3)	35.8	13	16	71	0.6	0.57
Fe-Co(0.17)/K(0.3)	33.7	14	18	68	0.7	0.52
Fe-Co(0.17)/K(0.5)	33.6	13	19	68	1.5	0.50
Fe-Co(0.17)/K(1.0)	31.0	18	13	69	5.2	0.53
Fe-Co(0.25)/K(0.3)	32.0	38	15	47	0.2	0.40
Fe-Co(0.50)/K(0.3)	50.3	1	63	36	0.0	0.20
Co/K(0.3)	60.6	1	96	3	0.0	0.10
Fe-Mn-K [c]	19.4	50	7	43	5.1	0.51

[a] Olefin to paraffin ratio of $C_2 - C_4$ hydrocarbons

[b] Alpha (chain growth probability) were calculated from mass fractions of C_1-C_7 hydrocarbons

[c] Prepared by a wet co-impregnation method (Fe = 17 wt%, K = 8wt% and Mn = 12 wt%, support weight basis)

[d] Including small amounts of alcohols

The product selectivities of K-promoted Fe-Co bimetallic catalysts with different Co/(Co + Fe) atomic ratios are also summarized in Table 4.1. The C_2^+ hydrocarbon selectivity and chain growth probability of gas-phase hydrocarbons were notably enhanced by the addition of K, while CH_4 selectivity drastically decreased. CH_4 selectivity of Fe-Co(0.17)/K(0.3)/Al_2O_3 catalyst was relatively similar to that of Fe/K(0.3)/Al_2O_3 catalyst, but the former catalysts exhibited higher C_2^+ hydrocarbons selectivity compared to the latter one. Furthermore, the Fe-Co(0.17)/K(0.3)/Al_2O_3 catalyst showed higher CO_2 conversions and C_2^+ selectivity than the K-promoted Fe-Mn catalyst with higher Fe loading as shown in Table 4.1. The influence of the catalyst preparation methods, namely pore-filling incipient wetness impregnation and wet co-impregnation methods was also investigated. The result showed that the CO_2 hydrogenation activities and selectivities of Fe-Co(0.17)/Al_2O_3 catalyst were hardly dependent on the preparation methods (Table 4.1). Hence, these results revealed the effectiveness of Fe-Co-K combination than Fe-Mn-K for CO_2 hydrogenation to C_2^+ hydrocarbons.

4.5 Effect of K/Fe Atomic Ratios

To study the effect of K content on the activities and selectivities of Fe-Co bimetallic catalysts in more details, the K concentration was adjusted to obtain wide range of K/Fe atomic ratios (0.0 - 1.0). The catalysts were tested for CO_2 hydrogenation at 573 K and 1.1 MPa and the results are shown in Figure 4.4. The addition of K (K/Fe = 0.3 atom $atom^{-1}$) to Fe-Co(0.17)/Al_2O_3 increased the C_2-C_7 STY significantly, but further increasing K loading did not cause clear changes in the C_2-C_7 STY, while CH_4 STY decreased linearly with an increase in the K loading. These results revealed that the addition of K to Fe-Co/Al_2O_3 catalysts enhanced the chain propagation of hydrocarbons.

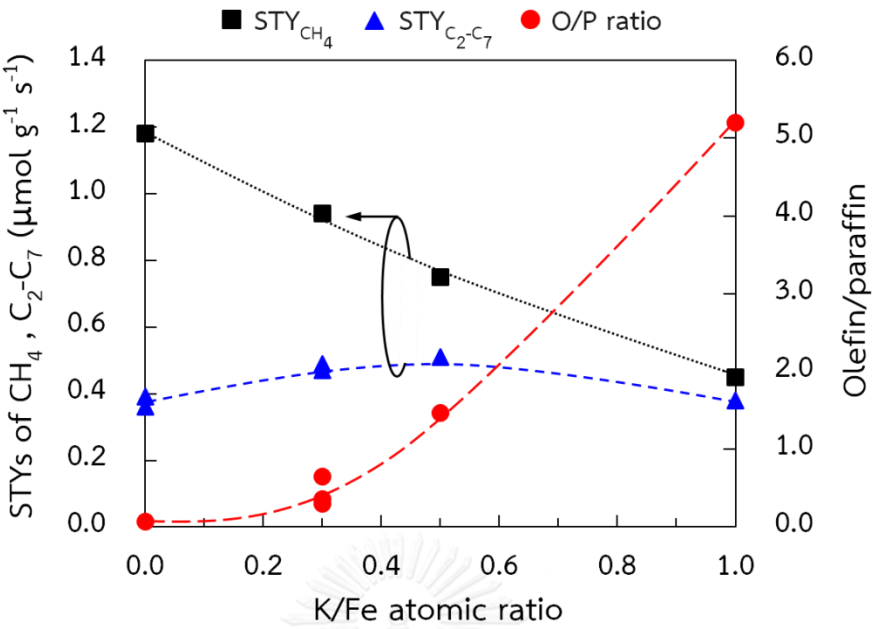

Figure 4.4 Effect of K/Fe atomic ratio on STYs of CH_4 and C_2-C_7 hydrocarbons and the olefin to paraffin ratio of C_2-C_4 hydrocarbons over Fe-Co(0.17)/K(Y)/Al_2O_3 catalysts.

The addition of K also increased olefin to paraffin ratio (O/P) of C_2-C_4 hydrocarbons for all catalysts as summarized in Table 4.1. Olefin contents increased with increasing K loading, and olefins predominated in C_2^+ hydrocarbons when the catalysts were heavily alkalized (K/Fe $\geq$ 0.5 atom $atom^{-1}$). O/P ratio reached approximately 5 at the K/Fe atomic ratio of unity (see also Figure 4.6).

The liquid products were also analyzed after CO_2 hydrogenation using the Gas Chromatography-Mass Spectrometry (GC/MS). Figures 4.5a and 4.5b illustrate GC/MS total ion chromatograms of liquid products from CO_2 hydrogenation over Fe-Co(0.17)/K(0.3)/Al_2O_3 and Fe-Co(0.17)/K(1.0)/Al_2O_3 catalyst, respectively. Since hexadecane ($C_{16}H_{34}$) was used for extracting the hydrocarbon products from the liquid products from CO_2 hydrogenation, the mass spectrometer filament was turned off at its retention time in order to protect the instrument.

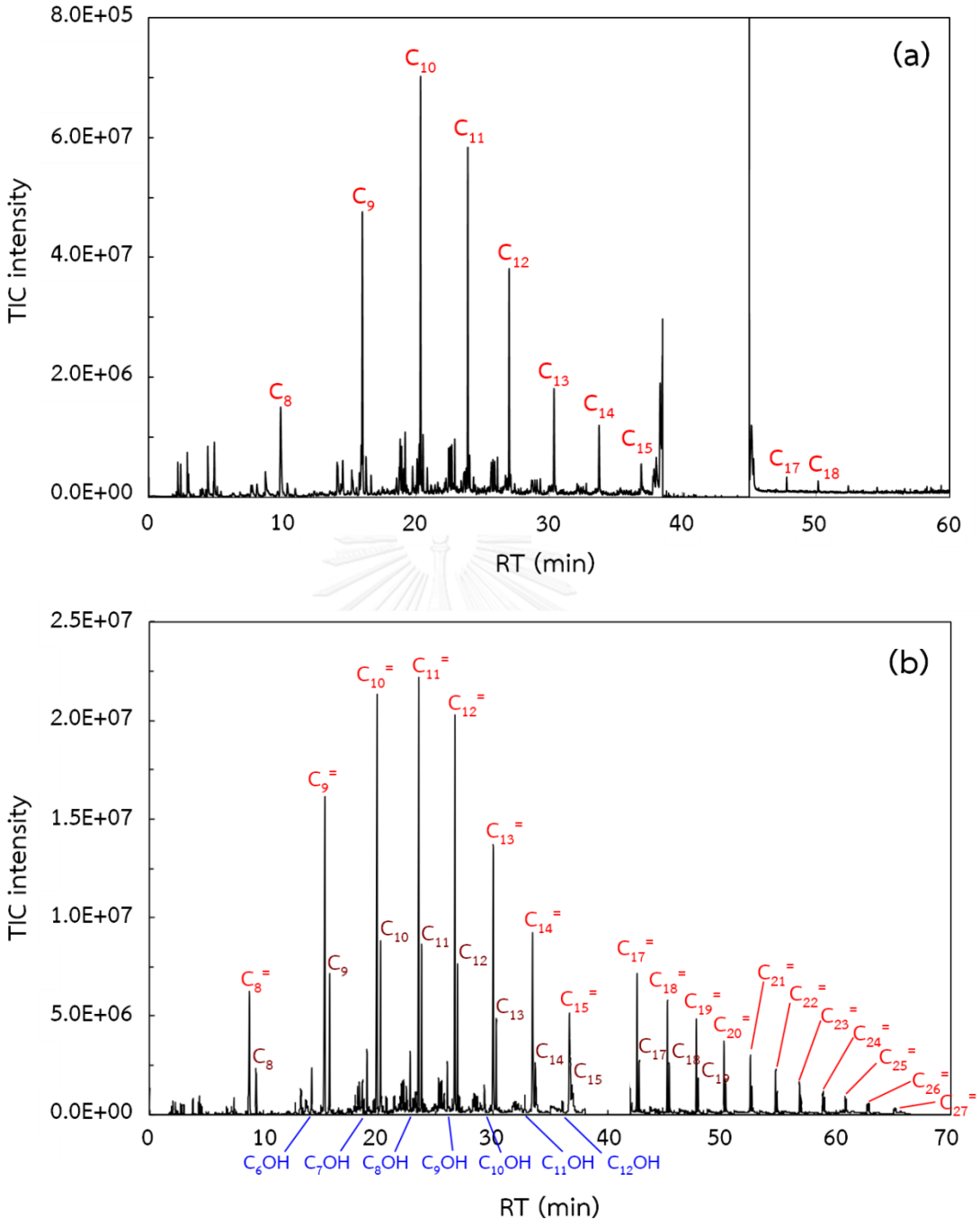

Figure 4.5 GC/MS total ion chromatogram of liquid products from CO_2 hydrogenation over (a) Fe-Co(0.17)/K(0.3)/Al_2O_3 and (b) Fe-Co(0.17)/K(1.0)/Al_2O_3 catalysts.

The hydrocarbon compounds from octane to octadecane were observed in the liquid product of Fe-Co(0.17)/K(0.3)/Al_2O_3 catalyst without olefin products (Figure 4.5a). This carbon number range was approximately corresponding to gasoline and jet fuel. In the case of highly alkalized Fe-Co catalyst (K/Fe = 1.0 atom $atom^{-1}$), the linear alpha olefins were main products with carbon numbers up to 27 (Figure 4.5b). The carbon number range of this liquid product was corresponding to gasoline, jet fuel (main) and also diesel fuel. Small amount of alcohols were also observed in the products.

From the Anderson–Schulz–Flory (ASF) distribution, where $\ln(M_N)$ (the mole fraction of hydrocarbons containing N carbon) is plotted with carbon number (N), the chain growth probability (α) could be derived from the slope of the line fitted to the data. The ASF plots of the liquid products were illustrated in Figure 4.6. The chain growth probability of liquid product from hydrogenation using Fe-Co(0.17)/K(1.0)/Al_2O_3 catalyst was 0.8, which higher than that from Fe-Co(0.17)/K(0.3)/Al_2O_3 catalyst (0.67), suggesting that chain growth probability of the liquid hydrocarbon products increased with K content. The chain growth probability of liquid product from hydrogenation using Fe-Co(0.17)/K(1.0)/Al_2O_3 was relative similar to those typically observed in FTS using Fe-based catalysts.

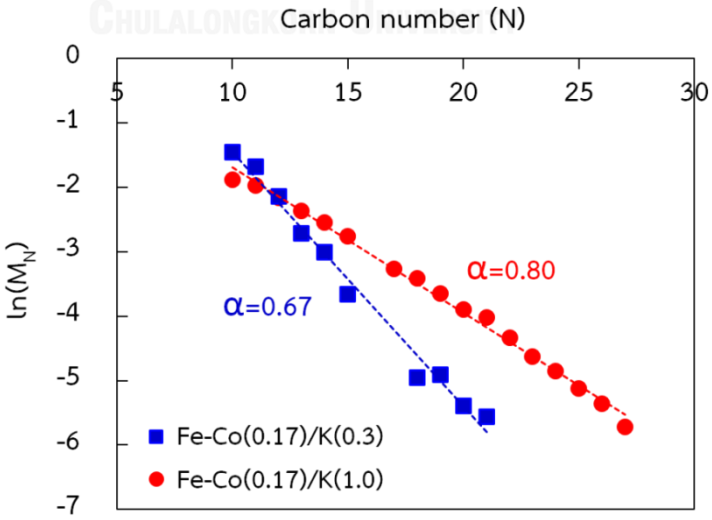

Figure 4.6 ASF plot of the liquid hydrocarbon products for the Fe-Co(0.17)/K(0.3)/Al_2O_3 and Fe-Co(0.17)/K(1.0)/Al_2O_3 catalysts.

CHAPTER V

H_2 AND CO_2 ADSORPTION PROPERTIES OF Fe-Co BIMETALLIC CATALYSTS AND THEIR ACTIVITIERS FOR CO_2 HYDROGENATION TO HIGHER HYDROCARBONS

5.1 Introduction

Fe-Co bimetallic catalysts have been used for CO hydrogenation to higher hydrocarbons for long time, and their physical and chemical properties have been studied in relation to their catalytic ability for CO hydrogenation [134,136,139,141,143-145]. However, these studies have mainly dealt with Co- (or Ni-) rich bimetallic catalysts [134,135,137]. In our work (Chapter IV), a significant promotion of higher hydrocarbon synthesis from CO_2 hydrogenation was observed over Fe-Co/Al_2O_3 bimetallic catalysts with a low Co content (Co/(Co + Fe) = 0.17 atom-Co atom^{-1}). The effect of combining Fe and a small amount of Co on the physicochemical properties of the catalysts has never been elucidated. In addition, there are only a limited number of studies that have evaluated the H_2 and CO_2 adsorption properties on these bimetallic catalysts. To develop a fundamental understanding of the Fe-Co bimetallic promotion of CO_2 hydrogenation, a systematic study of H_2 and CO_2 adsorption properties, and their relationship with CO_2 hydrogenation activities, is important.

In this work, Fe-Co bimetallic catalysts with different Co/(Co + Fe) atomic ratios (X) were characterized by X-ray diffraction (XRD), temperature-programmed reduction (TPR), temperature-programmed desorption (TPD) and diffuse reflectance Infrared Fourier transform spectroscopy (DRIFTS) in order to clarify the effect of combining Fe and Co on H_2 and CO_2 adsorption properties of the Fe-Co bimetallic catalysts, and their impact on the CO_2 hydrogenation activities.

5.2 Physical Properties of Calcined Catalysts

The physical properties of the calcined Fe-Co(X)/Al_2O_3 catalysts (X represents Co/(Co + Fe) atomic ratio) are summarized in Table 5.1. The Brunauer-Emmett-Teller (BET) surface area (SA) of the calcined Fe and Fe-rich Fe-Co (X ≤ 0.25) catalysts (137–145 m^2 g^{-1}) were somewhat close to that of the γ-Al_2O_3 support (139 m^2 g^{-1}), while the Co-rich Fe-Co(0.50)/Al_2O_3 SA was about 1.05-fold lower. In the presence of the metal oxides, the pore volume (PV) and average pore diameter (D_p) were dramatically decreased from 1.37- to 1.45-fold and 1.33-fold, respectively. However, the BET SA and PV of the calcined Co catalyst were 10–20% smaller than those of the γ-Al_2O_3 support. The average D_p of the support was reduced 1.33-fold with the addition of Fe, but was barely changed with the incorporation of Co oxide. The physical properties of the calcined Fe and Fe-rich Fe-Co catalysts suggested that small metal oxide particles were well dispersed inside the pores of the γ-Al_2O_3 support, while the Co oxide particles agglomerated to some extent in the calcined Co catalyst. This was supported by the XRD analysis, where agglomerated Co_3O_4 species was detected in the calcined Co catalyst but no polycrystalline phases of Fe and Co species were observed for the calcined Fe and Fe-Co (X ≤ 0.25) catalysts (Figure 5.2, see section 5.4).

Table 5.1 Metal loadings, physical properties and CO_2 hydrogenation activities and selectivity's of Fe-Co(X)/Al_2O_3 catalysts.

Catalyst	Loading[a] (wt%)		SA	PV	D_p	STY[b),c)] (μmol g^{-1} s^{-1})			Selectivity[b)] (%, carbon based)		
	Fe	Co	(m^2 g^{-1})	(cm^3 g^{-1})	(nm)	CH_4	C_{2-7}	CO	CH_4	C_2^{+} [d)]	CO
Al_2O_3	-	-	139	1.03	24	-	-	-	-	-	-
Fe/Al_2O_3	15.0	0	137	0.71	18	0.68	0.26	0.44	26	59	16
Fe-Co(0.10)/Al_2O_3	13.4	1.6	145	0.75	18	0.67	0.22	0.65	33	39	28
Fe-Co(0.17)/Al_2O_3	12.4	2.6	138	0.72	18	1.18	0.39	0.48	44	43	13
Fe-Co(0.25)/Al_2O_3	11.1	3.9	140	0.74	19	1.53	0.33	0.28	54	36	10
Fe-Co(0.50)/Al_2O_3	7.3	7.7	132	0.77	20	3.56	0.05	0.02	87	12	1
Co/Al_2O_3	0	15.0	121	0.86	23	3.91	0.01	0.10	97	1	2

[a)] Support weight basis

[b)] From ref. [115]

[c)] Space-time yield (μmol of product formed per g-cat per second)

[d)] Including small amounts of alcohols

5.3 Reducibility of Supported Metal Oxides

The TPR profiles of the calcined Fe-Co/Al_2O_3 catalysts with various Co/(Co + Fe) atomic ratios (X), along with the degree of reduction (DR) of the supported metal oxides are shown in Figure 5.1. The DR of the supported metal oxides was defined as the ratio of the measured H_2 consumption from TPR analysis to the theoretical H_2 consumption. The measured H_2 consumption was calculated by integrating the whole TPR profile, while the theoretical H_2 consumption was the amount of H_2 required for the reduction of the supported Fe and Co oxides to their metallic states according to the stoichiometry of the Eq. (5.1) and (5.2). Calibration of the H_2 consumption was done by reduction of Co_3O_4 powder (99.5%).

$$Fe_2O_3 + 3H_2 \leftrightarrow 2Fe^0 + 3H_2O \quad (5.1)$$

$$Co_3O_4 + 4H_2 \leftrightarrow 3Co^0 + 4H_2O \quad (5.2)$$

A major reduction peak was observed at 618 K for the calcined Fe/Al_2O_3 catalyst (X = 0) with much two smaller peaks at 780 K and 987 K. These three peaks were attributed to the sequential reduction steps of Fe_2O_3 to Fe^0 via Fe_3O_4 and FeO (Eq. (5.3) - (5.5)) [143,146].

$$3Fe_2O_3 + H_2 \leftrightarrow 2Fe_3O_4 + H_2O \quad (5.3)$$

$$Fe_3O_4 + H_2 \leftrightarrow 3FeO + H_2O \quad (5.4)$$

$$FeO + H_2 \leftrightarrow Fe^0 + H_2O \quad (5.5)$$

However, the DR of the supported Fe oxide was only 41%. The less intense peaks at higher temperatures (780 K and 987 K) indicated that the reduction of Fe_3O_4 to Fe^0 was strongly suppressed in the calcined Fe catalyst. This suggests that the intermediate Fe_3O_4 and/or FeO reacted with the Al_2O_3 surface during the TPR of calcined Fe catalyst, resulting in the formation of large amount of reduction-resistant Fe-Al-O species [143].

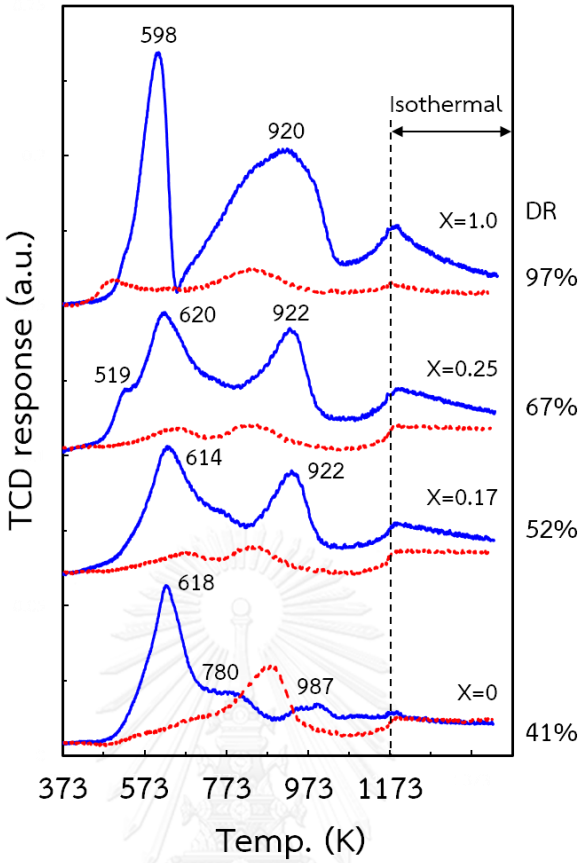

Figure 5.1 Effect of combining Fe and Co on the H_2-TPR profiles of the calcined (———) and reduced (---------) Fe-Co(X)/Al_2O_3 catalysts. The degree of reduction (% DR) of the supported metal oxides is also indicated.

The TPR profile of Fe/Al_2O_3 catalyst was obviously changed by combining Fe and Co. The second peak at 920 K was clearly observed in the Co-containing catalysts and was accompanied by a significant increase in the DR of the supported metal oxides (Figure 5.1). If the Fe/Al_2O_3 and Co/Al_2O_3 catalysts were physically mixed, the calculated DR would be 50% and 55% for X = 0.17 and 0.25, respectively. Since the measured DR of Fe-Co(0.17)/Al_2O_3 and Fe-Co(0.25)/Al_2O_3 were higher than those calculated values, the supported metal oxides possibly become reducible by alloying with Fe and Co [134,143]. However, the DR of the calcined Fe-Co(0.17)/Al_2O_3 catalyst was still 52%, indicating that a certain amount of reduction-resistant metal oxide was still present in this catalyst.

To investigate the extent of the reduction of the supported metal oxides after isothermal H_2 reduction, the calcined catalyst was pre-reduced in situ with H_2 at 673 K for 2 h before the TPR analysis. A clearly visible broad peak was observed in the TPR profiles of the reduced Fe/Al_2O_3 catalyst (Figure 5.1), indicating the presence of a large amount of unreduced Fe oxides. However, much lower intensity peaks were observed for the Co-containing catalysts. Moreover, the combination of Fe and Co also increased the extent of reduction of the supported metal oxides after isothermal reduction. In other words, more metallic sites were formed after H_2 reduction by combining Fe and Co.

5.4 Phases of Calcined and Spent Fe and Co Catalysts

XRD patterns of calcined and spent catalysts are illustrated in Figure 5.2. Diffraction peaks of γ-Al_2O_3 phase were solely observed in the XRD pattern of calcined Fe/Al_2O_3 catalyst. However, the formation of polycrystalline α-Fe_2O_3 in similar Fe/Al_2O_3 catalyst with 12 wt% Fe loading was reported earlier by Lögdberg et. al. [143]. Hence, the absence of polycrystalline α-Fe_2O_3 in Fe catalyst in this work indicating a good dispersion state of Fe_2O_3 on the γ-Al_2O_3 support. The diffraction pattern of calcined catalyst was not changed by combining Fe and a small amount of Co (X=0.17) as shown in Figure 5.2. For the calcined $Fe\text{-}Co(0.5)/Al_2O_3$ and Co/Al_2O_3 catalysts, polycrystalline Co_3O_4 was detected, which indicated that Co oxide particles agglomerated on the high Co-containing catalysts.

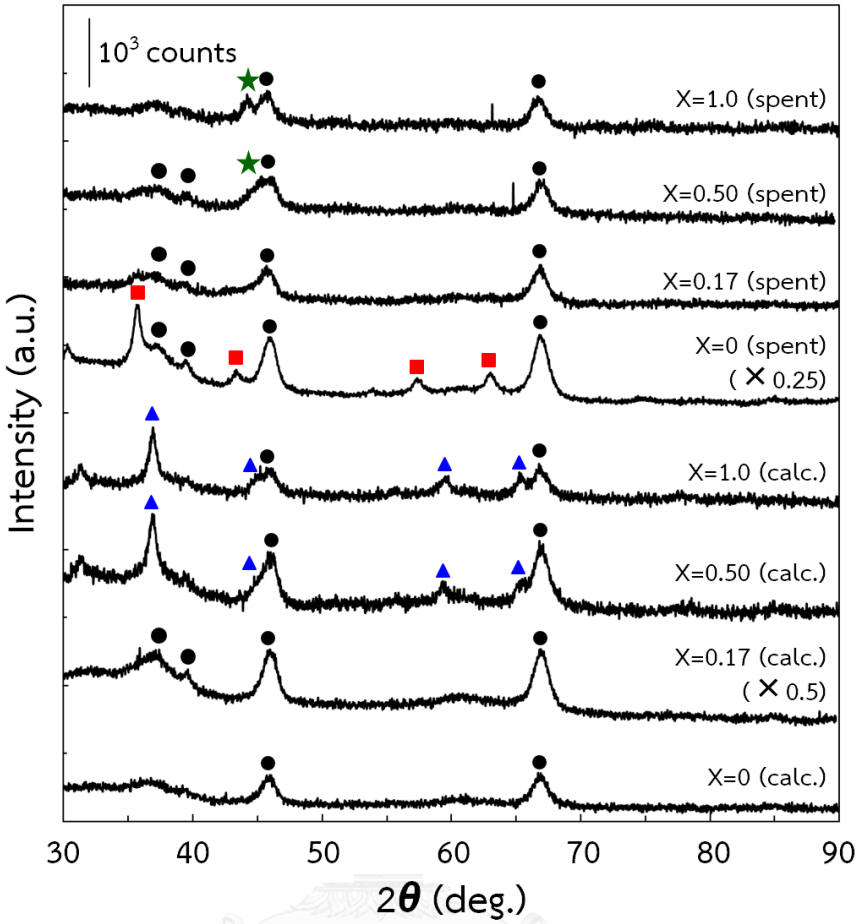

Figure 5.2 XRD patterns of calcined and spent Fe-Co(X)/Al_2O_3 catalysts. ● γ-Al_2O_3, ■ Fe_3O_4 (or Fe_2AlO_4), ▲ Co_3O_4, ★ Co^0

For spent catalyst, several new peaks emerged in the XRD pattern of Fe/Al_2O_3 catalyst at 2θ = 36, 43, 51 and 63°. These peaks are ascribed to polycrystalline Fe_3O_4 (or Fe_2AlO_4 [143]), while metallic and carbidic phases were not detected. However, the diffraction peaks of polycrystalline Fe oxide were completely disappeared from the XRD patterns of spent Fe-Co and Co catalysts. Furthermore, polycrystalline Co^0 was observed in spent Fe-Co(0.5)/Al_2O_3 and Co/Al_2O_3 catalyst without Co_3O_4 being detected, implying that bulk oxidation of Fe and Co species unlikely occurred during CO_2 hydrogenation and passivation of the spent catalyst. Therefore, polycrystalline Fe oxide observed in spent Fe/Al_2O_3 catalyst could be resulted from incomplete reduction of Fe_2O_3 as confirmed by the TPR experiment of reduced Fe catalyst,

rather than oxidation of metallic and/or carbidic phases during CO_2 hydrogenation and the subsequent passivation process. This result could be explained by the TPR results that the combination of Fe and Co improved the reduction degree of supported metal oxide, leading to disappearance of the diffraction peaks of Fe oxides.

For spent Fe-Co(0.17)/Al_2O_3 catalyst, the peak of Fe and Co phases was not observed in the XRD pattern, although the results of TPR suggested Fe-Co alloy formation in this catalyst. This is possibly due to that Fe-Co alloy is in a highly dispersed state in this bimetallic catalyst, and could not be detected by XRD analysis.

5.5 Surface Adsorbed Species on the Spent Catalyst

The surface adsorbed species formed during CO_2 hydrogenation were studied by DRIFTS analysis of the spent catalyst. The DRIFT spectra of the spent Fe-Co(0.17)/Al_2O_3 and Co/Al_2O_3 catalysts after flushing the DRIFTS cell with N_2 at ambient temperature for 1 h are shown in Figure 5.3a. The DRIFT spectra revealed major IR bands at 1590, 1394 and 1377 cm^{-1} , which were ascribed to the $\nu(OCO)_{as}$, $\delta(CH)$ and $\nu(OCO)_s$ vibrational bands of adsorbed formate species, respectively [147-149]. Weak IR bands at 1634 and 1443 cm^{-1} were assigned to the $\nu(OCO)_{as}$ and $\nu(OCO)_s$ vibrational bands of adsorbed bicarbonate species [147,148,150]. An additional band at 1460 cm^{-1} appeared only in the spectrum of the spent Fe-Co(0.17)/Al_2O_3 catalyst, showing the presence of adsorbed hydrocarbon species [151,152].

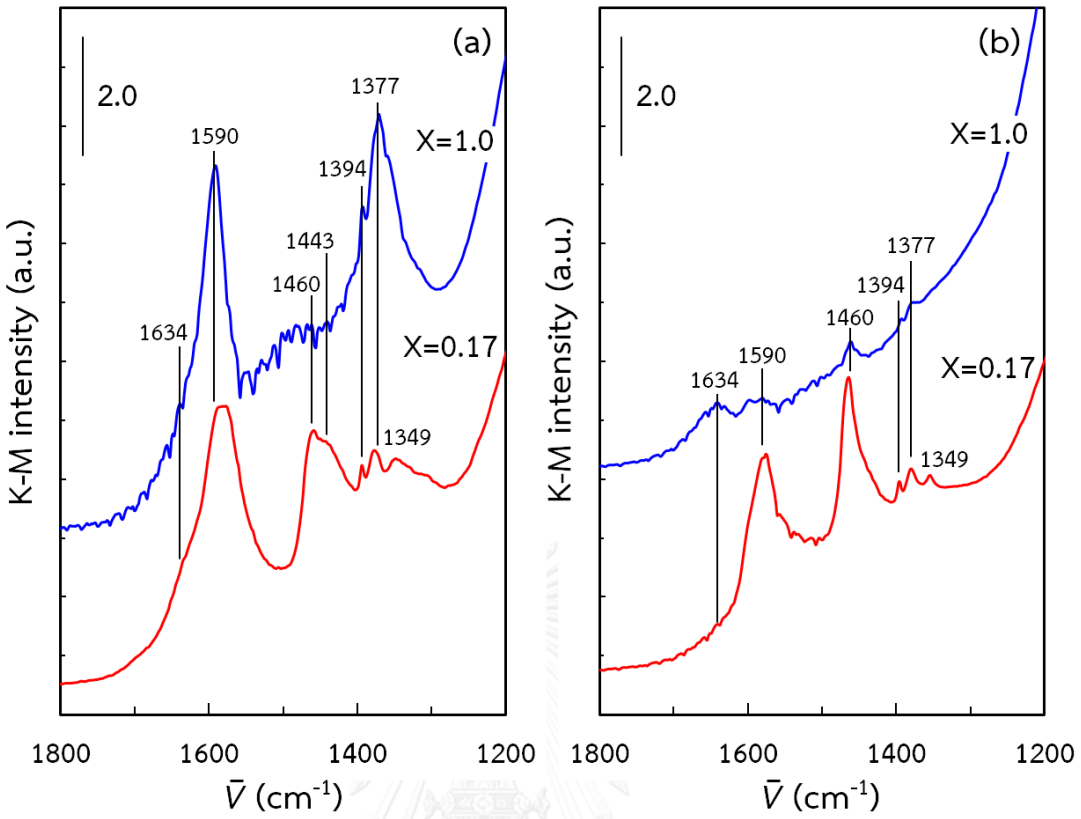

Figure 5.3 DRIFT spectra of the surface adsorbed species on spent Fe-Co(X)/Al_2O_3 catalysts after (a) N_2 purge at 298 K for 1 h and then (b) followed by H_2 reduction at 573 K for 2 h.

The spent catalysts were then reduced in a H_2 stream at 673 K for 2 h followed by flushing with N_2. The DRIFT spectra revealed that the intensities of the IR bands of adsorbed formate and bicarbonate species on the spent Co/Al_2O_3 catalyst were almost disappeared after H_2 reduction (Figure 5.3b). However, in the case of reduced-spent Fe-Co(0.17)/Al_2O_3 catalyst, only the IR bands of the adsorbed bicarbonate species (1634 and 1443 cm^{-1}) disappeared after reduction. The adsorbed formate and hydrocarbon species still being present in the spectrum of Fe-Co catalyst. DRIFTS analysis of the spent catalysts confirmed that the adsorbed bicarbonate and formate species were formed on both the Fe-Co and Co catalysts during CO_2 hydrogenation, but the formate species had a much higher stability on the Fe-Co bimetallic catalyst than on the Co catalyst.

5.6 H_2 Adsorption Properties of Fe-Co Catalysts

5.6.1 H_2-TPD Profiles of Reduced and Spent Catalysts

The adsorption states of H_2 on the Al_2O_3 supported monometallic and Fe-Co bimetallic catalysts were studied by H_2-TPD. Before the H_2-TPD experiment, the calcined catalysts were pre-reduced *in situ* at 673 K under a 50 mL min^{-1} H_2 flow for 2 h. H_2 desorption on the reduced Fe/Al_2O_3 (X = 0) catalyst mainly occurred at 770 K with several minor desorption peaks at 383, 472 and 1056 K (Figure 5.4a). The combination of Fe and a small amount of Co (X = 0.17) slightly enhanced the H_2 desorption at 770 K, whilst further increasing the Co content significantly suppressed the H_2 desorption at this temperature, but increased the amount of H_2 desorbed below 600 K. The H_2-TPD profiles of the Fe-Co bimetallic catalysts generally had similar features to that of the monometallic Fe catalyst, suggesting the segregation of Fe atoms on the Fe-Co alloy surface [134,136,143]. Interestingly, the H_2-TPD profile of the reduced Co/Al_2O_3 catalyst (X = 1) was greatly different from those of the other catalysts, where the H_2 desorption in the range of 600–900 K from the Co catalyst was negligible. Moderately adsorbed hydrogen (desorbed at 770 K) was observed only for the Fe-containing catalysts.

In the case of spent catalysts, the catalysts were pre-reduced *in situ* at 573 K under a 50 mL min^{-1} H_2 flow for 2 h prior to the H_2-TPD experiments. The adsorption states of H_2 on the spent catalysts (Figure 5.4b) were broadly similar to those of the corresponding reduced catalysts (Figure 5.4a), where the H_2 desorption mainly occurring at 700 - 720 K for the spent Fe and Fe-Co catalysts, while only a minor H_2 desorption was observed in this temperature range for the spent Co catalyst. These results indicate that the nature of the adsorption sites for H_2 on the reduced catalysts mostly remain unchanged during CO_2 hydrogenation. However, the H_2-TPD results show that the main desorption peaks observed for the fresh Fe and Fe-Co catalysts (Figure 5.4a) shifted to lower temperatures after CO_2 hydrogenation followed by passivation (Figure 5.4b). In addition, no desorption peak appeared above 1000 K for the spent Fe catalyst. These minor differences in the H_2-TPD

profiles between the corresponding reduced and spent catalysts could reflect structural changes of the Fe and Co species during CO_2 hydrogenation, such as transformation from Fe^0 to FeC_x. However, XRD analysis did not provide evidence for the formation of polycrystalline carbide species (Figure 5.2).

With respect to the H_2-TPD profiles of the spent catalysts (Figure 5.4b), it is also important to note that the peak at 340 K became more intense with increasing Co/(Co + Fe) atomic ratios at the expense of the peak at 520 K. The higher temperature peak disappeared at a Co/(Co + Fe) atomic ratio of 1, and two peaks were observed at 305 K and 440 K in this low temperature region. These changes indicate that weakly adsorbed H_2 (desorbed at ca. 300–440 K) becomes predominate on the metal surface in the presence of high Co concentrations (X ≥ 0.5).

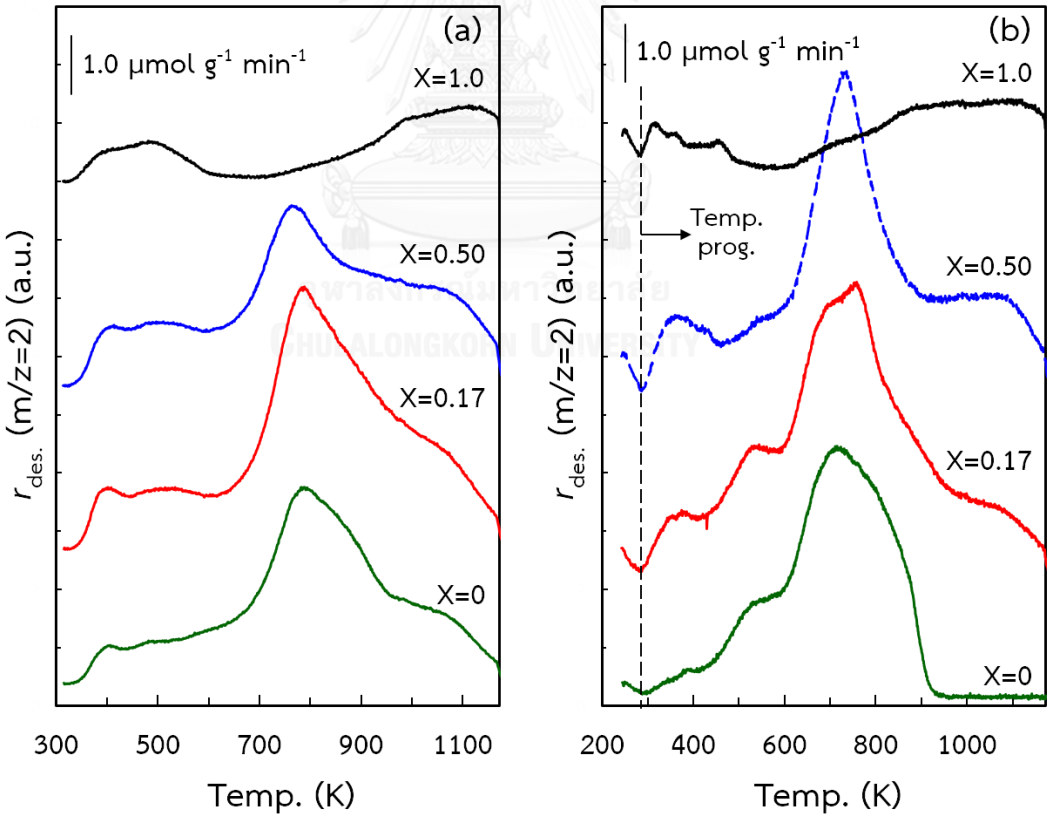

Figure 5.4 H_2-TPD profiles of the (a) reduced and (b) spent Fe-Co(X)/Al_2O_3 catalysts.

5.6.2 Decomposition of Adsorbed Formate Species during TPD

During the H_2-TPD analyses of the spent catalysts, CO and CO_2 were also detected by mass spectrometry at relatively high temperatures. The formation of CO (m/z = 28) and CO_2 (m/z = 44) during the H_2-TPD analysis of the spent Fe/Al_2O_3 and $Fe\text{-}Co(0.17)/Al_2O_3$ catalysts are shown in Figures 5.5a and 5.5b, respectively, along with their H_2 desorption profiles. CO and CO_2 were formed at the same temperature, and their formations overlapped with the H_2 desorption. Similarly, CO and CO_2 formations were also observed for the spent $Fe\text{-}Co(0.50)/Al_2O_3$ and Co/Al_2O_3 catalysts as shown in Figures 5.5c and 5.5d, respectively. DRIFTS analysis showed that the formate species still remained on the spent Fe-Co(0.17) catalyst even after H_2 reduction at 573 K (Figure 5.3b), indicating that the CO and CO_2 desorptions during H_2-TPD are caused by the decomposition of the formate species. Much weaker CO and CO_2 peaks for the spent Co catalyst were simply due to that the adsorbed formate species were almost entirely removed from the catalyst surface after H_2 reduction.

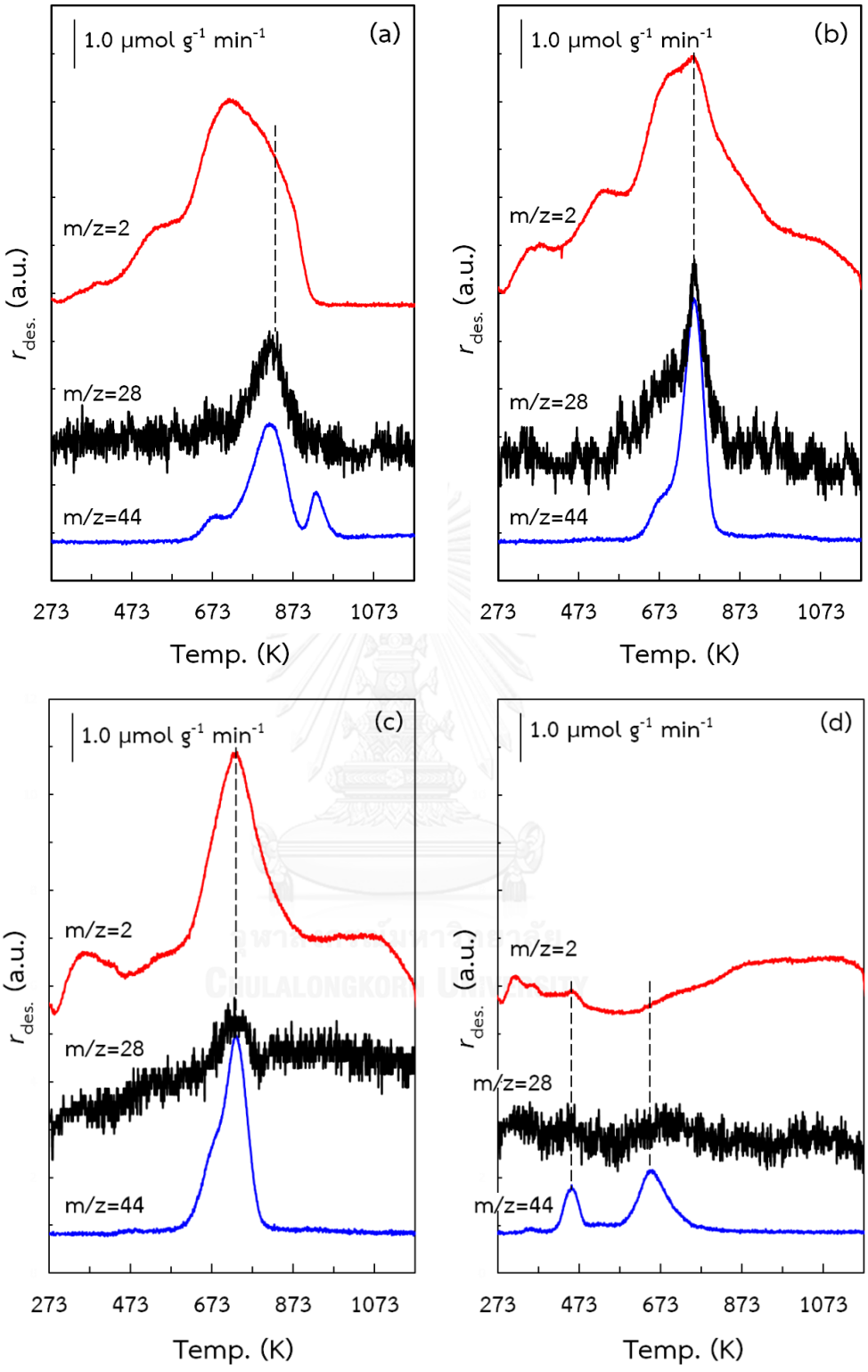

Figure 5.5 Mass traces of CO (m/z = 28) and CO_2 (m/z = 44) during the H_2-TPD of the spent (a) Fe/Al_2O_3, (b) $Fe\text{-}Co(0.17)/Al_2O_3$, (c) $Fe\text{-}Co(0.5)/Al_2O_3$ and (d) Co/Al_2O_3 catalysts along with their H_2-TPD profiles (m/z = 2).

5.6.3 Deconvolution Analysis of the H_2-TPD Profiles

To investigate the change in the H_2 adsorption properties as a function of the Co/(Co + Fe) atomic ratio, the overlapped peaks in the H_2-TPD profiles of the Fe and Fe-Co catalysts were deconvoluted using Gaussian functions. The deconvolution result for the reduced Fe/Al_2O_3 catalyst is shown in Figure 5.6. The curve created from the summation of the Gaussian peaks well fitted the experimental data. For clarity, these Gaussian peaks are denoted as types I - IV from low to high temperature, representing the different adsorption states of hydrogen on the catalyst surface. The H_2-TPD profile of the spent Fe/Al_2O_3 catalyst was also deconvoluted (Figure 5.6), where it should be noted that the fourth peak, which appeared at ca. 840 K (denoted as type IV' H_2), was caused by the decomposition of the adsorbed formate species (see section 5.6.2). Deconvolution results for the fresh and spent $Fe\text{-}Co(0.17)/Al_2O_3$ and $Fe\text{-}Co(0.5)/Al_2O_3$ catalysts are shown in Figures 5.6. Similar peaks were also observed in the TPD profiles of the spent Fe-Co bimetallic catalysts.

The adsorption states of H_2 on the monometallic Fe and Co surfaces have previously been studied by several researchers [153-156]. Two different H_2 chemisorption states, β_1 and β_2, which desorbed below ~500 K were reported on the Fe(110), Fe(100) and Fe(111) crystal surfaces [153]. Similarly, two adsorption states were reported on the reduced Co catalysts supported on amorphous silica [156]. In addition to these adsorption states, new adsorption states at higher binding energies (γ state) were reported in the H_2-TPD profiles of the supported Fe and Ni catalysts [154], and the appearance of these new states was explained by the presence of unreduced metal or support oxide species on the metal surface or in intimate contact with small metal crystallites.

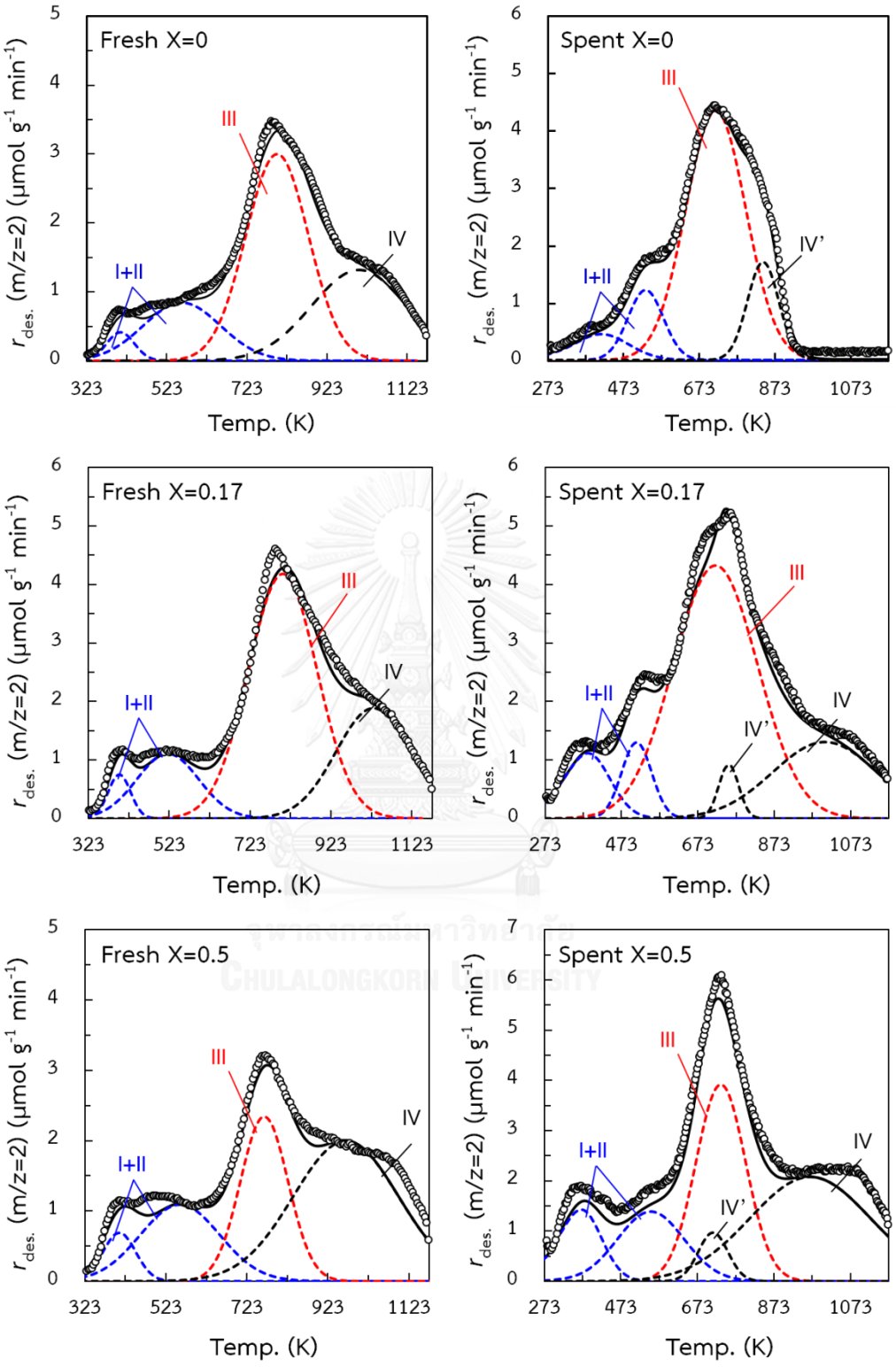

Figure 5.6 Deconvolution of the H_2-TPD profiles of reduced and spent Fe-Co(X)/Al_2O_3 catalysts. (°°°°°°) measured TPD profile, (---------) deconvoluted peaks, (———) summation of the deconvoluted peaks.

The H_2-TPD coupled with deconvolution analysis in this work revealed that 3–4 different adsorption states of H_2 were present on the reduced Fe-Co(X)/Al_2O_3 catalysts, and their quantity changed sensitively with the Co/(Co + Fe) atomic ratio of the catalyst. According to the previous reports, the weak desorption of H_2 at lower temperatures (types I and II; weakly adsorbed H_2) can be ascribed to atomic hydrogen adsorbed on the metal surface [153,156], while the major H_2 desorption observed for the Fe and Fe-Co catalysts (type III; moderately adsorbed H_2) originated from H_2 adsorbed on the Fe^0 or alloy surface decorated with unreduced metal oxide [154]. The latter assignment is consistent with the obtained TPR of the Fe and Fe-rich Fe-Co catalysts of this study, which demonstrated the presence of significant amounts of reduction-resistant metal oxides in these catalysts (section 5.3). The lack of this adsorption state on the reduced Co catalyst is possibly due to the fact that the supported Co oxide is almost completely reduced to the metallic state by H_2 reduction at 673 K. H_2 desorption was also observed above 1000 K (type IV) regardless of the Co/(Co + Fe) atomic ratio, which is possibly due to surface hydroxyl groups on the γ-Al_2O_3 surface. However, no desorption of H_2 was observed from the γ-Al_2O_3 support exposed to a H_2 stream at 673 K prior to TPD, suggesting that this peak is caused by desorption of hydrogen that had spilt-over onto the support surface rather than the hydrogen from the hydroxyl groups on the γ-Al_2O_3 surface.

5.6.4 Effect of Combining Fe and Co on H_2 Adsorption Properties

Deconvolution of the H_2-TPD profiles followed by integrating each peak gave important information about the influence of combining Fe and Co on the formation of different types of adsorbed H_2. The quantities of adsorbed H_2, as types (I + II) and III, were then plotted as a function of the Co/(Co + Fe) atomic ratio (X) in Figure 5.7. For the Co catalyst, H_2 desorbed below 600 K was regarded as type (I + II) H_2. The amount of weakly bound (type (I + II)) H_2 was weakly dependent on X, where it increased slightly with increasing Co concentration, showing a weak maximum at X = 0.4–0.5 (Figure 5.7). Since type (I + II) H_2 originates from atomic hydrogen adsorbed

on the metal surface, the amount of desorbed H_2 would be proportional to the SA of exposed metals when the stoichiometry of H_2 adsorption is assumed to be independent of the metal type. Accordingly, this small increase would reflect the increased DR of the supported metal oxides, leading to the increased metal SA. Lower metal SA of the Co catalyst was possibly due to an agglomeration of Co^0 as revealed by XRD analysis (Figure 5.2).

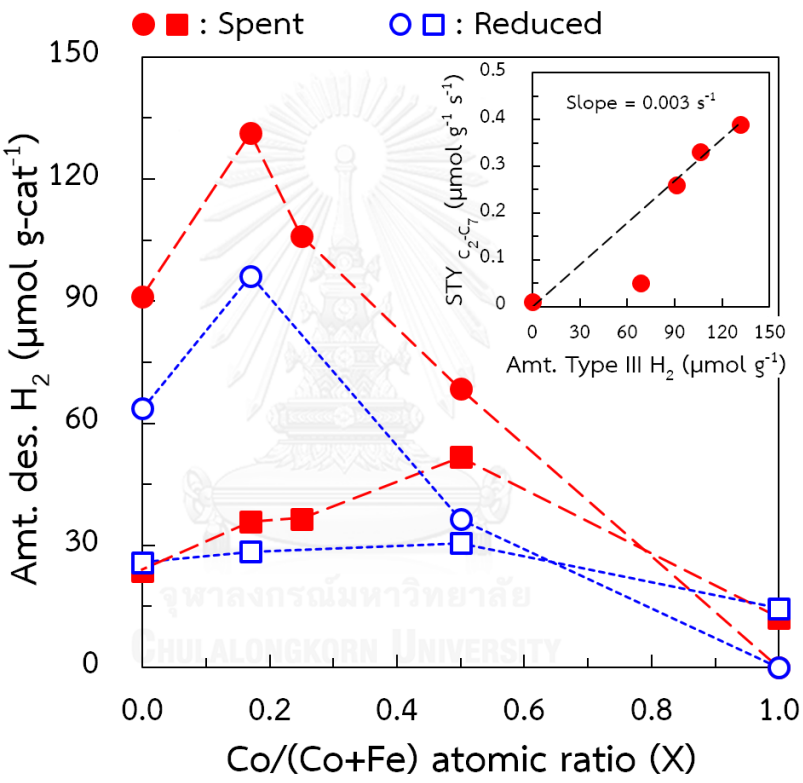

Figure 5.7 Effect of combining Fe and Co on the amount of desorbed H_2, type (I + II) H_2 (□,■) and type III H_2 (○,●), from the reduced and spent Fe-Co(X)/Al_2O_3 catalysts. The inset shows the linear relationship between the STYs of C_2-C_7 hydrocarbons (using the data from Table 5.1) and the amount of type III H_2 on the spent catalysts.

In contrast, the amount of type III H_2 (moderately adsorbed H_2) on both the reduced and spent catalysts were noticeably increased by the combination of Fe and a small amount of Co (X = 0.17), which was caused by the increased DR of the supported metal oxides, possibly through Fe-Co alloying, leading to an increased contact between the metal particles and unreduced oxides. At high Co/(Co + Fe) atomic ratios, the amount of type III H_2 sharply decreased because the DR of the supported metal oxides was significantly improved, resulting in a loss of contact with unreduced oxides. Only weakly adsorbed H_2 was observed on the Co catalyst. Schematic illustration of the proposed model for the adsorption states of hydrogen on Fe-Co(X)/Al_2O_3 catalysts is shown in Figure 5.8.

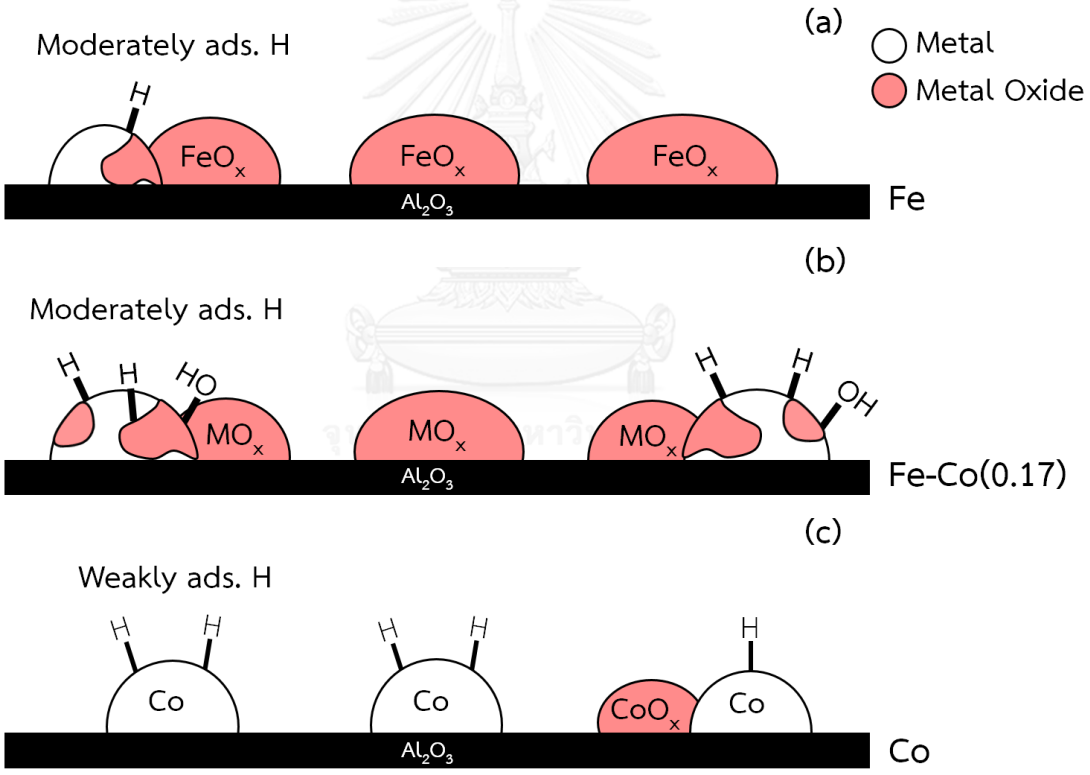

Figure 5.8 Schematic illustration of the proposed model for the adsorption states of hydrogen on the (a) Fe/Al_2O_3, (b) Fe-Co(0.17)/Al_2O_3 and (c) Co/Al_2O_3 catalysts.

5.7 Impact of the H_2 Adsorption States on the CO_2 Hydrogenation Activity

The product space-time yields (STYs) and CO_2 conversion on Fe-Co(X)/Al_2O_3 catalysts has been reported in Chapter IV [115], and are shown in Figure 5.9. The STYs of the C_2-C_7 hydrocarbons on these catalysts were maximal at 0.17 atom-Co $atom^{-1}$, and changed in a broadly similar way to the amount of type III H_2 (Figure 5.7). As shown in the inset of Figure 5.7, the STY of C_2-C_7 hydrocarbons increased linearly with the amount of type III H_2, except for the spent Fe-Co(0.5)/Al_2O_3 catalyst. This linear relationship indicated that moderately adsorbed H_2 may play an important role in the formation of C_2^+ hydrocarbons from CO_2 hydrogenation, which is quite different from CO hydrogenation on Co-Ni catalysts, where the presence of weakly adsorbed H_2 was crucial for the formation of higher hydrocarbons [135].

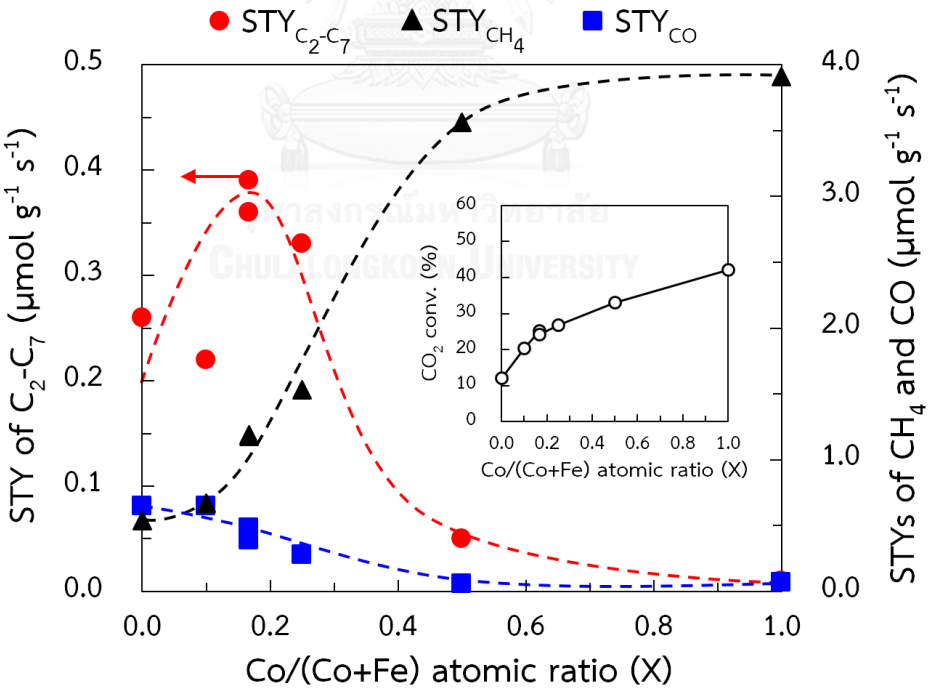

Figure 5.9 Effects of Co/(Co + Fe) atomic ratio on the STYs of C_2-C_7, CH_4 and CO hydrocarbons. The inset shows the CO_2 conversion as a function of Co/(Co + Fe) atomic ratio [115].

The different effects of the adsorbed H_2 on the CO and CO_2 hydrogenation can be explained in terms of the different coverage of CO on the metal surface. Kinetic analysis of the CO_2 hydrogenation to hydrocarbons over a Fe-based catalyst demonstrated that CO_2 is first hydrogenated to CO by the reverse water-gas shift (RWGS) reaction followed by CO hydrogenation to higher hydrocarbons by Fischer-Tropsch synthesis (FTS) [157]. Hence, in the case of CO_2 hydrogenation, the partial pressure of CO would be lower due to the thermodynamic barrier against the RWGS reaction and so the lower coverage of CO over the active metal surface. At a low CO coverage, moderately adsorbed H_2 becomes more important for the formation of higher hydrocarbons because the C_1 monomer, a chain growth carrier in the FTS, would be hydrogenated relatively slowly, providing more opportunities for carbon-carbon bond formation.

However, as shown in Figure 5.9 [115], the formation of C_2^+ hydrocarbons was significantly suppressed on the Fe-Co(0.5)/Al_2O_3 catalyst even in the presence of a significant amount of moderately adsorbed H_2. Rather, CH_4 formation accounted for 90% of the total hydrocarbon product with negligible amounts of CO formation. The lack of CO in the product from this catalysts indicated that CH_4 is mainly formed by direct hydrogenation of CO_2 [130]. Based on *in situ* DRIFTS observations, Schild et. al. [158] proposed that methanation of CO_2 on a Ni catalyst occurred by hydrogenation of the adsorbed formate species. In this work, formate was observed on both the Fe-Co and Co catalysts after CO_2 hydrogenation. Furthermore, H_2-TPD analysis of the spent catalysts revealed that weakly adsorbed H_2 (desorbed at ca. 300–440 K) became predominate at high Co loading levels. From these results, it could be inferred that the selective CH_4 formation on Fe-Co(0.5) and Co catalysts was caused by the rapid hydrogenation of the formate species in the presence of the weakly adsorbed H_2. In the absence of this adsorbed H_2, another reaction path for the RWGS reaction would become predominate on the Fe and Fe-rich Fe-Co bimetallic catalysts, since the formate species is also a crucial intermediate for RWGS reactions [159].

5.8 CO_2 Adsorption Properties of the Fe-Co Catalysts

The effect of the Fe-Co combination on the CO_2 adsorption properties of reduced and spent catalysts was also studied by TPD. The CO_2-TPD profiles of the reduced and spent Fe-Co(X)/Al_2O_3 catalysts are illustrated in Figure 5.10. The γ-Al_2O_3 support was also evaluated in the CO_2-TPD experiment as a reference, where CO_2 mainly desorbed at 350 K (Figure 5.10a). With respect to the reduced catalysts, additional shoulder peaks were observed at 550 K, otherwise the CO_2-TPD profiles of the reduced and spent catalysts were quite similar below 700 K. However, the CO_2-TPD profiles of the spent Fe and Fe-Co catalysts showed additional peaks at 720–793 K (Figure 5.10b), which were ascribed to the decomposition of the surface formate species. This is supported by the formation of CO_2 at almost the same temperatures during the H_2-TPD of the spent Fe and Fe-Co catalysts (Figure 5.5). In contrast to the H_2-TPD profiles, there was no significant difference in the CO_2-TPD profiles of the Fe, Fe-Co and Co catalysts.

The adsorption states of CO_2 on the reduced catalysts were also studied by DRIFTS analysis coupled with CO_2 adsorption, where Figure 5.11 shows the changes in the obtained DRIFT spectra of the adsorbed CO_2 with different adsorption times. Once the γ-Al_2O_3 powder was exposed to the CO_2, four IR bands emerged at 1649, 1523, 1439 and 1231 cm^{-1} (Figure 5.11a), corresponding to bicarbonate species [147,150]. Similar IR bands of the bicarbonate species were also observed in the reduced Co (Figure 5.11b) and Fe catalysts (Figure 5.11c). An additional broad band at 1495 cm^{-1} was only observed in the in DRIFT spectra of Fe catalysts, which was attributed to the carbonate species formed on the unreduced Fe oxide surface [147]. The formation of bicarbonate species on the γ-Al_2O_3 surface is consistent with a recent density functional theory based study, which demonstrated that bicarbonate is the most stable adsorbed species on a partially hydrated Al_2O_3 surface [150].

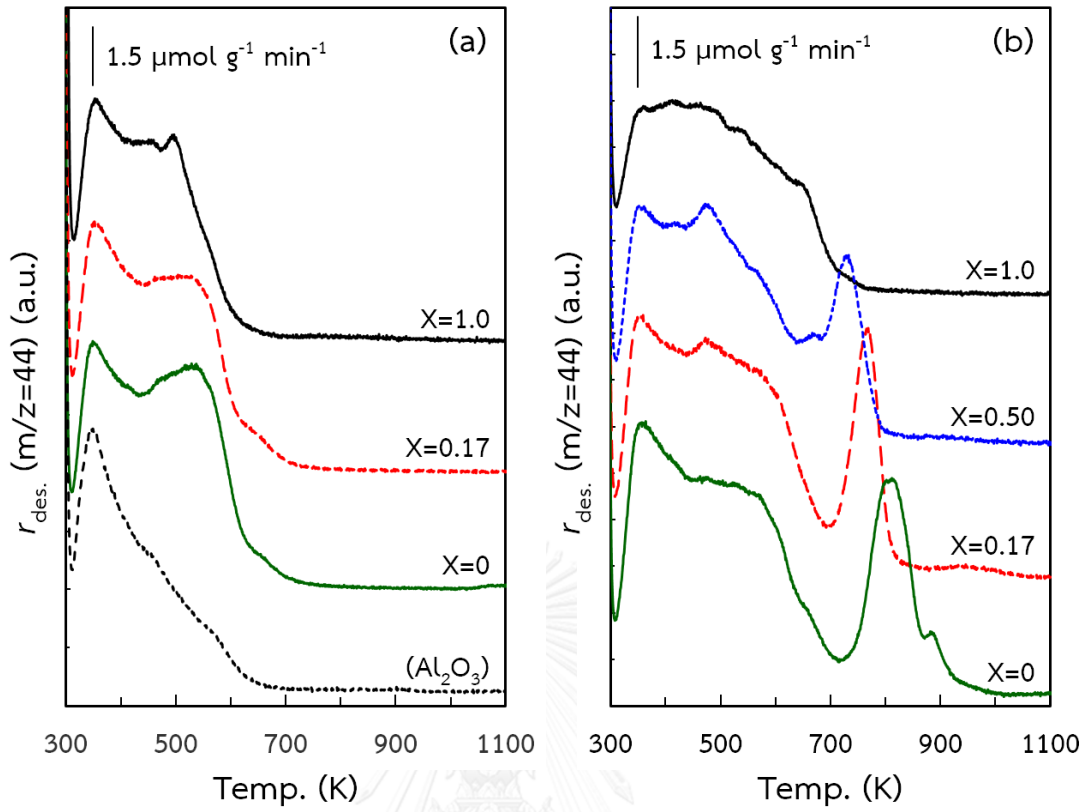

Figure 5.10 CO_2-TPD profiles of the (a) reduced and (b) spent Fe-Co(X)/Al_2O_3 catalysts.

Overall, the results of the CO_2-DRIFTS analysis showed that CO_2 desorption from the reduced catalysts mainly originates from bicarbonate and carbonate species formed on the γ-Al_2O_3 surface. The fact that CO_2 mainly interacts with the support surface rather than the metal surface would explain why the adsorption states of CO_2 were almost independent of the Co/(Co + Fe) atomic ratio of the catalyst.

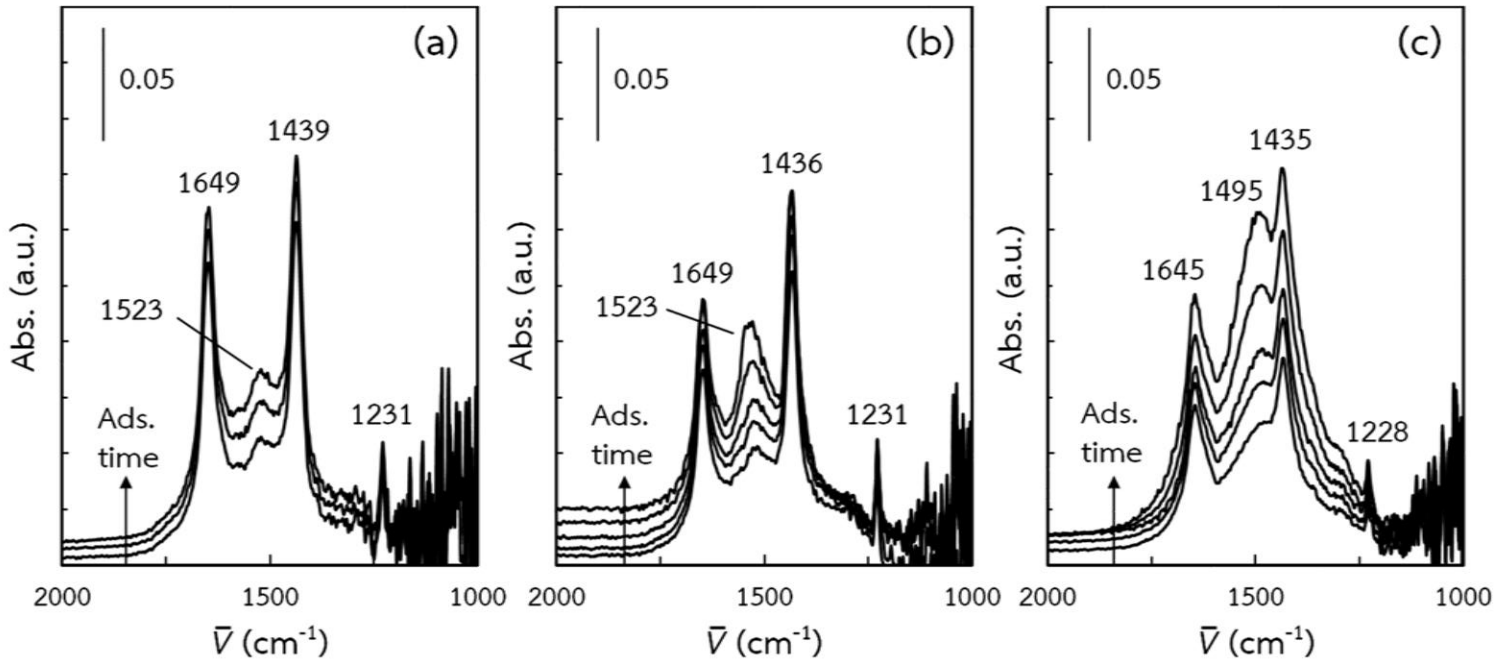

Figure 5.11 Change in the DRIFT spectra of CO_2 adsorbed on the (a) Al_2O_3 support, (b) reduced Co/Al_2O_3, and (c) reduced Fe/Al_2O_3 catalysts in the course of an adsorption time of (bottom to top) 3, 10, 20, 60, and 120 min.

CHAPTER VI

LIGHT OLEFIN SYNTHESIS FROM CO_2 HYDROGENATION OVER K-PROMOTED IRON-COBALT BIMETALLIC CATALYSTS

6.1 Introduction

Light olefins (C_2-C_4) are important building blocks for petrochemicals and polymers. With proper catalysts, hydrogenation of CO_2 could turn CO_2 into light olefins, which could reduce both the current CO_2 emission levels and the dependence on the depleting fossil fuels [4,16-18]. A significant promotion of C_2^+ hydrocarbons formation from CO_2 hydrogenation over Fe-Co/Al_2O_3 bimetallic catalysts with a low Co content (Co/(Co + Fe) = 0.17 atom-Co atom^{-1}) was reported in Chapter IV. The K promoted Fe-Co catalyst would have high activity for light olefin formation from CO_2 hydrogenation.

Potassium has been known as an effective promoter for CO and CO_2 hydrogenation to olefin-rich higher hydrocarbons over Fe-based catalysts [20,22,133,115]. However, the effects of the K-promoter have mainly dealt with monometallic Fe catalysts [19,119,120,123], while the effect of K loading on C_2-C_4 olefin formation, and the pathways for these olefins formation on Fe-Co bimetallic catalysts have not been investigated. According to Chapter V, the combination of Fe and Co led to formation of unique adsorption properties for H_2 and CO_2. It is of great interest to investigate how the K addition affects the adsorption properties and relates with CO_2 hydrogenation activities of these catalysts.

In this work, the K-promoted Fe, Co and Fe-Co bimetallic catalysts (Co/(Co + Fe) = 0.17 atom-Co atom^{-1}) with different K/Fe atomic ratios were tested for CO_2 hydrogenation and characterized by temperature-programmed desorption (TPD) to elucidate the influence of K-promoter on adsorption properties of H_2 and CO_2 on the

Fe-Co bimetallic catalysts, and their impact on the olefin formation from CO_2 hydrogenation.

6.2 Pathway for Olefin Formation from CO_2 Hydrogenation

To investigate the pathway for olefin formation from CO_2 hydrogenation, the catalysts were tested over wide range of W/F and the condition was kept constant at 573 K and 1.1 MPa. Conversion and product selectivities at about 15 - 16 h on stream were used for evaluating the activity and selectivity of the catalysts. Stable CO_2 conversion and selectivity could be obtained after 3 - 4 h on stream for all catalysts. Effects of W/F on CO_2 conversion of Fe-Co(X)/K(0.3)/Al_2O_3 catalyst are shown in Figure 6.1. CO_2 conversion increased with increasing W/F and gradually reached constant values at high W/F for all catalysts.

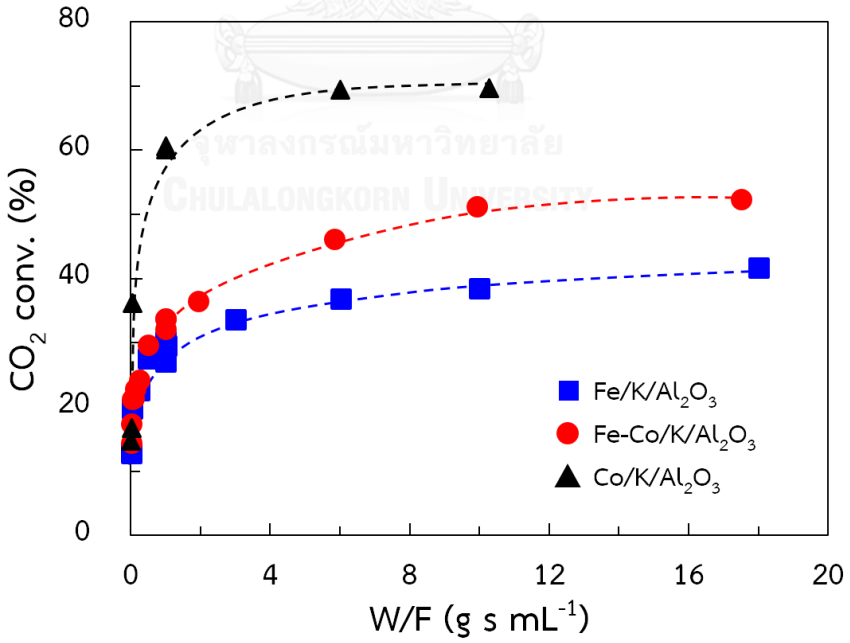

Figure 6.1 Effects of W/F on CO_2 conversion over Fe-Co(X)/K(0.3)/Al_2O_3 catalysts. (W = catalyst weight (g), F = feed gas flow rate (ml s^{-1}))

It is noted that the equilibrium CO_2 conversion at this reaction condition was around 74% (calculated using Aspen HYSYS 3.2, section 3.2). K-promoted Fe/Al_2O_3 catalyst provided lowest CO_2 hydrogenation activity, while $Co/K(0.3)/Al_2O_3$ catalyst exhibited highest activity and approached the equilibrium conversion at around W/F of 6 g s mL^{-1}. The results show that the addition of small amount of Co to Fe catalyst (Co/(Co + Fe) = 0.17 atom-Co $atom^{-1}$) could increase the CO_2 hydrogenation activity.

Figure 6.2 illustrates GC-FID chromatograms of gas-phase hydrocarbons from CO_2 hydrogenation over $Fe-Co(0.17)/K(0.3)/Al_2O_3$ catalyst at W/F of 1.01 g s mL^{-1} (the middle chromatogram). Linear paraffins were mainly observed together with a small amount of light olefins as the gas phase hydrocarbon products.

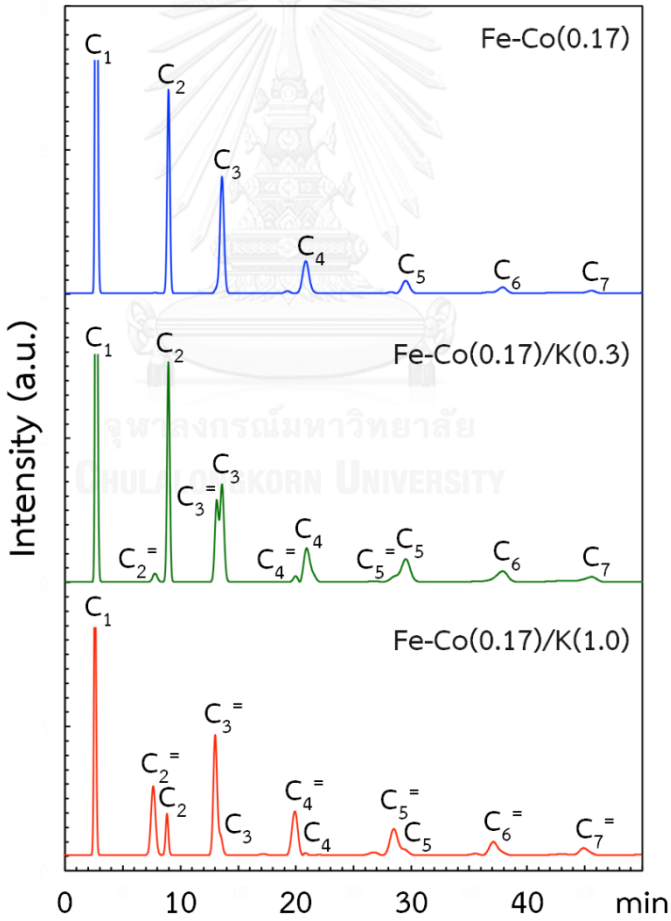

Figure 6.2 GC-FID chromatograms of gas-phase hydrocarbons from CO_2 hydrogenation on $Fe-Co(0.17)/K(Y)/Al_2O_3$ with different K/Fe atomic ratio at W/F of 1.01 g s mL^{-1}.

To investigate the pathways for these hydrocarbon formations, CO and hydrocarbon selectivity are plotted as a function of CO_2 conversion and shown in Figure 6.3. For all catalysts, the relatively similar trends were observed. The CO selectivity decreased with increasing CO_2 conversion, while hydrocarbon selectivity increased. These results suggest that CO mainly formed as a primary product from CO_2 hydrogenation (reverse water-gas shift reaction; RWGS) and the produced CO was then hydrogenated to hydrocarbons (FTS) [157], even for the K-promoted Co catalyst. The catalysts studied in this work were quite active at 573 K and 1.1 MPa, which was difficult to obtain very low conversion data. Thus, the presence of a direct hydrogenation route suggested by Riedel et al. [157] would not be excluded, but the contribution of such route would be small even if it present. Though K-promoted Co catalyst exhibited highest CO_2 hydrogenation activity, CO selectivity decreased quickly with increasing CO_2 conversion and CH_4 yield was high compared with those of Fe and Fe-Co catalysts (not shown here), due to the high hydrogenation ability of Co [115].

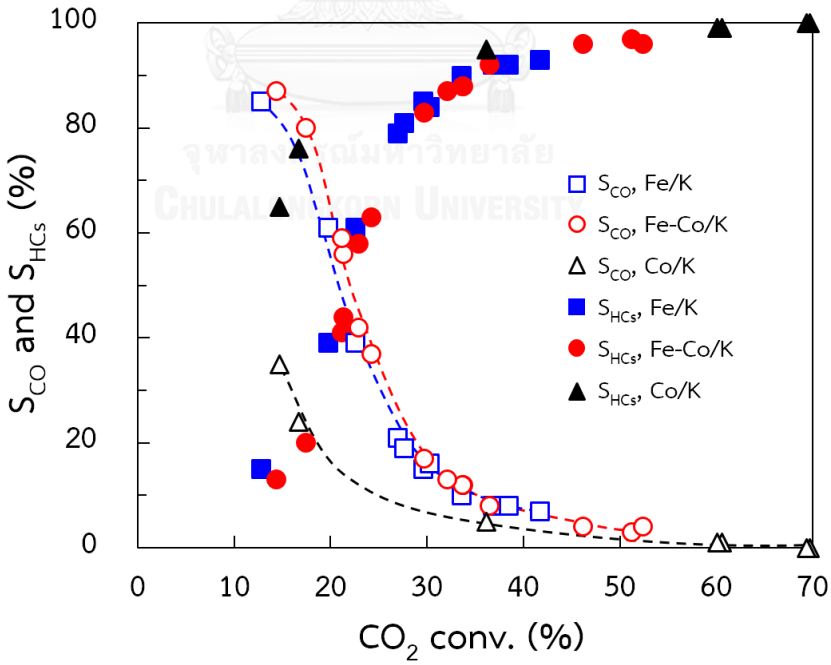

Figure 6.3 CO and hydrocarbon selectivity of Fe-Co(X)/K(0.3)/Al_2O_3 catalysts as a function of CO_2 conversion.

It is also worth noting that Fe-Co catalyst showed higher activity than Fe catalyst (Figure 6.1), but the changes of CO and hydrocarbon selectivity of both catalysts were almost similar. It could be concluded that the addition of small amount of Co increased both RWGS and FTS activities at a similar degree, resulting in an enhancement of CO_2 conversion without changing the product selectivity.

The light olefin and paraffin selectivity together with CO selectivity of Fe-Co(0.17)/K(0.3)/Al_2O_3 catalyst also plotted as a function of CO_2 conversion and shown in Figure 6.4. Both C_2-C_4 olefins and paraffins were observed at the CO_2 conversion of 14%. The paraffin selectivity increased drastically with the conversion, while the olefin selectivity increased approaching the maximum value (9%) and then decreased. Thus, light olefins and paraffins (C_2 - C_4) would form simultaneously from hydrogenation of the produced CO, but some of these olefins could be further hydrogenated to paraffins, depending on the concentration of chemisorbed hydrogen on the catalyst surface (Figure 6.5).

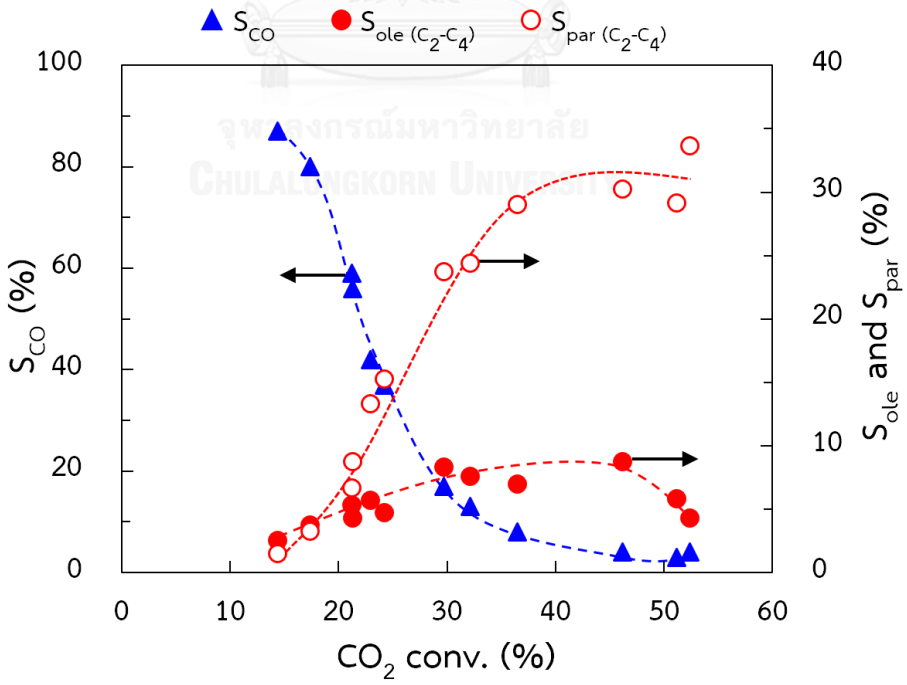

Figure 6.4 Product selectivity as a function of CO_2 conversion from hydrogenation over Fe-Co(0.17)/K(0.3)/Al_2O_3 catalysts.

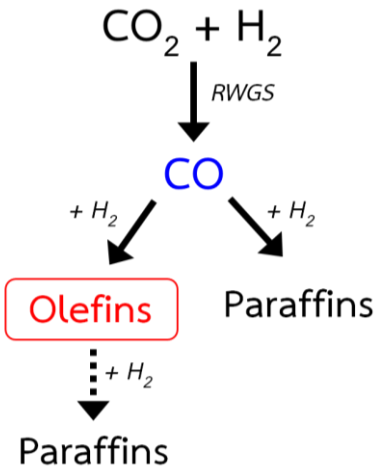

Figure 6.5 Proposed reaction pathway for CO_2 hydrogenation over K-promoted Fe-Co(0.17)/Al_2O_3 catalyst.

Hydrogenation of C_2-C_4 olefins was also confirmed by a sharp decrease in the olefin-paraffin ratio with increasing the conversion (see Figure 6.4). Therefore, suppressing olefin hydrogenation by tailoring the surface coverage of CO_2 and H_2 would cause the increase in the olefin content from CO_2 hydrogenation.

6.3 Light Olefins Synthesis from CO_2 Hydrogenation

To modify the surface coverage of H_2 and CO_2 on the catalyst surface, the amount of potassium promoter of Fe-Co catalysts was then varied. The activity and selectivity of Fe-Co(0.17)/K(Y)/Al_2O_3 catalysts (Y = 0 - 1) were investigated at hydrogenation condition of 573 K and 1.1 MPa (1.01 g s mL^{-1}). The product selectivity as a function of the K/Fe atomic ratio are shown in Figure 6.6. Without a K promoter (K/Fe = 0.0 atom $atom^{-1}$), no olefin was observed in the gas-phase hydrocarbon products (see Figure 6.2). Increasing K content resulted in a significant increase in light olefins (C_2-C_4) selectivity, at the expense of the light paraffin selectivity (Figure 6.6b).

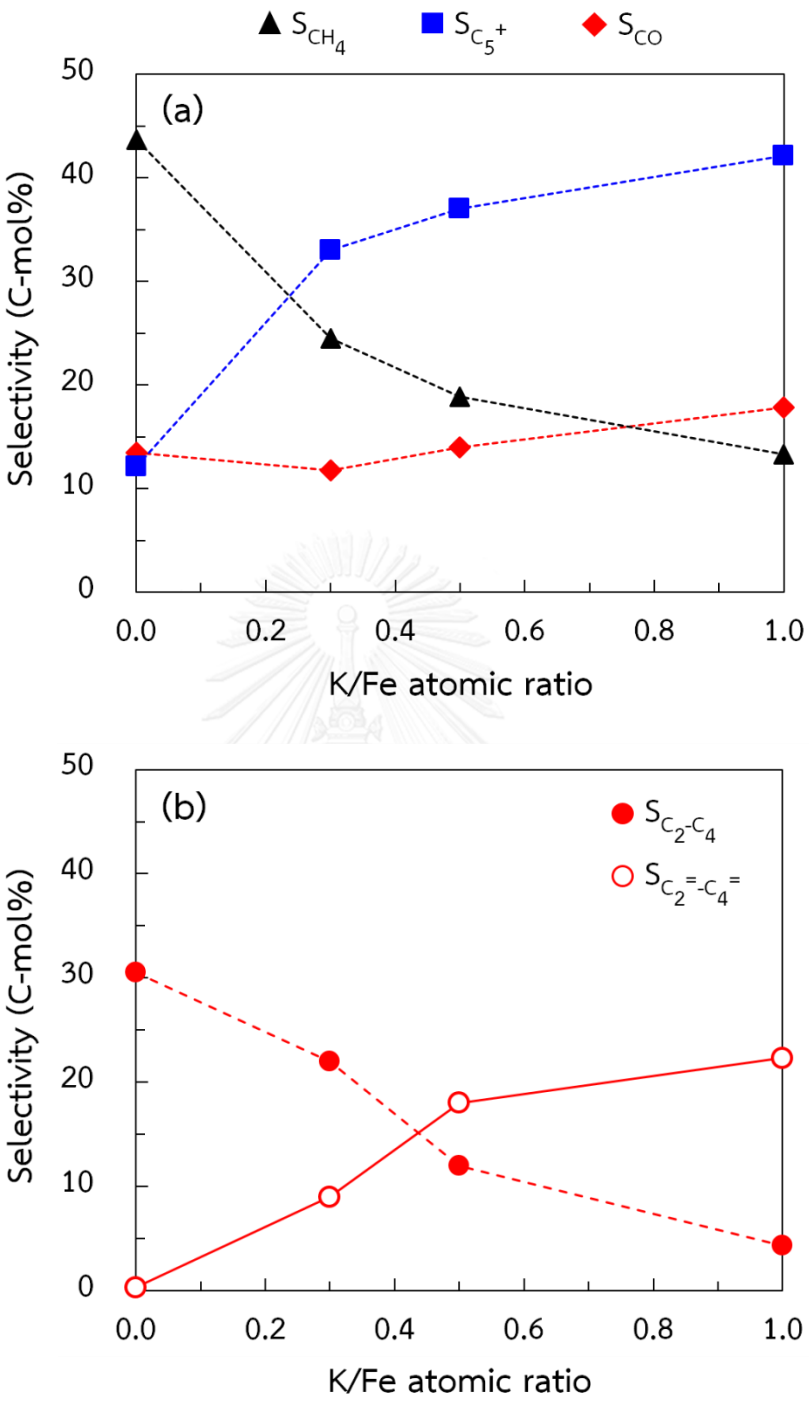

Figure 6.6 Effect of K/Fe atomic ratio (Y) on the selectivity of (a) CH_4, C_5^+ and CO, (b) C_2-C_4 and $C_2^=$-$C_4^=$ from CO_2 hydrogenation over Fe- Co(0.17)/K(Y)/Al_2O_3 catalysts.

It was also worth noting that CH_4 selectivity drastically decreased with increasing K content, while C_5^+ hydrocarbon notably increased (Figure 6.6a). Since the CO_2 conversion was hardly changed with the addition of K (Table 6.1), these results indicated that the catalyst adsorption properties of H_2 and CO_2 changed significantly with K content as discussed in the sections 6.5 and 6.6.

The light olefin yield and olefin to paraffin atomic ratio (O/P) for the Fe-Co/K catalysts are illustrated in Figure 6.7. Light olefin yield was significantly increased with increasing K promoter up to 0.5 atom atom^{-1}. Further increasing K content did not increase the olefin yield, while the O/P ratio increased sharply approaching 5 at K/Fe = 1 atom atom^{-1} [115]. These results clearly show that the K addition could suppress the olefin hydrogenation significantly, leading to a predominance of olefins in the light hydrocarbon products.

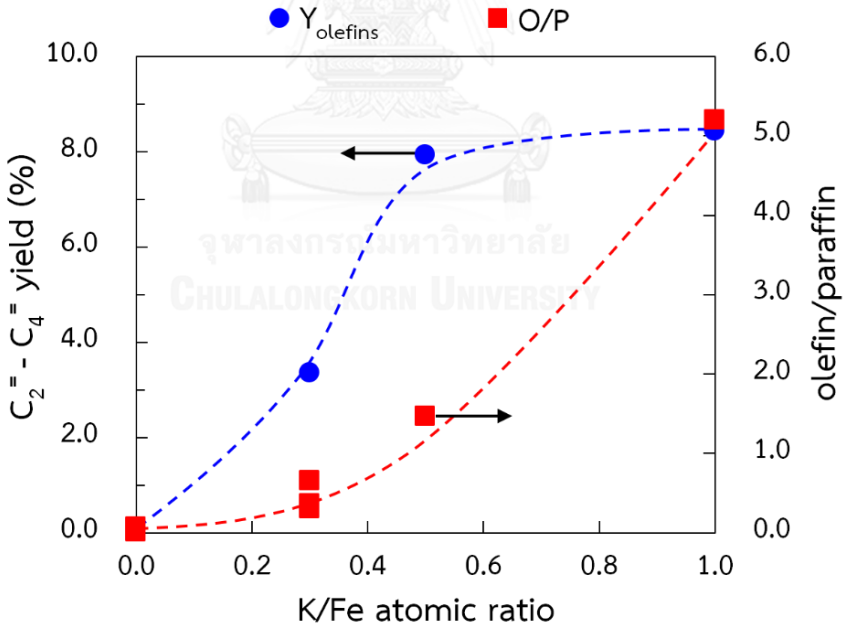

Figure 6.7 Effect of K/Fe atomic ratio (Y) on C_2-C_4 olefin yield and O/P ratio from CO_2 hydrogenation over Fe-Co(0.17)/K(Y)/Al_2O_3 catalysts [115].

Table 6.1 Physical properties and CO_2 hydrogenation activities and selectivity of Fe-Co(0.17)/K(Y)/Al_2O_3 and the catalysts from previous works.

Catalyst	SA ($m^2\ g^{-1}$)	PV ($cm^3\ g^{-1}$)	D_p (nm)	CO_2 conv. (%)	Selectivity (%, carbon based)			$C_2^=$ - $C_4^=$ yield (%)
					CH_4	C_2^{+} [e]	CO	
K/Al_2O_3	109	0.78	23	-	-	-	-	-
Fe-Co/Al_2O_3 [a), b)]	138	0.72	18	25	44	43	13	0
Fe-Co/K(0.3)/Al_2O_3 [a), b)]	127	0.66	17	34	25	64	12	3
Fe-Co/K(0.5)/Al_2O_3 [a)]	114	0.58	17	34	19	68	13	7
Fe-Co/K(1.0)/Al_2O_3 [a)]	82	0.59	22	31	13	69	18	7
Fe17 Mn12 K8/Al_2O_3 [b), c)]	N/A	N/A	N/A	19	7	69	18	4
Fe/HY [d)]	N/A	N/A	N/A	10	44	43	50	0
Fe/KY [d)]	N/A	N/A	N/A	18	8	17	39	4
Fe-Ce/HY [d)]	N/A	N/A	N/A	12	49	60	32	1
Fe-Ce/KY [d)]	N/A	N/A	N/A	20	6	20	31	5

[a)] From ref. [115]

[b)] From ref. [133]

[c)] Same composition and preparation procedure as [20]

[d)] 2.02 g s mL^{-1} (17 wt% metal loading) [128]

[e)] Including small amount of alcohols

CO_2 conversion and C_2-C_4 olefin yield of the K-promoted Fe-Co bimetallic catalyst are also compared with those of the catalysts reported previously (Table 6.1). A K-promoted Fe-Mn/Al_2O_3 catalyst was prepared according to the literature [20], and tested at hydrogenation condition of 573 K and 1.1 MPa. This table demonstrates that at the same reaction condition, Fe-Co bimetallic catalyst with K/Fe of 0.5 and 1.0 exhibited higher CO_2 conversion and light olefin yield than the promising Fe-based catalysts such as Y-zeolite supported Fe-Ce [128] and K-promoted Fe-Mn/Al_2O_3 catalysts.

6.4 Physical Properties of Calcined Catalysts

The physical properties of calcined K-promoted Fe-Co(0.17)/Al_2O_3 catalysts are provided in Table 6.1. The Brunauer-Emmett-Teller (BET) surface area (SA) and pore volume (PV) of the calcined catalysts decreased with increasing K content, while average pore diameter (D_p) barely changed. From the physical properties of the calcined K-promoted catalysts, some portions of alumina micropores were covered by potassium oxides, leading to the decrease in SA and PV of the support [19,121].

6.5 H_2 Adsorption Properties of K-Promoted Fe-Co Catalysts

6.5.1 H_2-TPD Profiles of Fe-Co(0.17)/K(Y)/Al_2O_3 Catalysts

The hydrogen adsorption states on the Al_2O_3 supported K-promoted Fe-Co bimetallic catalysts were studied by H_2-TPD (the Al_2O_3 support and K(1.0)/Al_2O_3 were also analyzed as references), the TPD profiles are illustrated in Figure 6.8. The H_2 desorption from the reduced Fe-Co(0.17)/Al_2O_3 (Y = 0) catalyst mainly occurred at 360, 565 (weakly adsorbed H_2) and 770 K (moderately adsorbed H_2) with a small desorption peak at 980 K (broken line, — — —). The weakly adsorbed H_2 on the Fe-containing catalysts was originated from atomic hydrogen adsorbed on the metal surface, while the moderately adsorbed H_2 was originated from hydrogen adsorbed on the Fe^0 or alloy surface in intimate contact with unreduced metal oxide [153,154,156]. The H_2 desorption at higher temperature (980 K) might be originated from H_2 that had spilt-over from metal onto the support surface rather than the surface hydroxyl groups on the γ-Al_2O_3 surface, since no H_2 desorption peak was observed from the H_2-TPD profile of γ-Al_2O_3 support.

The addition of a small amount of K (Y = 0.3) to Fe-Co catalysts suppressed the H_2 desorption especially the weakly adsorbed H_2, without changing the TPD profile. However, further increasing K content (Y = 1.0) (solid line) affected the TPD profile, where the peak intensity at 640 K increased. This peak would be ascribed to the desorption of hydrogen on K oxides or decomposition of $KAlH_4$ species [20], corresponding to the weak desorption peak observed at 650 K in the TPD profile of K(1.0)/Al_2O_3 (Figure 6.8).

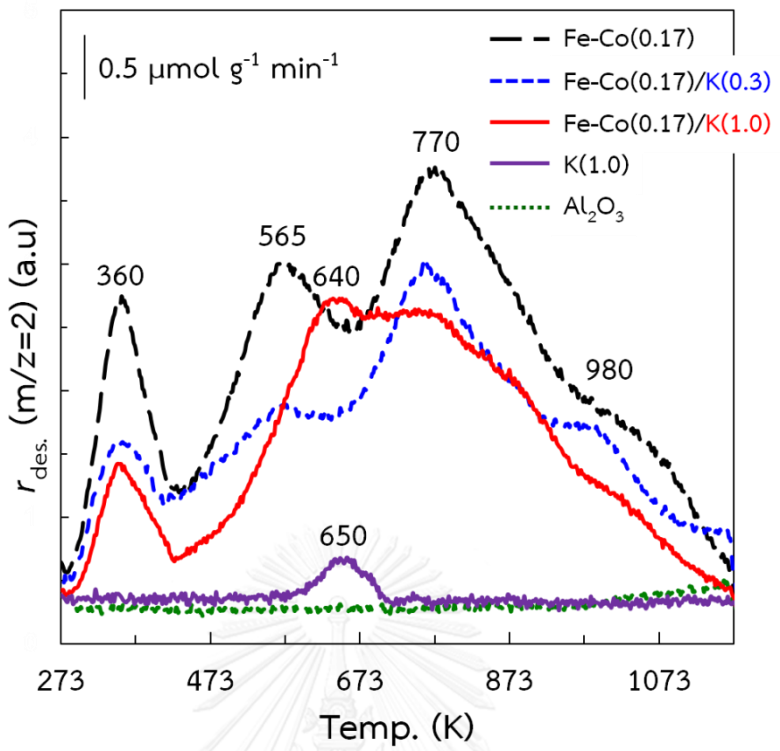

Figure 6.8 Effect of K/Fe atomic ratio (Y) on the H_2-TPD profiles of fresh Fe-Co(0.17)/K(Y)/Al_2O_3 catalysts.

6.5.2 Deconvolution Analysis of the H_2-TPD Profiles

To investigate the effect of K content on the change in the adsorption properties of H_2 quantitatively, the overlapped peaks in the H_2-TPD profiles of Fe-Co(0.17)/K(Y)/Al_2O_3 catalysts were deconvoluted using Gaussian functions. The quantities of different types of adsorbed hydrogen were achieved by integrating these Gaussian peaks, and presented in Table 6.2. Figure 6.9 also illustrates the deconvolution result of the reduced Fe-Co(0.17)/K(0.3)/Al_2O_3 catalyst as a representative example. The curve created from the summation of the Gaussian peaks fitted very well with the experimental data. These Gaussian peaks are then denoted as type I - IV from low to high temperature, representing the different adsorption states of hydrogen on the catalyst surface. The addition of small amount of K (K/Fe = 0.3) clearly decreased the amount of type (I + II) H_2 (weakly adsorbed H_2, desorbed below 600 K) from 80 to 60 μmol g-cat^{-1}, but further increase in the K/Fe

atomic ratio did not make significant change. Since type (I + II) H_2 originates from atomic hydrogen adsorbed on the metal surface, the deconvolution results indicate the coverage of the metal surface with K oxide species, as suggested for Fe catalysts [120], resulting in a decrease of weakly adsorbed H_2 (Figure 6.10a and 6.10b). The amount of type III H_2 (moderately adsorbed H_2, desorbed at 700 - 800 K) changed in a similar manner to the type (I+II) H_2. This is probably due to that some parts of the interface between reduced and unreduced metal oxides (origin of type III H_2) were also covered by K (Figure 6.10a and 6.10b). According to the H_2-TPD results in section 6.5.1, a small contribution of hydrogen from K oxide was observed in the TPD profile of K(1.0)/Al_2O_3, and denoted as type II' H_2. This peak could be ascribed to the desorption of hydrogen on K oxides or the decomposition of $KAlH_4$ species [20], but the amount of hydrogen desorbed in this temperature range was small compared to others (Figure 6.10c).

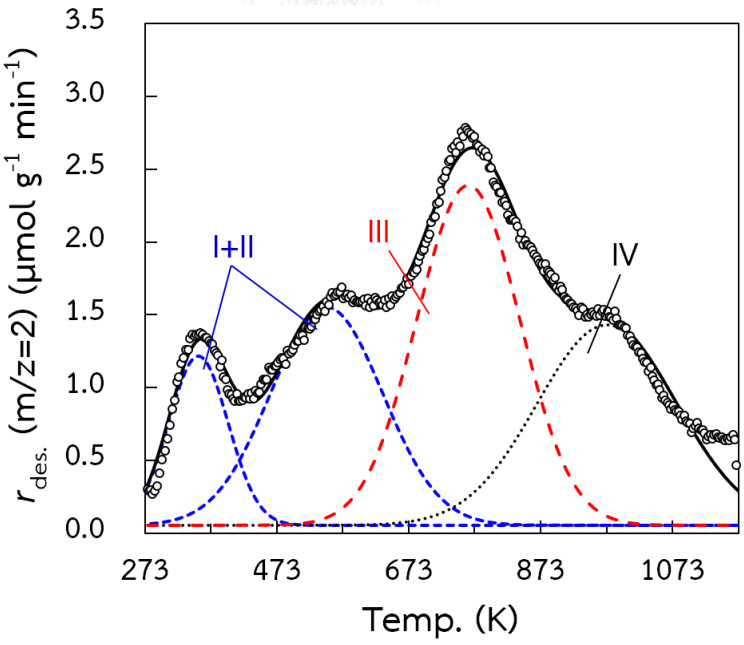

Figure 6.9 Deconvolution of the H_2-TPD profiles of the reduced Fe-Co(0.17)/K(0.3)/Al_2O_3 catalyst. (°°°°) measured TPD profile, (-------) deconvoluted peaks, (——) summation of the deconvoluted peaks (I-IV).

Table 6.2 Amount of adsorbed H_2 species over fresh Fe-Co(0.17)/K(Y)/Al_2O_3 catalysts.

Catalyst	Amount of adsorbed H_2 / μmol g-cat^{-1}					
	Type I	Type II	Type II'	Type III	Type IV	Type (I + II)
Al_2O_3 [a)]	0	0	0	0	0	0
Fe-Co(0.17)/Al_2O_3 [b)]	27.2	52.4	0.0	90.3	38.5	79.6
Fe-Co(0.17)/K(0.3)/Al_2O_3 [b)]	19.4	40.9	0.0	55.9	46.1	60.3
Fe-Co(0.17)/K(1.0)/Al_2O_3 [b)]	16.9	41.8	8.6	52.8	37.0	58.7
K(1.0)/Al_2O_3 [b)]	0	0	8.7	0	0	0

a) Reduction at 673 K for 2 h

b) Reduction at 673 K for 2 h and H_2 adsorption at 573 K (5 K min^{-1})

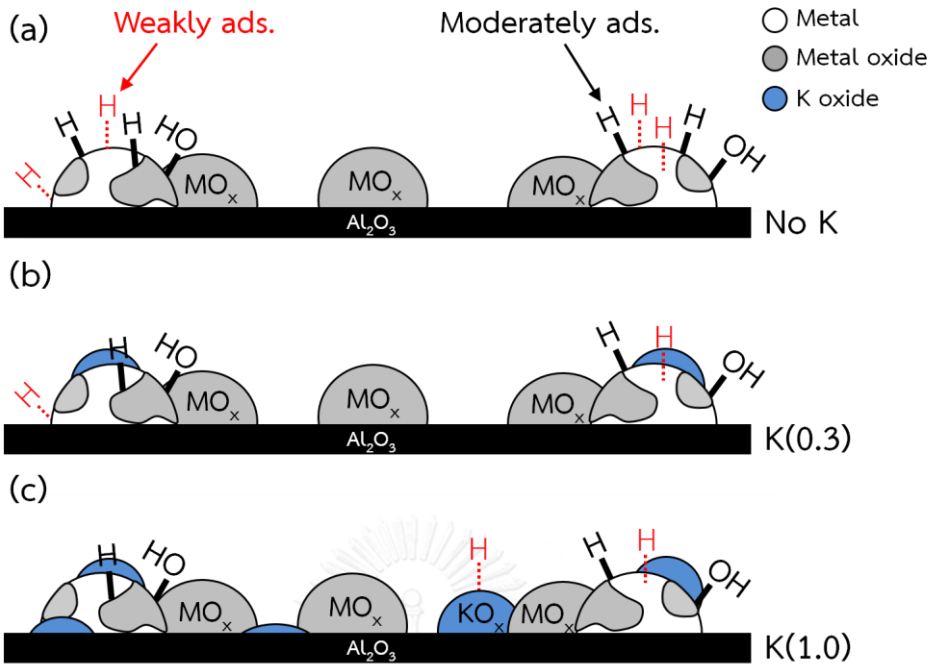

Figure 6.10 Schematic illustration of the proposed model for the adsorption states of hydrogen on the Fe-Co(0.17)/Al_2O_3 catalysts (a) without K, (b) with K/Fe = 0.3 and (c) K/Fe = 1.0 atomic ratio.

6.6 CO_2 Adsorption Properties of Fe-Co(0.17)/K(Y)/Al_2O_3 Catalysts

The effect of K addition on the CO_2 adsorption properties of reduced Fe-Co(0.17)/K(Y)/Al_2O_3 catalysts was studied by CO_2-TPD and the TPD profiles are shown in Figure 6.11. The γ-Al_2O_3 support was used as a reference, where CO_2 desorption was mainly occurred at 350 K (formation of bicarbonate species on a partially hydrated Al_2O_3 surface [150]). For the reduced Fe-Co(0.17)/Al_2O_3 catalysts (Y = 0) (broken line, — — —), CO_2 desorption was observed at 350 and 530 K, which mainly originated from bicarbonate and carbonate species formed on the γ-Al_2O_3 surface. The amount of desorbed CO_2 at 350 K drastically increased by the addition of a small amount of K (Y = 0.3). The CO_2-TPD profile significantly changed with further increase in K content (Y = 1.0). The weakly adsorbed CO_2 (desorbed at 350 K) was suppressed, while two desorption peaks at 630 and 880 were clearly observed (solid line). The desorption peaks at 630 and 880 K might be originated from a bidentate carbonate species and adsorbed CO_2 on potassium ferrite ($K_2Fe_2O_4$), respectively [160-162].

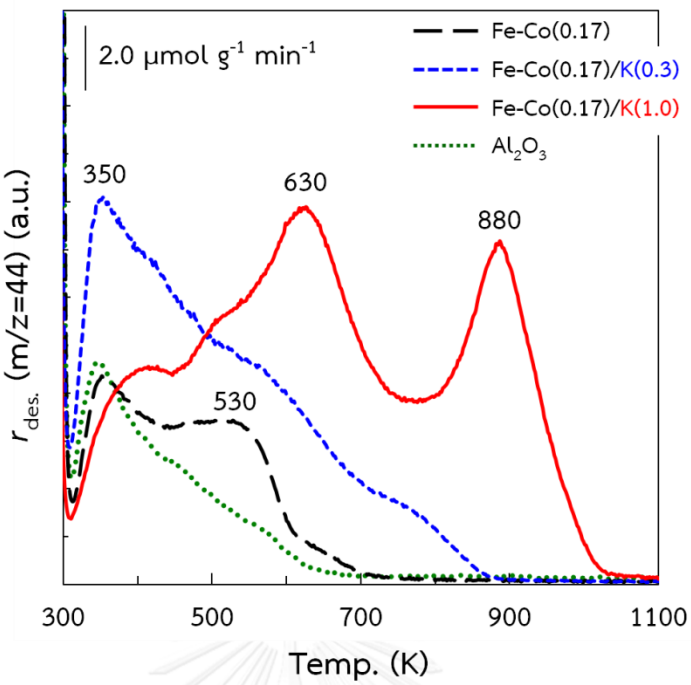

Figure 6.11 Effect of K/Fe atomic ratio (Y) on the CO_2-TPD profiles of fresh Fe-Co(0.17)/K(Y)/Al_2O_3 catalysts.

6.7 Surface Adsorbed Species on the Spent Catalysts

The surface adsorbed species on Fe-Co(0.17)/K(Y)/Al_2O_3 catalysts formed during CO_2 hydrogenation were studied by diffuse reflectance Infrared Fourier transform spectroscopy (DRIFTS) of the spent catalysts. After flushing the DRIFTS cell with N_2 at ambient temperature for 1 h, DRIFT spectrum were recorded, four major IR bands at 1580, 1460, 1410 and 1330 cm^{-1} were observed on all catalysts (Figure 6.12a). These bands at 1580, 1410 and 1330 cm^{-1} were ascribed to the ν(OCO)as, δ(CH) and ν(OCO)s vibrational bands of adsorbed formate species, respectively [34-36]. Weak IR bands at 1460 cm^{-1} showed the presence of adsorbed hydrocarbon species [38, 39]. The intensity of these IR bands significantly increased with increasing K content, suggesting more C_2^+ hydrocarbons were formed on K-promoted catalysts.

The spent catalysts were then reduced under flowing H_2 followed by flushing with N_2 and the DRIFT spectra were then recorded under N_2 flow. The DRIFT spectra revealed that, after H_2 reduction, the intensities of the IR bands of adsorbed formate species were slightly decreased, while the change of adsorbed hydrocarbon species was negligible (Figure 6.12b). DRIFTS analysis of the spent catalysts revealed that the adsorbed formate species were formed on all Fe-Co(0.17)/K(Y)/Al_2O_3 catalysts during CO_2 hydrogenation, and K could facilitate the adsorption of these formate intermediate species.

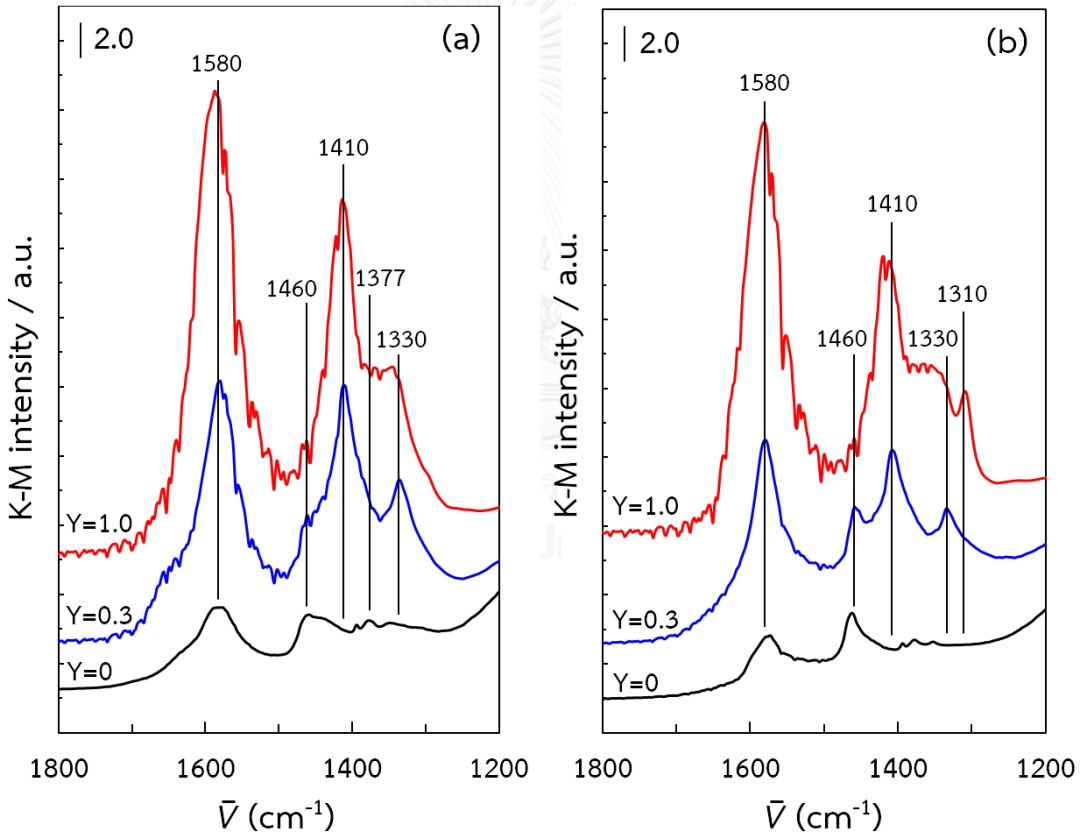

Figure 6.12 DRIFT spectra of the surface adsorbed species on spent Fe-Co(0.17)/K(Y)/Al_2O_3 catalysts after (a) N_2 purge at 298 K for 1 h and then (b) followed by H_2 reduction at 573 K for 2 h.

6.8 Effects of H_2 and CO_2 Adsorption Properties on CO_2 Hydrogenation Activity

As discussed in section 6.3, the K addition resulted in a significant increase in light olefin (C_2-C_4) selectivity, at the expense of light paraffin selectivity. Moreover, CH_4 selectivity drastically decreased with K content, while C_5^+ hydrocarbon notably increased. These results could be explained by changes of H_2 and CO_2 adsorption properties of catalysts with the K content. According to the H_2-TPD results (section 6.5, Figure 6.8), increasing K content of catalyst resulted in the decrease in the amount of weakly adsorbed H_2 (type I + II), which was important for further hydrogenation of produced olefins and CH_4 formation [19,119-123]. From CO_2-TPD results, the CO_2 adsorption drastically increased with K content (section 6.6, Figure 6.11), providing more chances of C-C bond formation. These changes in H_2 and CO_2 adsorption properties of theses catalysts resulted in an increase in light olefin and C_5^+ hydrocarbons selectivity. CO selectivity also slightly increased with K/Fe atomic ratio due to that K could promote the RWGS activity of the catalysts by providing the additional active sites to generate the formate species (intermediate species of RWGS reaction). This reason was in accordance with the DRIFTS results that the adsorbed formate species increased with K content (section 6.7, Figure 6.12) [35].

CHAPTER VII

CONCLUSIONS AND RECOMMENDATIONS

7.1 Conclusions

(i) Comparative Study of Fe-based Bimetallic Catalysts for CO_2 Hydrogenation to Higher Hydrocarbons

The effect of combining Fe and the second transition metals such as Co, Ni, Cu, Pd on the CO_2 hydrogenation activity and selectivity of Al_2O_3-supported catalysts for higher hydrocarbon synthesis was studied at 573 K and 1.1 MPa. The monometallic catalysts were also prepared and studied under the same reaction condition as references. Among the monometallic catalysts studied in this work, only Fe catalyst could synthesize C_2^+ hydrocarbons, while Ni and Co catalysts selectively yielded CH_4 as a product. CO_2 conversion on Ni catalyst was closed to an equilibrium CO_2 conversion (ca. 74%) at this reaction condition, which made this catalyst suitable for synthesizing the synthetic natural gas via hydrogenation of CO_2.

The combination of Fe and a small amount of each of the second transition metals (Co, Cu, Pd; X = 0.1 atom atom^{-1}) resulted in a notable enhancement of higher hydrocarbon formation from CO_2 hydrogenation, where Fe-Cu catalyst (without K) exhibited highest C_2^+ hydrocarbon yields. Though the combination of Fe and Ni at X = 0.1 atom atom^{-1} provided the strongest enhancement of CO_2 conversion but this catalyst yielded CH_4 selectively. Much lower Ni content was required for promoting the higher hydrocarbon formation compared to others, due to the strong hydrogenating ability of Ni. These results indicate an importance of tailoring the adsorption properties of hydrogen and carbon species for facilitating higher hydrocarbon formation from CO_2 hydrogenation. The results also show that K was an effective promoter for both Fe-Co and Fe-Cu bimetallic catalysts, where K-promoted Fe-Co(0.1) catalysts exhibited highest C_2^+ hydrocarbon yields.

(ii) CO_2 Hydrogenation to Higher Hydrocarbons over Fe-Co Bimetallic Catalysts

The effects of Co content in the Al_2O_3-supported Fe-Co bimetallic catalysts on the CO_2 hydrogenation activity and selectivity were investigated. A strong bimetallic promotion of C_2^+ hydrocarbons formation from CO_2 hydrogenation was obtained by combining Fe and a small amount of Co. The results show that the space-time yield (STY) of C_2-C_7 hydrocarbons approached the maximum at the Co/(Co + Fe) ~ 0.17 atom atom^{-1}, while the STY of CH_4 increased almost linearly with increasing the Co/(Co + Fe) atomic ratio up to 0.50. It is also worth noting that the maximum STY of C_2-C_7 hydrocarbons is notably higher than the simple summation of those over the monometallic Fe/Al_2O_3 and Co/Al_2O_3 catalysts, indicating a significant bimetallic promotion of CO_2 hydrogenation to C_2^+ hydrocarbons by combining Fe and a small amount of Co.

The addition of K to Fe-Co bimetallic catalysts further enhance CO_2 conversion and the STY of C_2-C_7 hydrocarbons, while it suppressed CH_4 formation. The olefin content in the product also increased with the K content, and olefins predominated in the higher hydrocarbons when the catalysts contained large amount of K (K/Fe $\geq$ 0.5 atom atom^{-1}). The liquid product containing linear alpha olefins as a main products with carbon numbers up to 27 was successfully synthesized from CO_2 hydrogenation using the Fe-Co bimetallic catalyst with high K/Fe atomic ratio (1.0 atom atom^{-1}).

The K-promoted Fe-Co bimetallic catalysts with desired compositions also show significant advantages in higher hydrocarbons synthesis over the K-promoted Fe/Al_2O_3 and Fe-Mn/Al_2O_3 catalysts with higher Fe loadings under the same reaction conditions. These results are important for developing the new catalysts and fundamental understanding of the mechanism involved in activation of CO_2 and H_2 towards carbon – carbon bond formation for higher hydrocarbons synthesis.

(iii) H_2 and CO_2 Adsorption Properties of Fe-Co Bimetallic Catalysts and Their Activities for CO_2 Hydrogenation to higher Hydrocarbons

Physicochemical properties of the Al_2O_3-supported Fe-Co bimetallic catalysts with various Co/(Co + Fe) atomic ratios were studied to develop a fundamental understanding of the bimetallic promotion of C_2^+ hydrocarbons formation from CO_2 hydrogenation. The temperature-programmed reduction (TPR) results showed that the TPR profile of Fe/Al_2O_3 catalyst was clearly changed by combining Fe with Co. The degree of reduction of the supported metal oxides also increased with the Co content, which possibly due to the formation of Fe-Co alloy.

The surface species formed during CO_2 hydrogenation were studied by the diffuse reflectance infrared Fourier transform spectroscopy (DRIFTS). The results indicated that the adsorbed bicarbonate and formate species were formed on both the Fe-Co and Co catalysts during CO_2 hydrogenation, but the adsorbed formate species on the Fe-Co bimetallic catalyst had much higher stability than those on the Co catalyst.

The temperature-programmed desorption of H_2 (H_2-TPD) revealed that the moderately adsorbed H_2 (type (III) H_2) was the major adsorbed species on the Fe and Fe-rich Fe-Co bimetallic catalysts. This moderately adsorbed H_2 could hydrogenate the C_1 monomer relatively slow, resulting in a higher chance for carbon-carbon bonds of hydrocarbons to be formed. The amount of this type III H_2 was increased by the combination of Fe and a small amount of Co, leading to the bimetallic promotion of C_2^+ hydrocarbons formation. H_2-TPD analysis also suggested a crucial role of the weakly adsorbed H_2 in the selective CH_4 formation on catalysts with high Co/(Co + Fe) atomic ratios (≥ 0.5). In contrast to the H_2-TPD profiles, there was no significant difference in the CO_2-TPD profiles of the Fe, Fe-Co and Co catalysts. These results imply the importance of governing the H_2 adsorption states for improving the formation of C_2^+ hydrocarbons and suppressing the undesirable formation of CH_4.

(iv) Light Olefin Synthesis from CO_2 Hydrogenation over K-Promoted Fe-Co Bimetallic Catalysts

K-promoted Fe, Co and Fe-Co catalysts were tested for CO_2 hydrogenation at 573 K and 1.1 MPa over wide range of W/F in order to investigate the pathway for olefin formation from CO_2 hydrogenation. K-promoted Co/Al_2O_3 exhibited highest CO_2 conversion followed by Fe-Co(0.17)/Al_2O_3 and Fe/Al_2O_3 catalysts, respectively. For all catalysts, CO mainly formed as a primary product from CO_2 hydrogenation via reverse water-gas shift (RWGS) reaction, and the produced CO was then hydrogenated to light olefins and paraffins simultaneously via Fischer-Tropsch synthesis (FTS). Some of these olefins could be further hydrogenated to paraffins, depending on the concentration of chemisorbed hydrogen on the catalyst surface. Although Fe-Co catalyst showed higher activity than Fe catalyst, but the changes of CO and hydrocarbon selectivity of both catalysts were almost similar, suggests that the addition of small amount of Co increased both RWGS reaction and FTS activities at a similar degree, resulting in an enhancement of CO_2 conversion without changing selectivity of the product.

The K-promoted Fe-Co(0.17)/Al_2O_3 catalysts with various potassium content (K/Fe = 0 - 1 atom atom^{-1}) were also tested for the CO_2 hydrogenation. The highly alkalized Fe-Co catalyst (K/Fe = 1 atom atom^{-1}) was an effective catalyst for synthesizing light olefins from CO_2 hydrogenation. By increasing the K/Fe atomic ratio, the amount of weakly adsorbed H_2 decreased, while it increased CO_2 adsorption, which lowered the possibility for hydrogenation of the produced olefins. Moreover, at the same reaction condition, Fe-Co(0.17)/K(1.0)/Al_2O_3 catalyst also showed higher CO_2 conversion and light olefin yield than the K-promoted Fe-Ce and Fe-Mn/Al_2O_3, known as promising catalysts for olefin production from CO_2 hydrogenation.

7.2 Recommendations

In this work, the Fe-Co bimetallic catalyst exhibited promising CO_2 hydrogenation activity and selectivity to higher hydrocarbons. A further study of catalytic CO_2 hydrogenation to higher hydrocarbons over Fe-Co bimetallic catalysts should be concerned with the following aspects:

1. This research revealed that Fe-Co bimetallic promotion was closely related to the perimeter sites between small metal particles and unreduced metal oxide species, depending on the dispersion and reducibility of active metals. Many literatures reported that type of support materials played a critical role on them. Therefore, the effects of support materials for the Fe-Co bimetallic catalyst on the CO_2 hydrogenation activity and selectivity to higher hydrocarbons are of particular interest, especially carbon-based support that have a weak interaction with Fe and Co.
2. This work reveals that CO_2 hydrogenation to higher hydrocarbons over K-promoted Fe-Co bimetallic catalyst occurred via a two-step reaction, namely RWGS reaction and FTS. Since water is formed from both reactions, the equilibrium of these reactions could be shifted to the right by removing the produced water from the catalyst. Therefore, the modification of the catalysts for improving the hydrophobicity and the influence of the hydrophobicity on CO_2 hydrogenation activity and selectivity to higher hydrocarbons would be further studied.
3. The source of CO_2 in this work was a gas mixture containing 24 vol% CO_2/ 72 vol% H_2/ 4 vol% Ar. However, the flue gas from industry usually consists of other gases in addition to CO_2 such as N_2, CO and H_2O. To study the application of Fe-Co bimetallic catalyst for the direct hydrogenation of the CO_2 in the flue gas, CO_2 hydrogenation using the feed gas containing impurity close to the flue gas composition should be investigated.

REFERENCES

[1] Melillo, J.M., McGuire A.D., Kicklighter D.W., Moore B., Vorosmarty C.J., Schloss A.L. Global climate change and terrestrial net primary production. Nature 363 (1993): 234-240.

[2] Schimel, D.S. Terrestrial ecosystems and the carbon cycle. Global change biology 1 (1995): 77-91.

[3] Jacobson, M.Z. Review of solutions to global warming, air pollution, and energy security. Energy & Environmental Science 2 (2009): 148-173.

[4] Song, C. (2002) CO_2 Conversion and Utilization: An Overview. In: C. Song, A.F. Gaffney, Fujimoto K (eds) CO_2 Conversion and Utilization. American Chemical Society, Washington DC.

[5] Mikkelsen, M., Jorgensen M., Krebs F.C. The teraton challenge. A review of fixation and transformation of carbon dioxide. Energy & Environmental Science 3 (2010): 43-81.

[6] Balat, H., Öz C. Technical and economic aspects of carbon capture and storage–a review. Energy, Exploration & Exploitation 25 (2007): 357-392.

[7] Aresta, M., Dibenedetto A. Utilisation of CO_2 as a chemical feedstock: opportunities and challenges. Dalton Transactions (2007): 2975-2992.

[8] Olivier, J.G., Janssens-Maenhout G., Muntean M., Peters J.A. (2013) Trends in global CO_2 emissions: 2013 report, PBL Netherlands Environmental Assessment Agency,

[9] Zhao, Y., Wang L., Hao X., Wu J. The kinetic study of light alkene syntheses by CO_2 hydrogenation over Fe-Ni catalysts. Frontiers of Chemical Engineering in China 4 (2010): 153-162.

[10] Jiang, Z., Xiao T., Kuznetsov V.L., Edwards P.P. Turning carbon dioxide into fuel. Philos Trans R Soc, A 368 (2010): 3343-3364.

[11] Fulkerson, W., Judkins R.R., Sanghvi M.K. Energy from fossil fuels. Scientific American 263 (1990): 128-135.

[12] Marbán, G., Valdés-Solís T. Towards the hydrogen economy? International Journal of Hydrogen Energy 32 (2007): 1625-1637.

[13] Song, C., Schobert H.H. Opportunities for developing specialty chemicals and advanced materials from coals. Fuel Processing Technology 34 (1993): 157-196.

[14] Schobert, H.H., Song C. Chemicals and materials from coal in the 21st century. Fuel 81 (2002): 15-32.

[15] Weisz, P.B. Basic choices and constraints on long-term energy supplies. Physics Today 57 (2004): 47-52.

[16] Song, C. Global challenges and strategies for control, conversion and utilization of CO_2 for sustainable development involving energy, catalysis, adsorption and chemical processing. Catalysis Today 115 (2006): 2-32.

[17] Centi, G., Perathoner S. Opportunities and prospects in the chemical recycling of carbon dioxide to fuels. Catalysis Today 148 (2009): 191-205.

[18] Wang, W., Wang S., Ma X., Gong J. Recent advances in catalytic hydrogenation of carbon dioxide. Chemical Society Reviews 40 (2011): 3703-3727.

[19] Choi, P.H., Jun K.-W., Lee S.-J., Choi M.-J., Lee K.-W. Hydrogenation of carbon dioxide over alumina supported Fe-K catalysts. Catalysis Letters 40 (1996): 115-118.

[20] Dorner, R.W., Hardy D.R., Williams F.W., Willauer H.D. K and Mn doped iron-based CO_2 hydrogenation catalysts: Detection of $KAlH_4$ as part of the catalyst's active phase. Applied Catalysis A: General 373 (2010): 112-121.

[21] Nam, S.-S., Kim H., Kishan G., Choi M.-J., Lee K.-W. Catalytic conversion of carbon dioxide into hydrocarbons over iron supported on alkali ion-exchanged Y-zeolite catalysts. Applied Catalysis A: General 179 (1999): 155-163.

[22] Dorner, R.W., Hardy D.R., Williams F.W., Willauer H.D. C_2-C_5^+ olefin production from CO_2 hydrogenation using ceria modified Fe/Mn/K catalysts. Catalysis Communications 15 (2011): 88-92.

[23] DOE/EPA Fuel Economy. Internet Resource Developed by U.S. Department of Energy and U.S. Environmental Protection Agency. Accessed May 20, 2001.

[24] Manzer, L.E. (2002) CO_2 Emission Reductions: An Opportunity for New Catalytic Technology. In: C. Song, A.F. Gaffney, Fujimoto K (eds) CO_2 Conversion and Utilization. American Chemical Society, Washington DC.

[25] Metz, B., Davidson O., de Coninck H., Loos M., Meyer L. (2005) IPCC special report on carbon dioxide capture and storage. Intergovernmental Panel on Climate Change, Geneva (Switzerland). Working Group III,

[26] Susan, S. (2007) Climate change 2007-the physical science basis: Working group I contribution to the fourth assessment report of the IPCC, Cambridge University Press,

[27] Arakawa, H., Aresta M., Armor J.N., Barteau M.A., Beckman E.J., Bell A.T., Bercaw J.E., Creutz C., Dinjus E., Dixon D.A., Domen K., DuBois D.L., Eckert J., Fujita E., Gibson D.H., Goddard W.A., Goodman D.W., Keller J., Kubas G.J., Kung H.H., Lyons J.E., Manzer L.E., Marks T.J., Morokuma K., Nicholas K.M., Periana R., Que L., Rostrup-Nielson J., Sachtler W.M.H., Schmidt L.D., Sen A., Somorjai G.A., Stair P.C., Stults B.R., Tumas W. Catalysis Research of Relevance to Carbon Management: Progress, Challenges, and Opportunities. Chemical Reviews 101 (2001): 953-996.

[28] Olah, G.A. Beyond Oil and Gas: The Methanol Economy. Angewandte Chemie International Edition 44 (2005): 2636-2639.

[29] Rohde, M.P., Unruh D., Schaub G. Membrane application in Fischer–Tropsch synthesis reactors—Overview of concepts. Catalysis Today 106 (2005): 143-148.

[30] Rohde, M.P., Unruh D., Schaub G. Membrane Application in Fischer–Tropsch Synthesis to Enhance CO_2 Hydrogenation. Industrial & Engineering Chemistry Research 44 (2005): 9653-9658.

[31] Faur Ghenciu, A. Review of fuel processing catalysts for hydrogen production in PEM fuel cell systems. Current Opinion in Solid State and Materials Science 6 (2002): 389-399.

[32] Tanaka, Y., Utaka T., Kikuchi R., Sasaki K., Eguchi K. CO removal from reformed fuel over $Cu/ZnO/Al_2O_3$ catalysts prepared by impregnation and coprecipitation methods. Applied Catalysis A: General 238 (2003): 11-18.

[33] Liu, Y., Liu D. Study of bimetallic Cu–Ni/ γ -Al_2O_3 catalysts for carbon dioxide hydrogenation. International Journal of Hydrogen Energy 24 (1999): 351-354.

[34] Stone, F., Waller D. Cu–ZnO and Cu–ZnO/Al_2O_3 Catalysts for the Reverse Water-Gas Shift Reaction. The Effect of the Cu/Zn Ratio on Precursor Characteristics and on the Activity of the Derived Catalysts. Topics in Catalysis 22 (2003): 305-318.

[35] Chen, C.-S., Cheng W.-H., Lin S.-S. Study of reverse water gas shift reaction by TPD, TPR and CO_2 hydrogenation over potassium-promoted Cu/SiO_2 catalyst. Applied Catalysis A: General 238 (2003): 55-67.

[36] Wang, L., Zhang S., Liu Y. Reverse water gas shift reaction over Co-precipitated Ni-CeO_2 catalysts. Journal of Rare Earths 26 (2008): 66-70.

[37] Goguet, A., Meunier F., Breen J.P., Burch R., Petch M.I., Faur Ghenciu A. Study of the origin of the deactivation of a Pt/CeO_2 catalyst during reverse water gas shift (RWGS) reaction. Journal of Catalysis 226 (2004): 382-392.

[38] Gorte, R.J., Zhao S. Studies of the water-gas-shift reaction with ceria-supported precious metals. Catalysis Today 104 (2005): 18-24.

[39] Goguet, A., Shekhtman S.O., Burch R., Hardacre C., Meunier F.C., Yablonsky G.S. Pulse-response TAP studies of the reverse water–gas shift reaction over a Pt/CeO_2 catalyst. Journal of Catalysis 237 (2006): 102-110.

[40] Ernst, K.-H., Campbell C.T., Moretti G. Kinetics of the reverse water-gas shift reaction over Cu(110). Journal of Catalysis 134 (1992): 66-74.

[41] Fujita, S.-I., Usui M., Takezawa N. Mechanism of the reverse water gas shift reaction over Cu/ZnO catalyst. Journal of Catalysis 134 (1992): 220-225.

[42] Chen, C.S., Wu J.H., Lai T.W. Carbon Dioxide Hydrogenation on Cu Nanoparticles. The Journal of Physical Chemistry C 114 (2010): 15021-15028.

[43] Goguet, A., Meunier F.C., Tibiletti D., Breen J.P., Burch R. Spectrokinetic Investigation of Reverse Water-Gas-Shift Reaction Intermediates over a Pt/CeO_2 Catalyst. The Journal of Physical Chemistry B 108 (2004): 20240-20246.

[44] Ma, J., Sun N., Zhang X., Zhao N., Xiao F., Wei W., Sun Y. A short review of catalysis for CO_2 conversion. Catalysis Today 148 (2009): 221-231.

[45] Nitta, Y., Suwata O., Ikeda Y., Okamoto Y., Imanaka T. Copper-zirconia catalysts for methanol synthesis from carbon dioxide: Effect of ZnO addition to Cu-ZrO_2 catalysts. Catalysis Letters 26 (1994): 345-354.

[46] Saito, M., Murata K. Development of high performance Cu/ZnO-based catalysts for methanol synthesis and the water-gas shift reaction. Catalysis Surveys from Asia 8 (2004): 285-294.

[47] Yang, C., Ma Z., Zhao N., Wei W., Hu T., Sun Y. Methanol synthesis from CO_2-rich syngas over a ZrO_2 doped CuZnO catalyst. Catalysis Today 115 (2006): 222-227.

[48] Liaw, B.J., Chen Y.Z. Liquid-phase synthesis of methanol from CO_2/H2 over ultrafine CuB catalysts. Applied Catalysis A: General 206 (2001): 245-256.

[49] Arena, F., Barbera K., Italiano G., Bonura G., Spadaro L., Frusteri F. Synthesis, characterization and activity pattern of Cu–ZnO/ZrO_2 catalysts in the hydrogenation of carbon dioxide to methanol. Journal of Catalysis 249 (2007): 185-194.

[50] Guo, X., Mao D., Lu G., Wang S., Wu G. Glycine–nitrate combustion synthesis of CuO–ZnO–ZrO_2 catalysts for methanol synthesis from CO_2 hydrogenation. Journal of Catalysis 271 (2010): 178-185.

[51] Jung, K., Bell A. Effects of Zirconia Phase on the Synthesis of Methanol over Zirconia-Supported Copper. Catalysis Letters 80 (2002): 63-68.

[52] Arena, F., Italiano G., Barbera K., Bordiga S., Bonura G., Spadaro L., Frusteri F. Solid-state interactions, adsorption sites and functionality of Cu-ZnO/ZrO_2 catalysts in the CO_2 hydrogenation to CH_3OH. Applied Catalysis A: General 350 (2008): 16-23.

[53] Fisher, I.A., Bell A.T. In-SituInfrared Study of Methanol Synthesis from H_2/CO_2 over Cu/SiO_2 and Cu/ZrO_2/SiO_2. Journal of Catalysis 172 (1997): 222-237.

[54] Jung, K.-D., Bell A.T. Role of Hydrogen Spillover in Methanol Synthesis over Cu/ZrO_2. Journal of Catalysis 193 (2000): 207-223.

[55] Liu, X.-M., Lu G.Q., Yan Z.-F. Nanocrystalline zirconia as catalyst support in methanol synthesis. Applied Catalysis A: General 279 (2005): 241-245.

[56] Słoczyński, J., Grabowski R., Olszewski P., Kozłowska A., Stoch J., Lachowska M., Skrzypek J. Effect of metal oxide additives on the activity and stability of $Cu/ZnO/ZrO_2$ catalysts in the synthesis of methanol from CO_2 and H_2. Applied Catalysis A: General 310 (2006): 127-137.

[57] Toyir, J., de la Piscina P.R.r., Fierro J.L.G., Homs N.s. Highly effective conversion of CO_2 to methanol over supported and promoted copper-based catalysts: influence of support and promoter. Applied Catalysis B: Environmental 29 (2001): 207-215.

[58] Liang, X.-L., Dong X., Lin G.-D., Zhang H.-B. Carbon nanotube-supported Pd–ZnO catalyst for hydrogenation of CO_2 to methanol. Applied Catalysis B: Environmental 88 (2009): 315-322.

[59] Koizumi, N., Jiang X., Kugai J., Song C. Effects of mesoporous silica supports and alkaline promoters on activity of Pd catalysts in CO_2 hydrogenation for methanol synthesis. Catalysis Today 194 (2012): 16-24.

[60] Kusama, H., Okabe K., Sayama K., Arakawa H. CO_2 hydrogenation to ethanol over promoted Rh/SiO_2 catalysts. Catalysis Today 28 (1996): 261-266.

[61] Kusama, H., Okabe K., Sayama K., Arakawa H. Ethanol synthesis by catalytic hydrogenation of CO_2 over $Rh.FeSiO_2$ catalysts. Energy 22 (1997): 343-348.

[62] Inui, T., Yamamoto T. Effective synthesis of ethanol from CO_2 on polyfunctional composite catalysts. Catalysis Today 45 (1998): 209-214.

[63] Inui, T., Yamamoto T., Inoue M., Hara H., Takeguchi T., Kim J.-B. Highly effective synthesis of ethanol by CO_2-hydrogenation on well balanced multi-functional FT-type composite catalysts. Applied Catalysis A: General 186 (1999): 395-406.

[64] Arakawa, H. (1998) Research and development on new synthetic routes for basic chemicals by catalytic hydrogenation of CO_2. In: T. Inui MAKISY, Yamaguchi T (eds) Studies in Surface Science and Catalysis. Elsevier,

[65] Takagawa, M., Okamoto A., Fujimura H., Izawa Y., Arakawa H. (1998) Ethanol synthesis from carbon dioxide and hydrogen. In: T. Inui MAKISY, Yamaguchi T (eds) Studies in Surface Science and Catalysis. Elsevier,

[66] Pan, X., Fan Z., Chen W., Ding Y., Luo H., Bao X. Enhanced ethanol production inside carbon-nanotube reactors containing catalytic particles. Nat Mater 6 (2007): 507-511.

[67] Fan, Z., Chen W., Pan X., Bao X. Catalytic conversion of syngas into C_2 oxygenates over Rh-based catalysts—Effect of carbon supports. Catalysis Today 147 (2009): 86-93.

[68] Semelsberger, T.A., Borup R.L., Greene H.L. Dimethyl ether (DME) as an alternative fuel. Journal of Power Sources 156 (2006): 497-511.

[69] Köppel, R.A., Stöcker C., Baiker A. Copper- and Silver–Zirconia Aerogels: Preparation, Structural Properties and Catalytic Behavior in Methanol Synthesis from Carbon Dioxide. Journal of Catalysis 179 (1998): 515-527.

[70] Yaripour, F., Baghaei F., Schmidt I., Perregaard J. Synthesis of dimethyl ether from methanol over aluminium phosphate and silica–titania catalysts. Catalysis Communications 6 (2005): 542-549.

[71] Aguayo, A.T., Ereña J., Mier D., Arandes J.M., Olazar M., Bilbao J. Kinetic Modeling of Dimethyl Ether Synthesis in a Single Step on a CuO–ZnO–Al2O3/ γ -Al2O3 Catalyst. Industrial & Engineering Chemistry Research 46 (2007): 5522-5530.

[72] Olah, G.A., Goeppert A., Prakash G.K.S. Chemical Recycling of Carbon Dioxide to Methanol and Dimethyl Ether: From Greenhouse Gas to Renewable, Environmentally Carbon Neutral Fuels and Synthetic Hydrocarbons. The Journal of Organic Chemistry 74 (2008): 487-498.

[73] Aguayo, A.T., Ereña J., Sierra I., Olazar M., Bilbao J. Deactivation and regeneration of hybrid catalysts in the single-step synthesis of dimethyl ether from syngas and CO_2. Catalysis Today 106 (2005): 265-270.

[74] Tao, J.-L., Jun K.-W., Lee K.-W. Co-production of dimethyl ether and methanol from CO_2 hydrogenation: development of a stable hybrid catalyst. Applied Organometallic Chemistry 15 (2001): 105-108.

[75] Wang, S., Mao D., Guo X., Wu G., Lu G. Dimethyl ether synthesis via CO_2 hydrogenation over CuO–TiO_2–ZrO_2/HZSM-5 bifunctional catalysts. Catalysis Communications 10 (2009): 1367-1370.

[76] An, X., Zuo Y.-Z., Zhang Q., Wang D.-z., Wang J.-F. Dimethyl Ether Synthesis from CO_2 Hydrogenation on a CuO–ZnO–Al_2O_3–ZrO_2/HZSM-5 Bifunctional Catalyst. Industrial & Engineering Chemistry Research 47 (2008): 6547-6554.

[77] Stöcker, M. Methanol-to-hydrocarbons: catalytic materials and their behavior. Microporous and Mesoporous Materials 29 (1999): 3-48.

[78] Vishwanathan, V., Jun K.-W., Kim J.-W., Roh H.-S. Vapour phase dehydration of crude methanol to dimethyl ether over Na-modified H-ZSM-5 catalysts. Applied Catalysis A: General 276 (2004): 251-255.

[79] Gao, W., Wang H., Wang Y., Guo W., Jia M. Dimethyl ether synthesis from CO_2 hydrogenation on La-modified CuO-ZnO-Al_2O_3/HZSM-5 bifunctional catalysts. Journal of Rare Earths 31 (2013): 470-476.

[80] Zhang, Z., Hu S., Song J., Li W., Yang G., Han B. Hydrogenation of CO_2 to Formic Acid Promoted by a Diamine-Functionalized Ionic Liquid. ChemSusChem 2 (2009): 234-238.

[81] Federsel, C., Jackstell R., Beller M. State-of-the-Art Catalysts for Hydrogenation of Carbon Dioxide. Angewandte Chemie International Edition 49 (2010): 6254-6257.

[82] Johnson, T.C., Morris D.J., Wills M. Hydrogen generation from formic acid and alcohols using homogeneous catalysts. Chemical Society Reviews 39 (2010): 81-88.

[83] Omae, I. Aspects of carbon dioxide utilization. Catalysis Today 115 (2006): 33-52.

[84] Ezhova, N.N., Kolesnichenko N.V., Bulygin A.V., Slivinskii E.V., Han S. Hydrogenation of CO_2 to formic acid in the presence of the Wilkinson complex. Russian Chemical Bulletin 51 (2002): 2165-2169.

[85] Inoue, Y., Izumida H., Sasaki Y., Hashimoto H. Catalytic fixation of carbon dioxide to formic acid by transition-metal complexes under mild conditions. Chemistry Letters 5 (1976): 863-864.

[86] Jessop, P.G., Hsiao Y., Ikariya T., Noyori R. Homogeneous Catalysis in Supercritical Fluids: Hydrogenation of Supercritical Carbon Dioxide to Formic Acid, Alkyl Formates, and Formamides. Journal of the American Chemical Society 118 (1996): 344-355.

[87] Tsai, J.C., Nicholas K.M. Rhodium-catalyzed hydrogenation of carbon dioxide to formic acid. Journal of the American Chemical Society 114 (1992): 5117-5124.

[88] Yin, C., Xu Z., Yang S.-Y., Ng S.M., Wong K.Y., Lin Z., Lau C.P. Promoting Effect of Water in Ruthenium-Catalyzed Hydrogenation of Carbon Dioxide to Formic Acid. Organometallics 20 (2001): 1216-1222.

[89] Himeda, Y., Onozawa-Komatsuzaki N., Sugihara H., Kasuga K. Simultaneous Tuning of Activity and Water Solubility of Complex Catalysts by Acid–Base Equilibrium of Ligands for Conversion of Carbon Dioxide. Organometallics 26 (2007): 702-712.

[90] Zhang, Y., Fei J., Yu Y., Zheng X. Silica immobilized ruthenium catalyst used for carbon dioxide hydrogenation to formic acid (I): the effect of functionalizing group and additive on the catalyst performance. Catalysis Communications 5 (2004): 643-646.

[91] Park, J.-N., McFarland E.W. A highly dispersed Pd–Mg/SiO_2 catalyst active for methanation of CO_2. Journal of Catalysis 266 (2009): 92-97.

[92] Chang, F.-W., Kuo M.-S., Tsay M.-T., Hsieh M.-C. Hydrogenation of CO_2 over nickel catalysts on rice husk ash-alumina prepared by incipient wetness impregnation. Applied Catalysis A: General 247 (2003): 309-320.

[93] Chang, F.-W., Hsiao T.-J., Chung S.-W., Lo J.-J. Nickel supported on rice husk ash — activity and selectivity in CO2 methanation. Applied Catalysis A: General 164 (1997): 225-236.

[94] Chang, F.-W., Tsay M.-T., Liang S.-P. Hydrogenation of CO_2 over nickel catalysts supported on rice husk ash prepared by ion exchange. Applied Catalysis A: General 209 (2001): 217-227.

[95] Vance, C.K., Bartholomew C.H. Hydrogenation of carbon dioxide on group viii metals: III, Effects of support on activity/selectivity and adsorption properties of nickel. Applied Catalysis 7 (1983): 169-177.

[96] Du, G., Lim S., Yang Y., Wang C., Pfefferle L., Haller G.L. Methanation of carbon dioxide on Ni-incorporated MCM-41 catalysts: The influence of catalyst pretreatment and study of steady-state reaction. Journal of Catalysis 249 (2007): 370-379.

[97] Agnelli, M., Kolb M., Mirodatos C. Co Hydrogenation on a Nickel Catalyst .: 1. Kinetics and Modeling of a Low-Temperature Sintering Process. Journal of Catalysis 148 (1994): 9-21.

[98] Kustov, A.L., Frey A.M., Larsen K.E., Johannessen T., Nørskov J.K., Christensen C.H. CO methanation over supported bimetallic Ni–Fe catalysts: From computational studies towards catalyst optimization. Applied Catalysis A: General 320 (2007): 98-104.

[99] Kowalczyk, Z., Stołecki K., Raróg-Pilecka W., Miśkiewicz E., Wilczkowska E., Karpiński Z. Supported ruthenium catalysts for selective methanation of carbon oxides at very low CO_x/H_2 ratios. Applied Catalysis A: General 342 (2008): 35-39.

[100] Abe, T., Tanizawa M., Watanabe K., Taguchi A. CO_2 methanation property of Ru nanoparticle-loaded TiO_2 prepared by a polygonal barrel-sputtering method. Energy & Environmental Science 2 (2009): 315-321.

[101] Luo, L., Songjun L., Zhu Y. The effects of yttrium on the hydrogenation performance and surface properties of a ruthenium-supported catalyst. Journal of the Serbian Chemical Society 70 (2005): 1419-1425.

[102] Weatherbee, G.D., Bartholomew C.H. Hydrogenation of CO_2 on group VIII metals: II. Kinetics and mechanism of CO_2 hydrogenation on nickel. Journal of Catalysis 77 (1982): 460-472.

[103] Marwood, M., Doepper R., Renken A. In-situ surface and gas phase analysis for kinetic studies under transient conditions The catalytic hydrogenation of CO2. Applied Catalysis A: General 151 (1997): 223-246.

[104] Lapidus, A.L., Gaidai N.A., Nekrasov N.V., Tishkova L.A., Agafonov Y.A., Myshenkova T.N. The mechanism of carbon dioxide hydrogenation on copper and nickel catalysts. Petroleum Chemistry 47 (2007): 75-82.

[105] Fujita, S., Terunuma H., Kobayashi H., Takezawa N. Methanation of carbon monoxide and carbon dioxide over nickel catalyst under the transient state. Reaction Kinetics and Catalysis Letters 33 (1987): 179-184.

[106] Schild, C., Wokaun A., Baiker A. On the mechanism of CO and CO_2 hydrogenation reactions on zirconia-supported catalysts: a diffuse reflectance FTIR study: Part II. Surface species on copper/zirconia catalysts: implications for methanoi synthesis selectivity. Journal of Molecular Catalysis 63 (1990): 243-254.

[107] Pérez-Alonso, F.J., Ojeda M., Herranz T., Rojas S., González-Carballo J.M., Terreros P., Fierro J.L.G. Carbon dioxide hydrogenation over Fe–Ce catalysts. Catalysis Communications 9 (2008): 1945-1948.

[108] Krishnamoorthy, S., Li A., Iglesia E. Pathways for CO_2 Formation and Conversion During Fischer–Tropsch Synthesis on Iron-Based Catalysts. Catalysis Letters 80 (2002): 77-86.

[109] Weatherbee, G.D., Bartholomew C.H. Hydrogenation of CO_2 on group VIII metals: IV. Specific activities and selectivities of silica-supported Co, Fe, and Ru. Journal of Catalysis 87 (1984): 352-362.

[110] Prairie, M.R., Renken A., Highfield J.G., Ravindranathan Thampi K., Grätzel M. A fourier transform infrared spectroscopic study of CO_2 methanation on supported ruthenium. Journal of Catalysis 129 (1991): 130-144.

[111] Yesgar, P.W., Sheintuch M. Nickel-catalyzed methanation reactions studied with an in situ magnetic induction method: Experiments and modeling. Journal of Catalysis 127 (1991): 576-594.

[112] Visconti, C.G., Lietti L., Tronconi E., Forzatti P., Zennaro R., Finocchio E. Fischer–Tropsch synthesis on a Co/Al_2O_3 catalyst with CO_2 containing syngas. Applied Catalysis A: General 355 (2009): 61-68.

[113] Riedel, T., Claeys M., Schulz H., Schaub G., Nam S.-S., Jun K.-W., Choi M.-J., Kishan G., Lee K.-W. Comparative study of Fischer–Tropsch synthesis with H2/CO and H2/CO2 syngas using Fe- and Co-based catalysts. Applied Catalysis A: General 186 (1999): 201-213.

[114] Gnanamani, M.K., Shafer W.D., Sparks D.E., Davis B.H. Fischer – Tropsch synthesis: Effect of CO_2 containing syngas over Pt promoted Co/ γ -Al_2O_3 and K-promoted Fe catalysts. Catalysis Communications 12 (2011): 936-939.

[115] Satthawong, R., Koizumi N., Song C., Prasassarakich P. Bimetallic Fe–Co catalysts for CO_2 hydrogenation to higher hydrocarbons. Journal of CO2 Utilization 3–4 (2013): 102-106.

[116] Xu, L., Bao S., Houpt D.J., Lambert S.H., Davis B.H. Role of CO_2 in the initiation of chain growth and alcohol formation during the Fischer-Tropsch synthesis. Catalysis Today 36 (1997): 347-355.

[117] Lee, S.-C., Kim J.-S., Shin W.C., Choi M.-J., Choung S.-J. Catalyst deactivation during hydrogenation of carbon dioxide: Effect of catalyst position in the packed bed reactor. Journal of Molecular Catalysis A: Chemical 301 (2009): 98-105.

[118] Herranz, T., Rojas S., Pérez-Alonso F.J., Ojeda M., Terreros P., Fierro J.L.G. Hydrogenation of carbon oxides over promoted Fe-Mn catalysts prepared by the microemulsion methodology. Applied Catalysis A: General 311 (2006): 66-75.

[119] Zhao, G., Zhang C., Qin S., Xiang H., Li Y. Effect of interaction between potassium and structural promoters on Fischer–Tropsch performance in iron-based catalysts. Journal of Molecular Catalysis A: Chemical 286 (2008): 137-142.

[120] Cubeiro, M., Morales H., Goldwasser M., Pérez-Zurita M., González-Jiménez F. Promoter Effect of Potassium on an Iron Catalyst in the Carbon Dioxide

Hydrogenation Reaction. Reaction Kinetics and Catalysis Letters 69 (2000): 259-264.

[121] Wan, H., Wu B., Zhang C., Xiang H., Li Y. Promotional effects of Cu and K on precipitated iron-based catalysts for Fischer–Tropsch synthesis. Journal of Molecular Catalysis A: Chemical 283 (2008): 33-42.

[122] Trépanier, M., Tavasoli A., Dalai A.K., Abatzoglou N. Co, Ru and K loadings effects on the activity and selectivity of carbon nanotubes supported cobalt catalyst in Fischer–Tropsch synthesis. Applied Catalysis A: General 353 (2009): 193-202.

[123] Yang, Y., Xiang H.-W., Xu Y.-Y., Bai L., Li Y.-W. Effect of potassium promoter on precipitated iron-manganese catalyst for Fischer–Tropsch synthesis. Applied Catalysis A: General 266 (2004): 181-194.

[124] Li, T., Yang Y., Zhang C., An X., Wan H., Tao Z., Xiang H., Li Y., Yi F., Xu B. Effect of manganese on an iron-based Fischer–Tropsch synthesis catalyst prepared from ferrous sulfate. Fuel 86 (2007): 921-928.

[125] Ning, W., Koizumi N., Yamada M. Researching Fe Catalyst Suitable for CO_2-Containing Syngas for Fischer–Tropsch Synthesis. Energy & Fuels 23 (2009): 4696-4700.

[126] Sai Prasad, P.S., Bae J., Jun K.-W., Lee K.-W. Fischer–Tropsch Synthesis by Carbon Dioxide Hydrogenation on Fe-Based Catalysts. Catalysis Surveys from Asia 12 (2008): 170-183.

[127] Fujiwara, M., Kieffer R., Ando H., Xu Q., Souma Y. Change of catalytic properties of FeZnO/zeolite composite catalyst in the hydrogenation of carbon dioxide. Applied Catalysis A: General 154 (1997): 87-101.

[128] Nam, S.-S., Kishan G., Lee M.-W., Choi M.-J., Lee K.-W. Selective Synthesis of C_2-C_4 Olefins and C_5^+ Hydrocarbons over Unpromoted and Cerium-promoted Iron Catalysts Supported on Ion Exchanged (H, K) Zeolite-Y. Journal of Chemical Research, Synopses (1999): 344-345.

[129] Riedel, T., Schulz H., Schaub G., Jun K.-W., Hwang J.-S., Lee K.-W. Fischer–Tropsch on Iron with H_2/CO and H_2/CO_2 as Synthesis Gases: The Episodes of

Formation of the Fischer–Tropsch Regime and Construction of the Catalyst. Topics in Catalysis 26 (2003): 41-54.

[130] Dorner, R.W., Hardy D.R., Williams F.W., Davis B.H., Willauer H.D. Influence of Gas Feed Composition and Pressure on the Catalytic Conversion of CO_2 to Hydrocarbons Using a Traditional Cobalt-Based Fischer–Tropsch Catalyst. Energy & Fuels 23 (2009): 4190-4195.

[131] Makino, T., Okada M. CO adsorption on regularly stepped Cu(410) surface. Surface Science 628 (2014): 36-40.

[132] Kaichev, V.V., Prosvirin I.P., Bukhtiyarov V.I., Unterhalt H., Rupprechter G., Freund H.-J. High-Pressure Studies of CO Adsorption on Pd(111) by X-ray Photoelectron Spectroscopy and Sum-Frequency Generation. The Journal of Physical Chemistry B 107 (2003): 3522-3527.

[133] Satthawong, R., Koizumi N., Song C., Prasassarakich P. Comparative Study on CO_2 Hydrogenation to Higher Hydrocarbons over Fe-Based Bimetallic Catalysts. Topics in Catalysis 57 (2014): 588-594.

[134] Ishihara, T., Eguchi K., Arai H. Hydrogenation of carbon monoxide over SiO_2-supported Fe-Co, Co-Ni and Ni-Fe bimetallic catalysts. Applied Catalysis 30 (1987): 225-238.

[135] Ishihara, T., Horiuchi N., Inoue T., Eguchi K., Takita Y., Arai H. Effect of alloying on CO hydrogenation activity over SiO_2-supported Co.Ni alloy catalysts. Journal of Catalysis 136 (1992): 232-241.

[136] Duvenhage, D.J., Coville N.J. Fe:CoTiO_2 bimetallic catalysts for the Fischer-Tropsch reaction I. Characterization and reactor studies. Applied Catalysis A: General 153 (1997): 43-67.

[137] Duvenhage, D.J., Coville N.J. Fe:Co/TiO_2 bimetallic catalysts for the Fischer–Tropsch reaction: Part 3: The effect of Fe:Co ratio, mixing and loading on FT product selectivity. Applied Catalysis A: General 289 (2005): 231-239.

[138] Tihay, F., Roger A.C., Pourroy G., Kiennemann A. Role of the Alloy and Spinel in the Catalytic Behavior of Fe–Co/Cobalt Magnetite Composites under CO and CO_2 Hydrogenation. Energy & Fuels 16 (2002): 1271-1276.

[139] Tavasoli, A., Trépanier M., Malek Abbaslou R.M., Dalai A.K., Abatzoglou N. Fischer–Tropsch synthesis on mono- and bimetallic Co and Fe catalysts supported on carbon nanotubes. Fuel Processing Technology 90 (2009): 1486-1494.

[140] Ma, X., Sun Q., Ying W., Fang D. Effects of the ratio of Fe to Co over Fe-Co/SiO2 bimetallic catalysts on their catalytic performance for Fischer-Tropsch synthesis. Journal of Natural Gas Chemistry 18 (2009): 232-236.

[141] Mirzaei, A.A., babaei A.B., Galavy M., Youssefi A. A silica supported Fe–Co bimetallic catalyst prepared by the sol/gel technique: Operating conditions, catalytic properties and characterization. Fuel Processing Technology 91 (2010): 335-347.

[142] Park, S.E., Nam S.S., Choi M.J., Lee K.W. Catalytic reduction of carbon dioxide. The effects of catalysts and reductants. Energy Conversion and Management 36 (1995): 573-576.

[143] Lögdberg, S., Tristantini D., Borg Ø., Ilver L., Gevert B., Järås S., Blekkan E.A., Holmen A. Hydrocarbon production via Fischer–Tropsch synthesis from H_2-poor syngas over different Fe-Co/ γ -Al_2O_3 bimetallic catalysts. Applied Catalysis B: Environmental 89 (2009): 167-182.

[144] de la Peña O'Shea, V.A., Álvarez-Galván M.C., Campos-Martín J.M., Fierro J.L.G. Fischer–Tropsch synthesis on mono- and bimetallic Co and Fe catalysts in fixed-bed and slurry reactors. Applied Catalysis A: General 326 (2007): 65-73.

[145] Mirzaei, A.A., Habibpour R., Faizi M., Kashi E. Characterization of iron-cobalt oxide catalysts: Effect of different supports and promoters upon the structure and morphology of precursors and catalysts. Applied Catalysis A: General 301 (2006): 272-283.

[146] Jozwiak, W.K., Kaczmarek E., Maniecki T.P., Ignaczak W., Maniukiewicz W. Reduction behavior of iron oxides in hydrogen and carbon monoxide atmospheres. Applied Catalysis A: General 326 (2007): 17-27.

[147] Busca, G., Lorenzelli V. Infrared spectroscopic identification of species arising from reactive adsorption of carbon oxides on metal oxide surfaces. Materials Chemistry 7 (1982): 89-126.

[148] Rethwisch, D.G., Dumesic J.A. Effect of metal-oxygen bond strength on properties of oxides. 1. Infrared spectroscopy of adsorbed carbon monoxide and carbon dioxide. Langmuir 2 (1986): 73-79.

[149] Gopal, P.G., Schneider R.L., Watters K.L. Evidence for production of surface formate upon direct reaction of CO with alumina and magnesia. Journal of Catalysis 105 (1987): 366-372.

[150] Pan, Y., Liu C.-j., Ge Q. Adsorption and Protonation of CO_2 on Partially Hydroxylated γ -Al_2O_3 Surfaces: A Density Functional Theory Study. Langmuir 24 (2008): 12410-12419.

[151] Snyder, R.G. Vibrational Study of the Chain Conformation of the Liquid n-Paraffins and Molten Polyethylene. Journal of Chemical Physics 47 (1967): 1316-1360.

[152] Cieślik-Boczula, K., Czarnik-Matusewicz B., Perevozkina M., Filarowski A., Boens N., De Borggraeve W.M., Koll A. ATR-IR spectroscopic study of the structural changes in the hydrophobic region of ICPAN/DPPC bilayers. Journal of Molecular Structure 878 (2008): 162-168.

[153] Bozso, F., Ertl G., Grunze M., Weiss M. Chemisorption of hydrogen on iron surfaces. Applications of Surface Science 1 (1977): 103-119.

[154] Bartholomew, C. Hydrogen adsorption on supported cobalt, iron, and nickel. Catalysis Letters 7 (1990): 27-51.

[155] Zhang, C., Zhao G., Liu K., Yang Y., Xiang H., Li Y. Adsorption and reaction of CO and hydrogen on iron-based Fischer–Tropsch synthesis catalysts. Journal of Molecular Catalysis A: Chemical 328 (2010): 35-43.

[156] Zowtiak, J.M., Bartholomew C.H. The kinetics of H_2 adsorption on and desorption from cobalt and the effects of support thereon. Journal of Catalysis 83 (1983): 107-120.

[157] Riedel, T., Schaub G., Jun K.-W., Lee K.-W. Kinetics of CO_2 Hydrogenation on a K-Promoted Fe Catalyst. Industrial & Engineering Chemistry Research 40 (2001): 1355-1363.

[158] Schild, C., Wokaun A., Koeppel R.A., Baiker A. Carbon dioxide hydrogenation over nickel/zirconia catalysts from amorphous precursors: on the mechanism of methane formation. Journal of Physical Chemistry 95 (1991): 6341-6346.

[159] Burch, R. Gold catalysts for pure hydrogen production in the water-gas shift reaction: activity, structure and reaction mechanism. Physical Chemistry Chemical Physics 8 (2006): 5483-5500.

[160] Montanari, T., Castoldi L., Lietti L., Busca G. Basic catalysis and catalysis assisted by basicity: FT-IR and TPD characterization of potassium-doped alumina. Applied Catalysis A: General 400 (2011): 61-69.

[161] Kantschewa, M., Albano E.V., Etrtl G., Kno ¨ zinger H. Infrared and x-ray photoelectron spectroscopy study of K_2CO_3/ γ -Al_2O_3. Applied Catalysis 8 (1983): 71-84.

[162] Hirano, T. Roles of potassium in potassium-promoted iron oxide catalyst for dehydrogenation of ethylbenzene. Applied Catalysis 26 (1986): 65-79.

APPENDICES

APPENDIX A

Gas Product Analysis

The gas products including Ar, CO, CH_4 and CO_2 were analyzed online with an Agilent 3000 micro GC with molecular sieve type column for Ar, CO, CH_4 and Plot-Q column for CO_2, respectively. The GC condition and temperature program used for the analyses are described in Table A-1.

Table A-1 Condition and temperature program for micro GC analysis.

Parameters	Molecular Sieve	Plot Q
Carrier gas	Helium	Helium
Internal standard	Argon	Argon
Injector temperature (°C)	100	100
Column temperature (°C)	60	70
Column pressure (psi)	20	20
Sample pump (s)	10	10
Injection time (ms)	100	100
Run time (s)	300	600

The gas-phase hydrocarbon products were analyzed online with SRI 8610C GC equipped with FID with Porapak Q column. The GC-FID condition and temperature program used for the analyses are described in Table A-2.

Table A-2 Condition and temperature program for GC-FID analysis.

Parameters	Value
Carrier gas	Helium
Injector temperature (°C)	165
Detector temperature (°C)	250
Injection volume (ml)	3
Oven temperature program	
Initial temperature (°C)	40
Hold time (min)	0
Ramp rate (°C min^{-1})	5
Final temperature (°C)	100
Hold time (min)	0
Ramp rate (°C min^{-1})	2.5
Final temperature (°C)	200
Hold time (min)	0

APPENDIX B

Liquid Hydrocarbon Product Analysis

The liquid hydrocarbons collected in an ice cooled condenser connected to the reactor were analyzed after the reaction with the GC/MS (Shimadzu, QP-5000) with a capillary column Rxi®-5HT (Crossbond® 5% diphenyl/ 95% dimethyl polysiloxane, 30 m x 0.25 mm i.d. x 0.25 μm film thickness). The conditions and temperature program for GC/MS are described in Table B-1.

Table B-1 Condition and temperature program for GC/MS analysis.

Parameters	Value
Carrier gas	Helium
Column inlet pressure (kPa)	23
Column flow (mL min^{-1})	0.7
Linear velocity (cm/s)	30.1
Split mode injector	20:1
Total flow (mL min^{-1})	15.2
Carrier gas flow rate (mL min^{-1})	15.2
Injector temperature (°C)	290
Detector temperature (°C)	270
Injection volume (μl)	1
Oven temperature program	
Initial temperature (°C)	35
Hold time (min)	10
Ramp rate (°C min^{-1})	5
Final temperature (°C)	120
Hold time (min)	2
Ramp rate (°C min^{-1})	4
Final temperature (°C)	250
Hold time (min)	5

APPENDIX C

Calculation of CO_2 Conversion and Product Selectivity

The CO_2 hydrogenation activity of the catalysts was obtained from GC-TCD analyses (using Ar as an internal standard) and expressed in terms of mole percent conversion of CO_2. Calculation procedures are as follow:

$$\text{CO}_2 \text{ conversion (\%)} = \left[1 - \frac{\left({}^{\text{CO}_2}/_{\text{Ar}}\right)_{\text{out}}}{\left({}^{\text{CO}_2}/_{\text{Ar}}\right)_{\text{in}}}\right] \times 100 \qquad \text{(C-1)}$$

where $\left({}^{\text{CO}_2}/_{\text{Ar}}\right)_{\text{in}}$ = ratio of CO_2 and Ar concentration at the reactor inlet

$\left({}^{\text{CO}_2}/_{\text{Ar}}\right)_{\text{out}}$ = ratio of CO_2 and Ar concentration in the reactor outlet

Example: CO_2 conversion of Fe-Co(0.17)/K(0.3)/Al_2O_3 catalyst

From Table C-1: at 14 hour-on-stream; Ar area = 504973, CO_2 area = 1028280

$(CO_2/Ar)_{out}$ = 1028280 / 504973 = 2.036

$(CO_2/Ar)_{in}$ can be calculated from the ratio of CO_2 area to Ar area measured at 1.1 MPa (ambient temperature) before CO_2 hydrogenation (Ar area = 369282, CO_2 area = 1132650).

$(CO_2/Ar)_{in}$ = 1132650 / 369282 = 3.066

So, CO_2 conversion = [1 - (2.036 / 3.066)] x 100 = 33.7 % #

Table C-1 GC-TCD data from CO_2 hydrogenation over Fe-Co(0.17)/K(0.3)/Al_2O_3 catalyst.

TOS (h)	Area			
	Ar	CH_4	CO	CO_2
0.0	448899	100325	102612	1077560
0.5	471267	109438	105812	1050630
1.0	495160	142746	108132	1044700
1.5	502928	162382	107626	1038550
2.0	512811	177874	108887	1036820
2.5	518296	187671	110158	1033010
3.0	516845	192953	110234	1032550
3.5	519034	198416	111366	1036760
4.0	522517	203094	112808	1036390
4.5	523278	206813	113502	1037710
5.0	519511	208529	113225	1036500
5.5	525251	213905	115112	1038390
6.0	516862	212864	114085	1036950
6.5	519284	215969	115501	1039200
7.0	519891	218100	116643	1038800
7.5	519390	219536	117593	1038230
8.0	517928	220546	118243	1038940
8.5	519239	222734	119556	1037320
9.0	512978	221247	119069	1039340
9.5	508606	220556	119016	1036640
10.0	512701	223590	120991	1038510
10.5	510418	223783	121279	1037020
11.0	508096	223792	121722	1037320
11.5	512408	226817	123656	1037030
12.0	512041	227323	124443	1037280
12.5	507504	225976	124195	1035590
13.0	506961	226872	124902	1036890
13.5	506919	227189	125831	1032900
14.0	504973	226332	126794	1028280
14.5	503044	225242	127664	1030750
15.0	503686	225511	129010	1031980

The product space-time yield (STY) was expressed in mole of product per weight of the catalyst per reaction time (μmol g^{-1} s^{-1}) and calculated as followed.

<u>CH_4 STY of Fe-Co(0.17)/K(0.3)/Al_2O_3 catalyst:</u>

Feed gas flow rate (24% CO_2/ 72% H_2/ 4% Ar) = 12 mL(STP) min^{-1}

Catalysts weight = 0.202 g

Gas constant = 0.082 L atm K^{-1} mol^{-1}

First the CO_2 flow rate is calculated;

CO_2 flow rate = [(Feed gas flow rate (mL(STP) min^{-1}) x 0.001 / 0.082 / 273.15 x 60) / (Catalysts weight (g) / 1000)] x 0.24

= [(12 x 0.001 / 0.082 / 273.15 x 60) / (0.202 / 1000)] x 0.24

= 38.19 mol kg-cat^{-1} h^{-1} #

To calculate the STY, calibration data of Ar, CH_4 and CO_2 for GC-TCD are needed. By plotting between gas concentration (y-axis) and area of the peak (x-axis) so we can get the slopes which will be used for qualitative calculation. From the calibration curve of Ar, CH_4 and CO_2 (not shown here), the slopes are listed below:

Slope of Ar curve = 1.51014E-05

Slope of CH_4 curve = 1.40412E-05

Slope of CO_2 curve = 2.3076E-05

From Table C-1 at 14 hour-on-stream; Ar area = 504973, CH_4 area = 226332

CH_4 STY = CO_2 flow rate x (CH_4 area x Slope of CH_4 curve) / (Ar area x Slope of Ar curve) / [$(CO_2/Ar)_{in}$ x (Slope of CO_2 curve/Slope of Ar curve)]

= 38.19 x (226332 x 1.40412E-05) / (504973 x 1.51014E-05) / [3.066 x (2.3076E-05/1.51014E-05)]

= 3.397 mol kg-cat^{-1} h^{-1}

= 0.944 μmol g-cat^{-1} s^{-1} #

The gaseous hydrocarbons were analyzed online by GC-FID. The selectivity of these gaseous hydrocarbons (C_1 - C_7) was expressed in carbon mole percent (%) and calculated as followed.

$$S_i = \left(\frac{C_i}{\sum_{i=1}^{n} C_i}\right) \times 100 \qquad \text{(C-2)}$$

where S_i = percent selectivity of hydrocarbon product i

C_i = concentration of hydrocarbon product i

n = number of hydrocarbon product from the reaction

Hydrocarbon selectivity of $Fe/K(0.3)/Al_2O_3$ catalyst:

From Table C-2: Total area of C_1 to C_7 = 2330.8595

So, CH_4 selectivity = (Area of CH_4 / Total area) x 100

= (665.6935 / 2330.8595) x 100

= 29 C-mole% #

C_2-C_7 selectivity = 100 - CH_4 selectivity

= 100 - 29 = 71 C-mole% #

Table C-2 GC-FID data from CO_2 hydrogenation over $Fe/K(0.3)/Al_2O_3$ catalyst.

Component	Retention time (min)	Area
CH_4	1.550	665.6935
C_2H_4	4.833	106.6960
C_2H_6	6.000	251.5145
C_3H_6	11.850	347.9135
C_3H_8	12.416	110.3610
C_4H_8	19.416	115.1270
C_4H_{10}	20.383	201.2585
C_5H_{10}	28.366	51.5790
C_5H_{12}	29.183	170.4795
C_6H_{14}	37.600	132.6405
C_7H_{16}	45.416	177.5965

APPENDIX D

Calculation of Chain Growth Probability

Since CO_2 hydrogenation over Fe-based catalysts mostly proceeds via reverse water-gas shift reaction followed by Fischer-Tropsch synthesis, so the hydrocarbon product distribution generally follows an Anderson–Schulz–Flory distribution, where the hydrocarbon chain is formed step-wise by insertion of C_1 intermediates with constant growth probability (α). The Anderson–Schulz–Flory distribution can be expressed as the following equation.

$$W_N = N(1-\alpha)^2 \alpha^{N-1} \quad \text{(D-1)}$$

$$\frac{W_N}{N} = \frac{(1-\alpha)^2}{\alpha} \alpha^N \quad \text{(D-2)}$$

$$\ln\left(\frac{W_N}{N}\right) = \ln\left[\frac{(1-\alpha)^2}{\alpha}\right] + N \ln\alpha \quad \text{(D-3)}$$

where W_N = carbon weight fraction of hydrocarbon containing N carbon

N = carbon number

α = chain growth probability

The chain growth probability (α) can be calculated from the slope of the plot between the carbon number (N) and natural logarithm of hydrocarbon weight fraction to carbon number ratio ($\ln(W_N/N)$) or natural logarithm of the carbon mole fraction of hydrocarbon containing N carbon ($\ln M_N$).

Example: Chain growth probability of gaseous product from CO_2 hydrogenation over Fe-Co(0.17)/K(1.0)/Al_2O_3 catalyst

Table D-1 GC-FID data from CO_2 hydrogenation over Fe-Co(0.17)/K(0.5)/Al_2O_3 catalyst.

Component	Retention time (min)	Area
CH_4	2.616	3767.6770
C_2H_4	7.666	717.5785
C_2H_6	8.833	1277.4875
C_3H_6	12.966	1981.1635
C_3H_8	N/A	497.0410
C_4H_8	19.783	947.0330
C_4H_{10}	20.650	711.8820
C_5H_{10}	28.283	454.3990
C_5H_{12}	29.116	388.7160
C_6H_{14}	37.000	498.0670
C_7H_{16}	44.933	387.6650

First calculate the area of each hydrocarbon containing N carbon,

Area of C_3 hydrocarbon = 1981.1635 + 497.0410 = 2478.2045 #

Carbon number (N)	Area
1	3767.6770
2	1995.0660
3	2478.2045
4	1658.9150
5	843.1150
6	498.0670
7	387.6650

The carbon weight fraction of hydrocarbon containing N carbon (W_N) is then calculated by divided the area of each hydrocarbon containing N carbon with the total area.

Total area = 11628.7095

W_3 = 2478.2045 / 11628.7095 = 0.2131 #

Then, calculate $\ln(W_N/N)$ and plot with carbon number (N).

Carbon number (N)	W_N	W_N/N	$\ln(W_N/N)$
1	0.3240	0.3240	-1.1270
2	0.1716	0.0858	-2.4559
3	0.2131	0.0710	-2.6446
4	0.1427	0.0357	-3.3336
5	0.0725	0.0145	-4.2336
6	0.0428	0.0071	-4.9423
7	0.0333	0.0048	-5.3470
Total	1.0000		

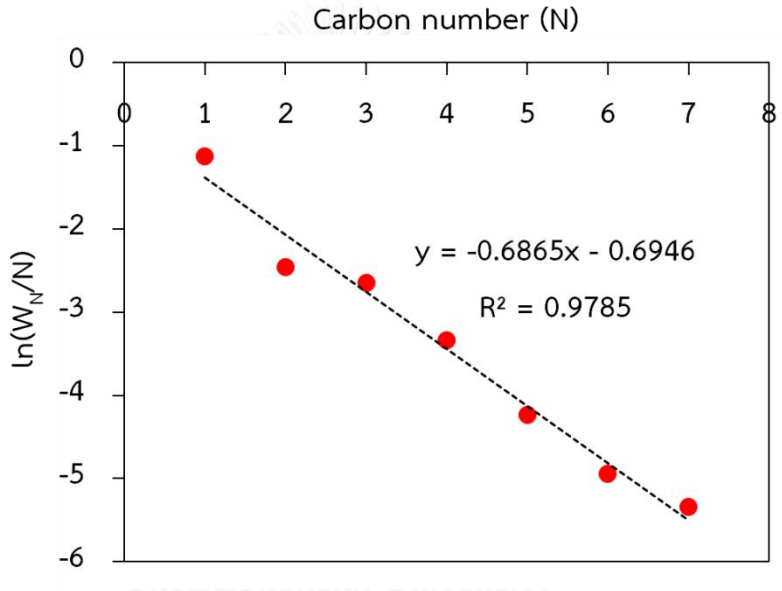

Figure D-1 ASF plot of the gaseous hydrocarbon products for the Fe-Co(0.17)/K(0.5)/Al_2O_3 catalysts.

According to Eq. D-3, the slope of Figure D-1 is $\ln(\alpha)$. Then, the chain growth probability (α) can be calculated.

$$\text{Slope} = \ln(\alpha) = -0.6865$$

$$\alpha = 0.50 \quad \#$$

APPENDIX E

Time-on-Stream Results from Hydrogenation using High Co-Containing Catalysts

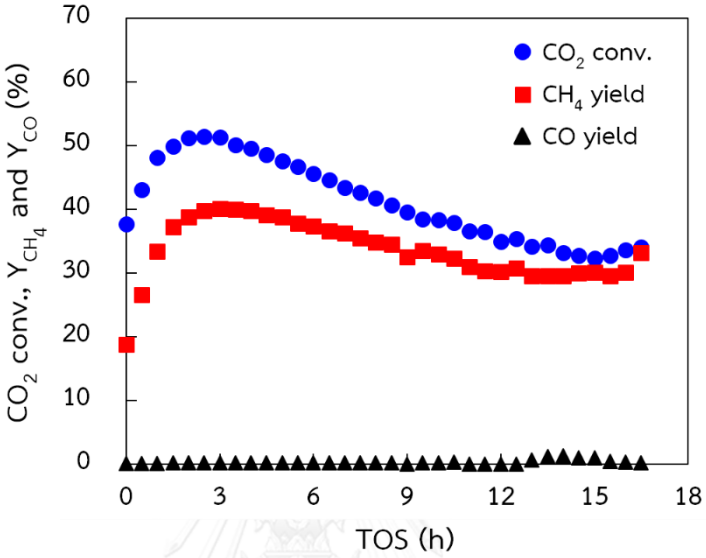

Figure E-1 Time-on-stream stabilities of CO_2 conversions and product yields over Fe-Co(0.50)/Al_2O_3 catalyst.

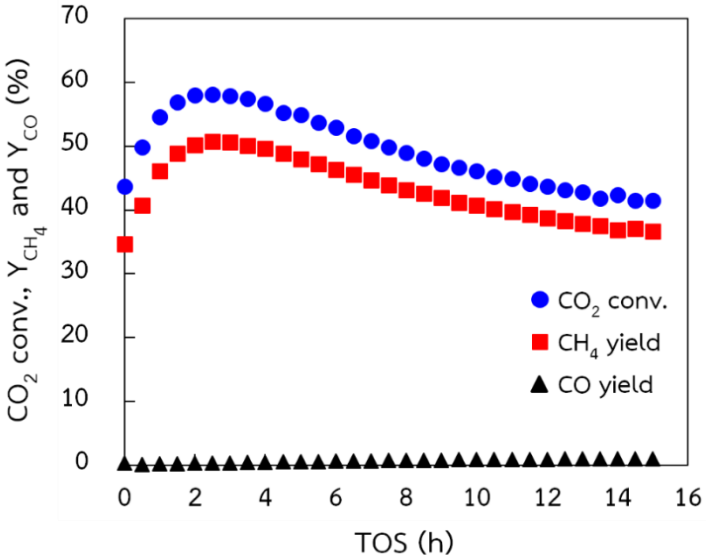

Figure E-2 Time-on-stream stabilities of CO_2 conversions and product yields over Co/Al_2O_3 catalyst.

VITA

Miss Ratchprapa Satthawong was born on November 1, 1987 in Bangkok, Thailand. She received her B.Sc. (Second class honors) degree from the Department of Chemical Technology, Chulalongkorn University in 2010. She continued studying for a Doctoral Degree in Chemical Technology, Chulalongkorn University. She has received the Royal Golden Jubilee Scholarship from Thailand Research Fund for her Ph.D. study. Ratchprapa also served as a teaching assistant for undergraduate courses “Chemical Engineering Thermodynamics”, “Process Dynamics and Control” and “Physicochemical Measurements II”. She carried out her Ph.D. research for two year (2012-2013) at Clean Fuel and Catalysis Program (CFCP) in the Energy Institute of the Pennsylvania State University (PSU), Pennsylvania, USA.

Journal Publication:

1. Satthawong, R., Koizumi, N., Song, C., and Prasassarakich, P. Bimetallic Fe–Co Catalysts for CO2 Hydrogenation to Higher Hydrocarbons. Journal of CO2 Utilization 3-4 (2013) 102-106.

2. Satthawong, R., Koizumi, N., Song, C., and Prasassarakich, P. Comparative Study on CO2 Hydrogenation to Higher Hydrocarbons over Fe-Based Bimetallic Catalysts. Topics in Catalysis 57 (2014) 588-594.

3. Satthawong, R., Koizumi, N., Song, C., and Prasassarakich, P. Light Olefin Synthesis from CO2 Hydrogenation over K-Promoted Fe-Co Bimetallic Catalysts. Submitted to Catalysis Today.

Conference Presentation (Oral presentation):

1. “Novel Bimetallic Catalysts for CO2 Hydrogenation to Olefin-Rich Higher Hydrocarbon”. ICCDU XII, Alexandria, VA, USA.

2. “Comparative Studies of Fe-Based Bimetallic Catalysts for CO2 Hydrogenation to Higher Hydrocarbons”. 9thMPSGC, University of Malaya, Malaysia.

3. “Comparative studies of Fe-M (M; Co, Ni, Cu, Pd) Bimetallic Catalysts for CO2 Hydrogenation to Higher Hydrocarbons”. RGJ-Ph.D Congress XV, Chonburi, Thailand.

4. “Light Olefins Synthesis from CO2 Hydrogenation over K-Promoted Fe-Co Bimetallic Catalysts”. TOCAT7, Kyoto, Japan.